NTNU

Norwegian University of
Science and Technology

Reliability assessments of concrete structures using non-linear finite element analyses

Hanna Eklund
Astrid Skorve
Arne Strand

Civil and Environmental Engineering
Submission date: June 2017
Supervisor: Max Hendriks, KT
Co-supervisor: Morten Engen, KT
Jochen Köhler, IBM

Norwegian University of Science and Technology
Department of Structural Engineering

Department of Structural Engineering
Faculty of Engineering Science and Technology
NTNU- Norwegian University of Science and Technology

ACCESSIBILITY

MASTER THESIS 2017

SUBJECT AREA:	DATE:	NO. OF PAGES:
Structural Design	11.06.2017	150

TITLE:

Reliability Assessments of Concrete Structures using Non-Linear Finite Element Analyses

Pålitelighetsanalyser av betongkonstruksjoner ved bruk av ikke-lineære elementanalyser

BY:

Hanna Eklund
Astrid Skorve
Arne Strand

SUMMARY:
Reliability assessment of slender concrete columns using Non-linear finite element analysis (NLFEA) is studied in this thesis. Several reliability methods in combination with NLFEA are applied and discussed to assess the consistency of the Eurocode design calculations in regard to reliability.
The Eurocode applies the safety format of Partial safety factor (PSF) which assumes a linear Limit state function (LSF). Using NLFEA may result in a non-linear limit state, hence violating the assumption of the PSF method. Still, the Eurocode recommends using the PSF format on non-linear problems when NLFEA are conducted. Current research on concrete structures involves formulating new safety formats that are applicable to NLFEA and non-linear LSFs.
This thesis further adapts the current research to the problem of slender columns subject to large second order effects. The reliability is assessed by a response surface method in combination with first and second order reliability methods. Both NLFEA and an analytic approach was used in the probabilistic design. The Monte Carlo method was applied as well to determine the accuracy of the methods. Five random variables were introduced, namely the concrete compressive strength, the reinforcement yield strength, the concrete stiffness, the eccentricity of the load and the load itself. The material and geometric uncertainty have been implemented, while some considerations were made towards the modelling uncertainty. Safety factors applicable to several case configurations were also sought by assessing different concrete grades and column slenderness.
Suggestions for improvements in a future version of Eurocode 2 is given. For slender columns, it may seem advantageous to propose a new set of safety factors that are calibrated to consider second order effects. In general, safety factors associated to second order effects should be increased, and safety factors associated to the cross-sectional resistance may be decreased or set to one.

RESPONSIBLE TEACHER: Max Hendriks

SUPERVISOR(S): Max Hendriks, Morten Engen, Jochen Köhler

CARRIED OUT AT: Department of Structural Engineering

Department of Structural Engineering

FACULTY OF ENGINEERING
NTNU – Norwegian University of Science and Technology

MASTER THESIS 2017

for

Hanna Eklund, Astrid Skorve and Arne Strand

Reliability Assessments of Concrete Structures using Non-Linear Finite Element Analyses

Pålitelighetsanalyser av betongkonstruksjoner ved bruk av ikke-lineære elementanalyser

Concrete structures are normally designed using the partial safety factor (PSF) method. Implicit in this method is the assumption of a linear limit state function (LSF), and this permits the calibration of partial safety factors that account for the target reliability, and the variability and assumed sensitivity of the respective basic variables. This approach represents generically a large range of design situations today.

Non-linear finite element analyses (NLFEA), if properly performed, provides the designer with realistic estimates of the structural behavior. However, with NLFEA the LSF might no longer be linear, and the underlying assumptions of the PSF method would then be violated. Parts of current research in the concrete community is related to formulating proper safety formats that are applicable in connection to NLFEA and possible non-linear LSFs.

In this project, the problem will be elaborated on by studying a seemingly simple problem: slender columns subjected to axial loading. Two 3.8 m long reinforced concrete columns with similar geometries but different concrete grades are considered.

Supervisor(s): Max Hendriks, Jochen Köhler, Morten Engen

NTNU, 17.01. 2017

Preface

This MSc thesis is written as the final part of the master program of Civil Engineering at the Norwegian University of Science and Technology in Trondheim. It is written for the Department of Structural Engineering in the period from January to June 2017.

The thesis concerns reliability assessment of concrete structures using NLFEA, and the feasibility of Eurocode calculation methods regarding highly non-linear problems. Structural reliability was a relatively new field of study for the authors, so digging into and trying to comprehend the methods and theory has been a great opportunity and challenge. The reliability assessments performed in this thesis were conducted with self-developed, integrated procedures with Matlab, Python, Diana and Command Prompt. The development was time consuming, but greatly increased the understanding of the potentials and limitations of different the methods.

The master thesis has been supervised by Professor Max Hendriks, Associate Professor Jochen Köhler and PhD candidate Morten Engen at Multiconsult. Gratitude is extended towards our supervisors for their patient and helpful guidance. We highly appreciate the good advice and long, motivating discussions. We are also thankful for the the insight and knowledge our supervisors shared concerning structural reliability, concrete structures and in programming.

Thanks are also extended to PhD candidate Finn Idar Grøtta Giske at Multiconsult for valuable information and understanding of the second order reliability method.

Trondheim, 11.06.2017

Hanna Eklund Astrid Skorve Arne Strand

Abstract

Reliability assessment of slender concrete columns using Non-linear finite element analysis (NLFEA) is studied in this thesis. Several reliability methods in combination with NLFEA are applied and discussed to assess the consistency of the Eurocode design calculations in regard to reliability.

The Eurocode applies the safety format of Partial safety factor (PSF) method which assumes a linear Limit state function (LSF). Using NLFEA may result in a non-linear limit state, hence violating the underlying assumption of the PSF method. Still, the Eurocode recommends using the PSF format on non-linear problems when NLFEA are conducted. Current research on concrete structures involves formulating new safety formats that are more applicable to NLFEA and non-linear LSFs.

This thesis further adapts the current research to the problem of slender columns subject to large second order effects. The reliability is assessed by a response surface method in combination with first and second order reliability methods. Both NLFEA and an analytic approach was used in the probabilistic design. The Monte Carlo method was applied as well to determine the accuracy of the methods. Five random variables were introduced, namely the concrete compressive strength, the reinforcement yield strength, the concrete stiffness, the eccentricity of the load and the load itself. The material and geometric uncertainty have been implemented, while some considerations were made towards the modelling uncertainty. Safety factors applicable to several case configurations were also sought by assessing different concrete grades and column slenderness.

Suggestions for improvements in a future version of Eurocode 2 is given. For slender columns, it may seem advantageous to propose a new set of safety factors that are calibrated to consider second order effects. In general, safety factors associated to second order effects should be increased, and safety factors associated to the cross-sectional resistance may be decreased or set to one.

Sammendrag

I denne oppgaven er det gjort pålitelighetsvurderinger av slanke betongsøyler ved bruk av ikkelineære elementanalyser. Forskjellige pålitelighetsmetoder blir implementert og diskutert for å vurdere pålitelighetsnivået i dagens Eurokode.

Eurokoden benytter partielle sikkerhetsfaktorerer (PSF) som sikkerhetsformat, der det forutsettes en lineær grensetilstand, eller *limit state* (LS). Bruk av ikkelineære analyser kan derimot føre til en ikkelineær LS, og dermed er den underliggende forutsetningen for PSF-metoden feil. Eurokoden anbefaler likevel å bruke PSF-formatet på problemer der ikkelineære elementanalyser utføres.

Dagens forskning innenfor betongkonstruksjoner innebærer blant annet å utforme nye sikkerhetsformater som er mer anvendelige for ikkelineære analyser og ikkelineær LS.

I denne oppgaven blir pålitelighetsvurderinger gjort på slanke søyler som er utsatt for store andreordens effekter.

Påliteligheten vurderes ved en *response surface* metode i kombinasjon med *first order reliability method* og *second order reliability method*. Både ikkelineære elementanalyser og en analytisk tilnærming ble brukt i den probabilistiske fremstillingen. Monte Carlo ble også benyttet for å vurdere nøyaktigheten av de tilnærmede metodene. Fem stokastiske variabler ble introdusert; betongens trykkfasthet, flytespenning i armering, E-modulen til betong, eksentrisiteten til lasten, og lasten. Usikkerhet knyttet til material og geometri har blitt inkludert i analysene, og modelleringsusikkerheten er diskutert. Det ble forsøkt foreslått et sett med sikkerhetsfaktorer som passer flere søyleoppsett ved å variere betongkvalitet og slankhet i analysene.

Noen forslag til forbedringer i en fremtidig versjon av Eurocode 2 kommer frem i oppgaven. For slanke søyler kan det virke fordelaktig å foreslå et nytt sett med sikkerhetsfaktorer som er kalibrert for å ta hensyn til store andreordens effekter. Generelt bør sikkerhetsfaktorer knyttet til andreordens effekter økes, og sikkerhetsfaktorer knyttet til tverrsnittsmotstanden kan reduseres eller settes til en.

Contents

List of Figures

List of Tables

List of Symbols

Φ	Standard normal distribution
Φ_n	n-dimensional cumulative standard normal distribution
Θ	Random variable to the Model uncertainty
α_R	Sensitivity of the resistance
α_S	Sensitivity of the load action
α_{cc}	Coefficient taking account of long term effects on the compressive strength and of unfavourable effects resulting from the way the load is applied
α_{fc}	Sensitivity of concrete strength
α_{fy}	Sensitivity of reinforcement yield strength
α_i	Sensitivity factors
β	Reliability index
β_σ^{min}	Minimum reduction factor of compressive strength due to lateral cracking
β_T	Target reliability index
β_{eq}	Equivalent reliability index
β_{sys}	System reliability index
η	Strain relation $\frac{\varepsilon_c}{\varepsilon_{c1}}$
γ_{CE}	Partial safety factor for the Youngs modulus
γ_G	Partial safety factor for permanent actions
γ_c	Partial safety factor for concrete
γ_O	Overall safety factor
γ_s	Partial safety factor for reinforcement steel
κ_i	Curvature

λ	Slenderness ratio
μ_E	Mean value of the Young's modulus of concrete
μ_M	Mean of the safety margin
μ_N	Mean of the applied load
μ_R	Mean of the resistance
μ_S	Mean of the load action
μ_e	Mean value of the total eccentricity
μ_{fc}	Mean concrete compressive strength
μ_{fy}	Mean steel yield strength
μ_{ln}	Lognormal mean value
μ_x	Mean value of random variable X
μ_Θ	Mean of the model uncertainty
ν	Poisson ratio
ϕ	Out of plumpness
σ	Standard deviation
σ_E	Standard deviation of the Young's modulus of concrete
σ_M	Standard deviation of the safety margin
σ_N	Standard deviation of the applied load
σ_R	Standard deviation of the resistance
σ_S	Standard deviation of the load
σ_c	Concrete compressive strength
σ_e	Standard deviation of the total eccentricity
σ_{fc}	Standard deviation of the concrete compressove strength
σ_{fy}	Standard deviation of the steel yield strength

σ_{ln}	Lognormal standard deviation
σ_x	Standard deviation of random variable X
σ_Θ	Standard deviation of the model uncertainty
ε_{FORM}	Convergence criteria for the first order reliability method
ε_{RSM}	Convergence criteria for the response surface method
ε_y	Steel yield strain
ζ	Factor used to scale the FORM probability of failure to SORM probability of failure
A_s	Reinforcement area
a_i	Constants of the first and second order reliability methods
a_{nom}	Nominal geometrical parameters
b	Cross-section width of concrete column
b_i	Constants of the second order reliability method
c	Concrete cover
D_{SN}	Normal stiffness
E	Modulus of elasticity
E_c	Modulus of elasticity of concrete
E_{cd}	Design modulus of elasticity of concrete
E_{cm}	Secant modulus of elasticity of concrete
E_s	Elastic modulus of steel
e	Total eccentricity
e_0	Average eccentricity
e_{1y}	Initial/Planned eccentricity of load application in y-direction
e_2	Second order deflection
e_d	Design eccentricity

e_i	Eccentricity found in EC2-1-1
f	Arbitrary factor
f_0	Initial curvature
f_c	Concrete compressive strength
$\tilde{f}_c$	Concrete compressive strength when used in non-linear analysis according to EC2-2
f_{cd}	Design concrete compressive strength
f_{ck}	Characteristic concrete compressive strength
f_{cm}	Mean value of concrete cylinder compressive strength
$f_{cm,is}$	Insitu values for the mean compressive strength of concrete [9]
f_{ct}	Concrete tensile strength
f_{ctd}	Design concrete tensile strength
f_{ctm}	Mean value of concrete tensile strength
f_y	Steel yield strength
$\tilde{f}_y$	Yield strength of reinforcement when used in non-linear analysis according to EC2-2
f_{yd}	Yield strength of reinforcement
f_{yk}	Characteristic yield strength of reinforcement steel
$f_{ym,is}$	Insitu values for the yield strength of steel [9]
G	Limit state function
G_c	Compressive fracture energy
G_F	Fracture energy
g	Realization of the limit state function
$\widetilde{g}$	Approximated realization of the limit state function
H	Horizontal load
h	Cross-section height of concrete column

h_c	Concrete element size
h_{eq}	Equivalent length (Crack-band width)
h_{max}	Maximum element size
I	Moment of inertia
k	Factor taking into account the mean concrete stiffness and strains
$k_{0.05}$	Inverse of the normal distribution for the 5%-fractile value
l	Length of concrete column
M	Safety margin
M_{0Ed}	First order moment
M_2	Nominal second order moment
N	Applied axial force
N_d	Design load
n	Number of random variables
P_f	Probability of failure
R	Resistance of a section or structure
R_d	Design resistance of a section or structure
R_n	Nominal resistance of a section or structure
S	Load action
U	Random variable in standard normal space
u	Realization of random variable U
u_2	Deflection in y-direction
V_Θ	Coefficient of variation of model uncertainty
V_E	Coefficient of variation of concrete stiffness
V_f	Coefficient of variation of material strength

V_{fc}	Coefficient of variation of concrete strength
V_{fy}	Coefficient of variation of reinforcement yield strength
V_G	Coefficient of variation of geometrical factor
V_N	Coefficient of variation of the applied load
V_{Pf}	Coefficient of variation of the failure probability
V_R	Coefficient of variation of the resistance
V_x	Coefficient of variation of random variable X
X	Random variable
X_f	Random variable to model the material uncertainty
X_G	Random variable to model the geometrical uncertainty
x	Realization of random variable X
$Y_{3,j}$	Log-normal variable representing additional variations due to the special placing, curing and hardening conditions of in situ concrete at job j
z	Number of Monte Carlo simulations

Abbreviations

CDF Cumulative density function

CHX60 Twenty-node isoparametric solid brick element

CL3CM Three-node curved line base element

CL9BE Three-node, two-dimensional class-III beam element

CPU Central processing unit

CQ16M Eight-node quadrilateral isoparametric plane stress element

CQ48I Interface element between two planes in a three-dimensional configuration

DIANA DIsplacement ANAlyser

EC2 Eurocode 2

EC2-1-1 Eurocode 2-1-1

EC2-2 Eurocode 2-2

FEA Finite element analysis

FORM First order reliability method

GRFM Global resistance factor method

IABSE The Internatinal Association for Bridge and Structural Engineering

JCSS Joint Committee on Structural Safety

LoA Level-of-Approximation

LSF Limit state function

LSFE Limit state function evaluation

MC Monte Carlo

NLFEA Non-linear finite element analysis

NPRA Norwegian Public Roads Administration

NR Newton-Raphson

PDF Probability density function

PSF Partial safety factor

RS Response surface

RSM Response surface method

SORM Second order reliability method

ULS Ultimate Limit State

1 Introduction

In the current state of design, concrete structures are normally designed using the Partial safety factor (PSF) method to satisfy safety and serviceability requirements. This is a semi-probabilistic method where a linear Limit state function (LSF) is assumed, which allows for calibration of partial safety factors to a certain reliability level. In the safety factors, there are underlying assumptions about the sensitivity and variability of the basic variables, and this safety format covers a large range of design situations today.

The PSF method is originally meant for component checks, where redistribution of forces and other global effects are not taken into account. To account for global effects, as well as assessing all failure modes collectively, non-linear analyses could be carried out. When assessing a structure with non-linear finite element software, the assumption of a linear limit state might be inaccurate, and the underlying assumptions of the PSF method are consequently violated. Still, the Eurocode suggests using the PSF format on non-linear problems when Non-linear finite element analysis (NLFEA) are conducted [10]. Current research on concrete structures involves formulating new safety formats that are applicable to NLFEA and non-linear LSFs.

In this project, the Eurocode's capability to adapt to slender structures will be investigated. Also, by developing a full probabilistic representation of the problem, the reliability level and other important assumptions of the Eurocode are examined. Both the methods and safety formats are of interest, and non-linear behavior is considered through NLFEA. To do this, NLFEA was used in combination with reliability methods, which is still a quite new field in structural engineering. When performing NLFEA a limit state function is not possible to access explicitly. To carry out reliability assessments, approximate methods should be used to evaluate the limit state. A challenge is to choose a feasible method that gives accurate results without being too time consuming. In order to test and validate the reliability methods, they were performed using analytic assessments as well.

The slender columns evaluated in this project are originally from an ongoing Round-Robin study by the International Association for Bridge and Structural Engineering (IABSE). They have asked academia to give capacity estimates of a slender column with NLFEA, before experimentally testing the columns. Two rounds of testing are performed, starting with a standard concrete grade, then shifting to high strength concrete. The material input should in the first

steps be following current codes. Further, a best estimate of the column capacity should be developed, mirroring the response expected in the experiments. The experimental results will be provided to academia after they have submitted their best estimate, and marks the start of the second round of testing. Later, material samples of both columns will be tested, and academia will have the chance to implement these results to the models. Unfortunately the present project was finished before the results of the high strength concrete experiments were distributed and material samples were tested. Each new step represents a higher knowledge level, which may or may not affect the modelling consistency and accuracy of the non-linear modelling.

Being a part of this study an ambition is to draw conclusions as to how much level of knowledge affects the accuracy and consistency in finite element analyses. Another interesting aspect of the IABSE project is how various engineers interpret and adapt the Eurocode differently.

Some limitations were made to this project to make the calculations more doable. The load was simplified as a point force originating from permanent actions, and the self weight of the columns were neglected. The failure modes considered were compression failure in the concrete and yielding in the reinforcement. Other possible failures such as compression failure at the point of load application were not considered.

In the probabilistic analyses, the number of basic variables and which basic variables included limit the scope. The variables that were included were concrete strength, yield strength, concrete stiffness, eccentricity which also includes the effect of imperfections, and the load.

The report is structured as follows:

Section 2: The case study from IABSE is presented with column specifications and experimental setup.

Section 3: Properties of the material, geometry and load inputs are presented. The extent of this project calls for different sets of properties, and all sets are presented in this section.

Section 4: The methods of calculating the design and best estimate capacities are given. Level of knowledge is presented with the best estimate evaluation. The Level-of-Approximation approach is also presented. The last subsection of this section summarizes the non-linear finite element modelling, which is implemented in the capacity calculations and in the non-linear reliability assessments.

Section 5: Structural reliability theory and methods are presented in the first couple of subsections. The implementation of these methods, analytically and with NLFEA, is then presented. The methods introduced and implemented are the Monte Carlo, First and Second Order Reliability Method and a Response Surface Method in conjunction with First and Second Order Reliability Method.

Section 6: All results are presented in this section. The section starts with the design capacity calculations which are organized after increasing level of approximation. Following, the best estimate and the Round-Robin results are given, organized after increasing level of knowledge. The reliability results come next. First the results of all methods are presented in terms of the original column setup. A sensitivity study on the reliability methods is given, before an extended study on different column setups is presented.

Section 7: Discussion of the results.

Section 8: Conclusions are drawn based on the most important findings in this project.

Section 9: At last, proposals for further work are given.

2 Case configuration

The case study of this master thesis is based on a column setup defined by The Internatinal Association for Bridge and Structural Engineering (IABSE). Two 3.8 m long reinforced concrete columns with similar geometries but different concrete grades are considered.

2.1 Column specifications

The most important features of the columns are given in this section. More detailed drawings produced by IABSE are given in Appendix A.

The columns are statically determined and free to rotate in both ends, as seen in Figure 2.1a. The critical length is assumed to be the length of the columns, l. The columns are loaded in compression as illustrated in Figure 2.1b. The load has an eccentricity, e_{1y}, that induces buckling about the weak axis.

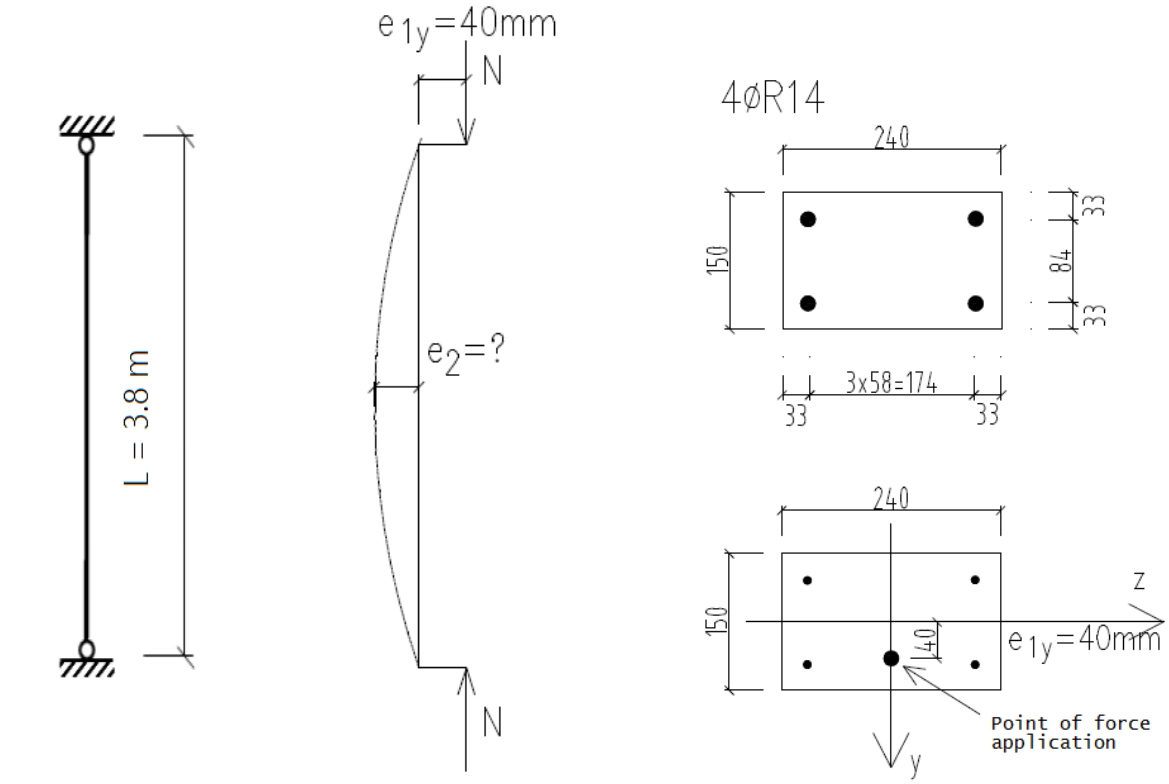

(a) Column setup

(b) Load application

(c) Cross-section

Figure 2.1: Column geometry and loading configuration

The column cross-section is rectangular and defined by the height, $h = 150mm$, and width,

$b = 240mm$, see Figure 2.1c. The concrete cover is $c = 33mm$ in both y- and z-direction. The force is applied at $e_{1y} = 40mm$ from the centroid of the cross-section as seen in Figure 2.1c.

The reinforcement layout is given in Figure 2.2. The longitudinal reinforcement is made up of Ø14 bars, while Ø6 bars are used for the stirrups. The top and bottom platens are welded to the 600 mm long longitudinal reinforcement.

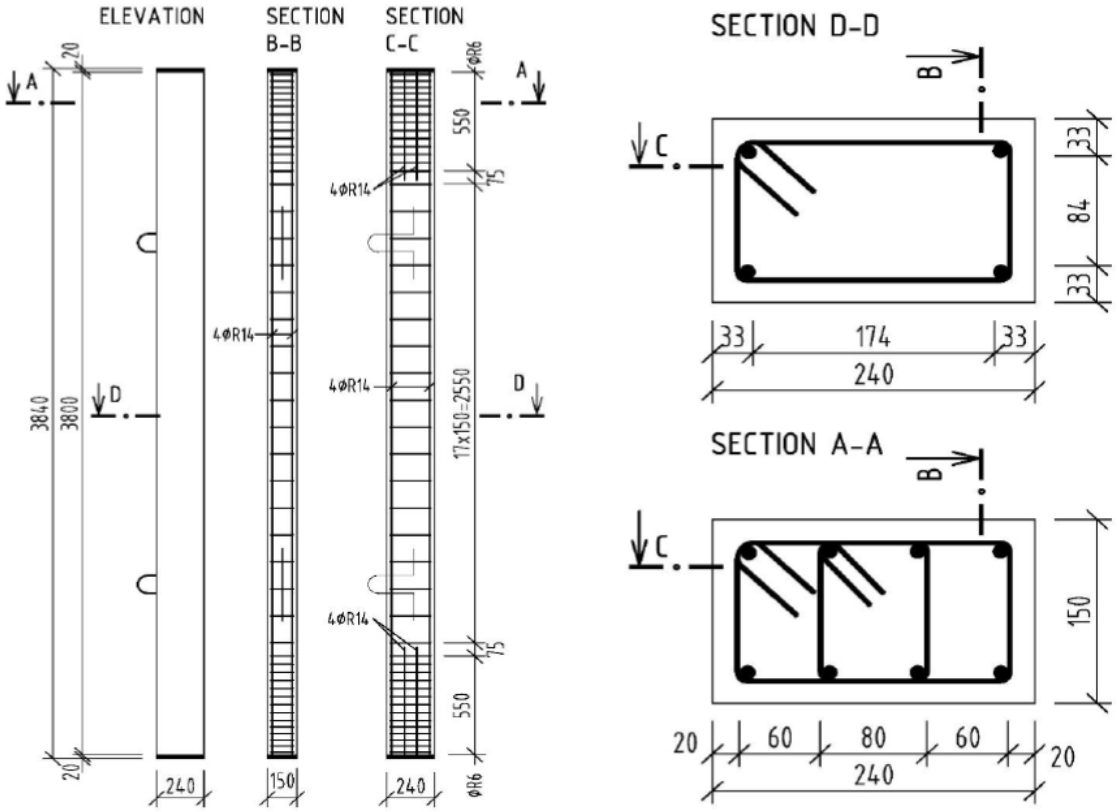

Figure 2.2: Reinforcement layout given by IABSE [1]

The material grades used for the two columns are shown in Table 2.1. Column A is made of a normal concrete type, while Column B is made of high-strength concrete. The curing period was assumed to be 28 days. Both columns are reinforced with the same steel type.

Column A	Column B
Concrete C45/55	Concrete C100/115
Steel B500B (R10505)	Steel B500B (R10505)

Table 2.1: Material grades and steel type used for the concrete columns

Creep is insignificant due to the short load duration of the columns and will be neglected in this thesis.

2.2 Experimental setup

The testing was performed by IABSE, and an illustration of the experimental setup is found in Figure 2.3.

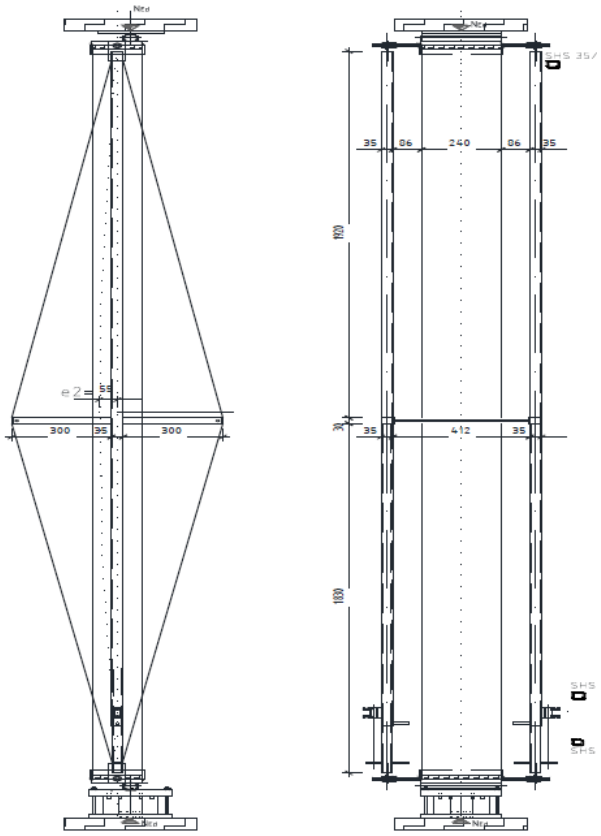

Figure 2.3: Experimental setup [1]

For Column A, in total six tests were performed. The tests titled S-1-1 to S-1-3 were cast as beams while the tests titled S-1-4 to S-1-6 were cast as columns. The difference is illustrated in Figure 2.4. The same figure also shows that the load was applied as a line load.

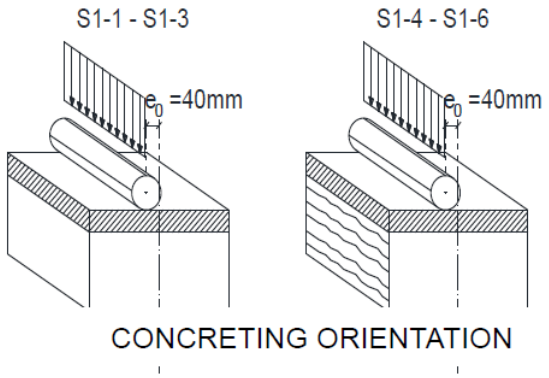

Figure 2.4: Load application and concreting orientation [1]

3 Properties of material, geometry and load

The capacity calculations described in Sections 4 and 5 were performed with different parameters and assumptions for material, eccentricity and load. The choices done in regard to these parameters will be described in this section.

3.1 Material

The relevant materials in this thesis are concrete and steel, and their parameters will be described next. In the calculation of design capacities according to the Eurocode and in the determination of the best estimate, only deterministic material parameters were applied. The structural reliability analyses on the other hand, considers some of the material parameters as stochastic variables.

3.1.1 Eurocode material parameters

All material parameters used in combination with the Eurocode capacity calculations are based upon equations given in Table 3.1 of Eurocode 2-1-1 (EC2-1-1) [2]. The main parameters implemented in the Eurocode analyses are the concrete compressive strength, f_c, the concrete stiffness, E_c, the concrete tensile strength, f_{ct}, and the reinforcement yield strength, f_y. The design values of each parameter for both Column A and B are listed in Table 3.1.

Parameters	Equation	Column A	Column B
Compressive strength [MPa]	$f_{cd} = \frac{f_{ck}}{\gamma_c}$	30.00	66.67
Tensile strength [MPa]	$f_{ctd}= \begin{cases} 0.3(f_{cd})^{\frac{2}{3}} \leq \text{C50}, \\ 2.12ln\big(1 + \frac{(f_{ck}+8)/\gamma_c}{10}\big) > \text{C50} \end{cases}$	2.90	3.20
Young's modulus [GPa]	$E_{cd} = 22\big(\frac{f_{ck}+8}{10}\big)^{0.3}/\gamma_{CE}$	30.24	37.43
Yield strength [MPa]	$f_{yd} = f_{yk}/\gamma_s$	434.78	

Table 3.1: Eurocode 2-1-1 Design material parameters

To determine a proper approximation of the design tensile strength, f_{ctd}, the equation of the mean tensile strength, f_{ctm}, was scaled by the partial safety factor of concrete, γ_c. To achieve the design concrete stiffness, E_{cd}, the mean concrete stiffness, E_{cm}, was simply divided by the partial safety factor of concrete stiffness, $\gamma_{CE}= 1.2$, as suggested in Section 5.8.6(3) of EC2-1-1 [2].

Both linear and non-linear constitutive relations for concrete were utilized for different Level-of-Approximation (LoA), explained in Section 4.1. For the most simple calculations with constant stress in the compression zone, the bi-linear relation seen in Figure 3.1a was used in combination with the reinforcement relation shown in Figure 3.1c using no post-yielding hardening. To model the problem more realistically, the relation in Figure 3.1b was used for concrete, and post-yielding hardening was included in the reinforcement.

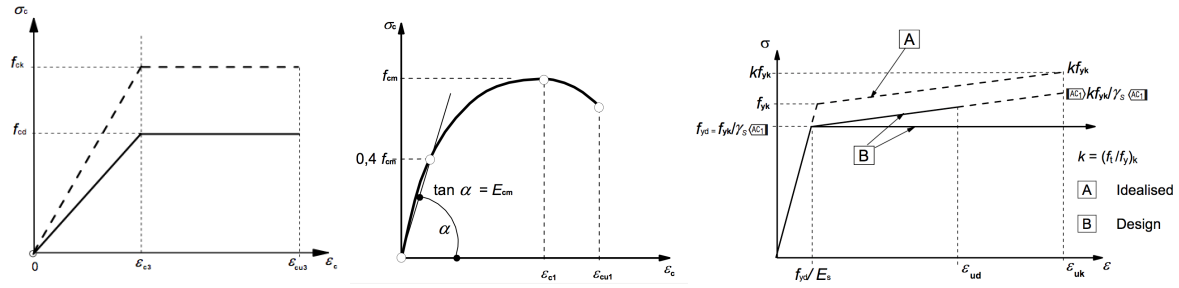

(a) Concrete linear *(b) Concrete non-linear* *(c) Reinforcement*

Figure 3.1: Eurocode constitutive material relations [2]

The parabolic relation shown in Figure 3.1b can be expressed by

$$\frac{\sigma_c}{f_{cm}} = \frac{k\eta - \eta^2}{1 + (k-2)\eta}. \tag{3.1}$$

Equation (3.1) is defined by the mean concrete strength, f_{cm}, the strain relation, η, and a factor, k, taking into account the mean concrete stiffness and strains [2]. To achieve the parabolic relation in terms of design values, f_{cm} and E_{cm} were simply substituted by the design concrete strength, f_{cd}, and design concrete stiffness, E_{cd}.

3.1.2 Best estimate material parameters

In the development of a best estimate model, mean material sets were implemented to achieve a more realistic representation. Primarily three different material sets were compared before the assumed most realistic was chosen. They were the following:

- Material A: The 50%-fractile value of the concrete strength and yield strength from an assumed lognormal distribution, adjusted to resemble the structural insitu strength [9].
- Material B: EC2-1-1, Table 3.1 with mean values [2]
- Material C: fib Model Code 2010 with mean values [4]

Two different parabolic constitutive relations were implemented to these material sets. For material B, the constitutive stress-strain relation in compression from the Eurocode 2, seen in Figures 3.1b and 4.4c, was chosen. For material sets A and C, the relation implemented was one recommended by the Guidelines of NLFEA [11] written by the Dutch Rijkswaterstaat Centre for Infrastructure, further referred to as the Guidelines of NLFEA. The relation can be seen in Figure 4.4b and is further described in Section 4.4.1. The fracture energy, G_F, for all material sets is retrieved from the fib model code 2010 [4], and the compressive fracture energy, G_c, from the Guidelines of NLFEA.

Material set A takes the sample mean of the cylinder strength, f_{cm}, and scales it by a factor of 1.15 to achieve the mean in-situ strength of concrete, $f_{cm,is}$. The factor of 1.15 accommodates the differences in concrete strength observed from laboratory samples to real structures, while $k_{0.05}$ is the inverse of the normal distribution for the 5%-fractile value, $\Phi^{-1}(0.05)$, and V_{fc} and V_{fy} are the coefficients of variation for concrete strength and steel yield strength. The difference between laboratory and in-situ is much less for the steel reinforcement and thus the steel is not scaled [9]. The other material parameters are calculated using equations from Table 3.1 in EC2-1-1, with the mean compressive strength, f_{cm}, substituted by $f_{cm,is}$. The equations and mean values used in material set A can be found in Table 3.2.

Parameters	Equation	Column A	Column B
Compressive strength [MPa]	$f_{cm,is} = \frac{f_{ck}}{1.15} e^{k_{0.05} V_{fc}}$	50.08	111.29
Tensile strength [MPa]	$f_{ctm,is} = \begin{cases} 0.3\left(\frac{f_{ck}}{1.15}\right)^{\frac{2}{3}} \leq \text{C50}, \\ 2.12 ln\left(1 + \frac{f_{cm,is}}{10}\right) > \text{C50} \end{cases}$	3.46	5.29
Young's modulus [GPa]	$E_{cm,is} = 22\left(\frac{f_{cm,is}}{10}\right)^{0.3}$	35.67	45.32
Poisson ratio [-]	ν	0.15	0.15
Fracture energy [N/mm]	$G_{F,is} = 0.073 f_{cm,is}^{0.18}$	0.148	0.171
Comp. fracture energy [N/mm]	$G_{C,is} = 250 G_{F,is}$	37.00	42.75
Yield strength [MPa]	$f_{ym,is} = f_{yk} e^{k_{0.05} V_{fy}}$	534.00	

Table 3.2: Parameters of material set A

Material set B and C consist of parameters that are quite similarly defined. They both use the mean compressive strength as defined in EC2-1-1 and adapted equations from EC2-1-1 Table 3.1. They differ in the definition of the Young's modulus and the Poisson ratio, ν. The equations

and definitions can be seen in Tables 3.3 and 3.4 for material set B and C respectively.

Parameters	Equation	Column A	Column B
Compressive strength [MPa]	$f_{cm} = f_{ck} + 8$	53.00	108.00
Tensile strength [MPa]	$f_{ctm}= \begin{cases} 0.3\big(f_{ck}\big)^{\frac{2}{3}} \leq \text{C50}, \\ 2.12ln\big(1+\frac{f_{cm}}{10}\big) > \text{C50} \end{cases}$	3.80	5.23
Young's modulus [GPa]	$E_{cm} = 22\big(\frac{f_{cm}}{10}\big)^{0.3}$	36.28	44.92
Poisson ratio [-]	ν	0.15	0.15
Fracture energy [N/mm]	$G_F = 0.073 f_{cm}^{0.18}$	0.149	0.170
Comp. fracture energy [N/mm]	$G_C = 250 G_F$	37.25	42.50
Yield strength [MPa]	f_{yk}	500.00	

Table 3.3: Parameters of material set B

Parameters	Equation	Column A	Column B
Compressive strength [MPa]	$f_{cm} = f_{ck} + 8$	53.00	108.00
Tensile strength [MPa]	$f_{ctm} = \begin{cases} 0.3\big(f_{ck}\big)^{\frac{2}{3}} \leq \text{C50}, \\ 2.12ln\big(1+0.1 f_{cm}\big) > \text{C50} \end{cases}$	3.80	5.23
Young's modulus [GPa]	$E_c = 21.5\big(\frac{f_{cm}}{10}\big)^{\frac{1}{3}}$	37.49	47.52
Poisson ratio [-]	ν	0.2	0.2
Fracture energy [N/mm]	$G_F = 0.073 f_{cm}^{0.18}$	0.149	0.170
Comp. fracture energy [N/mm]	$G_C = 250 G_F$	37.50	42.50
Yield strength [MPa]	f_{yk}	500.00	

Table 3.4: Parameters of material set C

3.1.3 Stochastic material variables

In this study, the material parameters considered to carry the most uncertainty, and further used as stochastic variables, are listed below. All material uncertainty is assumed to be covered by these variables. No correlation between the variables was assumed.

- Concrete compressive strength, f_c
- Reinforcement yield strength, f_y
- Concrete modulus of elasticity, E_c

The random variables representing the column resistance, f_c, f_y and E_c, were assumed to be

lognormally distributed. In many cases the normal distribution is a convenient representation of random variables, but the approximation fails when the coefficient of variation is large. The normal distribution also allows for negative values which sometimes must be avoided. The lognormal distribution is an accurate approach for both high and low coefficients of variations, and yields a null probability of occurrence of negative values as well [12].

Lognormally distributed parameters are represented by the mean and standard deviation of the distribution only. The mean, standard deviation and coefficient of variation corresponding to the stochastic material variables are summarized in Table 3.5, and will below be explained in closer detail. All other material parameters were assumed to be deterministic.

x	μ_x	σ_x	V_x	Probability density function (PDF)
f_c	$\frac{f_{ck}}{1.15}e^{1.645V_{fc}}$	$\mu_{fc}V_{fc}$	0.150	Lognormal
f_y	$f_{yk}e^{1.645V_{fy}}$	$\mu_{fy}V_{fy}$	0.040	Lognormal
E_c	$22\left(\frac{f_{cm,is}}{10}\right)^{0.3}$	$\mu_E V_E$	0.158	Lognormal

Table 3.5: Mean, standard deviation and coefficient of variation of the material parameters

The mean value of concrete and steel strength, μ_{fc} and μ_{fy}, were set to the insitu adjusted 50%-fractile values, $f_{cm,is}$ and $f_{ym,is}$, introduced in Section 3.1.2. The standard deviations of concrete and steel strength, σ_{fc} and σ_{fy}, were found using the coefficients of variation, V_{fc} and V_{fy}, given in Table 4.1. The mean value of the concrete stiffness, μ_E, was calculated using the equation given in Table 3.1 in EC2-1-1, while the coefficient of variation, V_E, was estimated through Equation (3.2) from the JCSS Model Code [3].

$$E_{c,ij} = 10.5 f_{c,ij}^{\frac{1}{3}} Y_{3,j} \tag{3.2}$$

The variable representing additional variations due to the special placing, curing and hardening conditions of insitu concrete at job j, $Y_{3,j}$, has a lognormal distribution with a mean of 1.0 and a coefficient of variation of 0.15. A total number of 10^8 random samples of $E_{c,ij}$ was generated, and the coefficient of variation of this random sample was found. The standard deviation of the concrete stiffness, σ_E, could then be determined.

3.2 Geometry and load

Regarding geometry and load conditions, the applied load and the eccentricity were the only changing parameters throughout the different assessments. In the capacity calculations, the

load is only a result of the analyses. No further deliberation on the load is needed in Sections 3.2.1 and 3.2.2. In probabilistic assessments, however, the load was regarded as a basic variable and needs further interpretation.

3.2.1 Eurocode 2 eccentricity

In the test setup, there is a planned load eccentricity, e_{1y}, of 40 mm. In addition, there may be some deviations in the geometry of the column and the positioning of the load. The unfavorable effects of this should be included in Ultimate Limit State (ULS) design, and is covered by Eurocode 2-1-1 Section 5.2. In this specific case, the column could be considered an isolated, braced member, which means that the imperfections could be modelled as either the eccentricity e_i, or a horizontal load H, as illustrated in Figure 3.2. In the present work, the effect of imperfections was added to the planned eccentricity. The eccentricity e_i was found to be 9.5 mm with the Eurocode, which means that the total eccentricity used in the column capacity design was 49.5 mm.

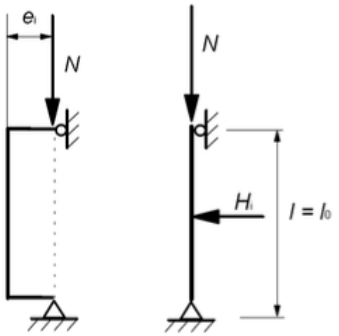

Figure 3.2: Accounting for imperfections with eccentric axial force or lateral force [2]

3.2.2 Best estimate eccentricity

The estimate of the applied eccentricity determined by Eurocode 2-1-1 can be considered conservative. Since the mean values of imperfections are zero [3], the eccentricity was changed to an expected value of 40mm for the best estimate design of Column A.

When determining the eccentricity of Column B, the higher level of knowledge was utilized. The JCSS Probabilistic Model Code [3] suggests an approach where absolute values of the eccentricities are found by considering the truncated probability distributions. JCSS divides the eccentricity into three parts; the average eccentricity, e_0, the initial curvature, f_0 and the out of plumpness, ϕ, as shown in Figure 3.3.

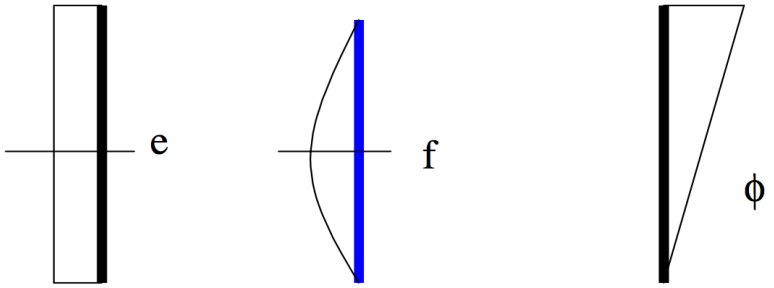

Figure 3.3: The three basic eccentricities [3]

In the best estimate of Column B, additionally to the planned load eccentricity, effects of curvature and out-of-plumbness were added. The curvature and plumbness are considered normally distributed and symmetrical around zero, with standard deviation of $l/1000$ for the straightness, and 0.0015 rad for the out-of-plumbness [3]. Since the absolute values were of interest, the truncated, half normal distributions with a mean of $\sigma\sqrt{2/\pi}$ [13], were applied. The total eccentricity used in the best estimate of Column B would then be

$$e = e_0 + \sqrt{\frac{2}{\pi}}\frac{l}{1000} + 0.0015l \approx 48mm,$$

where e_0 is set to the planned eccentricity e_{1y} = 40 mm, and l is the length of the column.

3.2.3 Stochastic load and geometry variables

The parameters of load and geometry expected to carry the most uncertainty, are listed below.

- Eccentricity, e
- Load, N

Here all uncertainty related to geometry is assumed covered by the eccentricity variable. A normal distributed eccentricity is recommended in the JCSS Probabilistic Model Code [3]. The load was assumed to originate from self-weight of overlying structures, both from material and installations, and was also assumed normally distributed. The mean, standard deviation and coefficient of variation corresponding to the stochastic load and geometry variables are summarized in Table 3.6, and is explained in closer detail below.

x	μ_x	σ_x	V_x	PDF
e	e_{1y}	$\frac{\sqrt{2}L}{1000}$	$\frac{\sigma_e}{\mu_e}$	Normal
N	$\frac{N}{1.35}$	$\mu_N V_N$	0.20	Normal

Table 3.6: Mean, standard deviation and coefficient of variation of the load and eccentricity

In the probabilistic representation of the problem, the definition of the eccentricity was taken from the JCSS Probabilistic Model code as shown in Figure 3.3. The out of plumbness was neglected for the reliability analyses. The planned eccentricity, $e_{1y}= 40mm$, the average eccentricity and the initial curvature were as a simplification merged to become one single stochastic variable. Both f_0 and e_o has a mean of 0 and a standard deviation of $l/1000$. This results in a mean value $\mu_e= 40mm$ and standard deviation $\sigma_e= \sqrt{2}l/1000$.

The self-weight was assumed to have a coefficient of variation, V_N, of 0.2. The mean load, μ_N, was found by dividing the design load by a safety factor, γ_G. In Equation 6.10a in EN 1990 [14], for situations where permanent loads are dominating, this factor is set to 1.35 [14]. The standard deviation, σ_N, was then calculated using the mean value and coefficient of variation.

4 Capacity calculation methods

4.1 Level of Approximation

Fib Model Code [4] describes the concept of Level-of-Approximation (LoA). This concept categorizes different design methods in their level of approximation/sophistication, where level I represents the simplest methods valid only for standard cases where high accuracy is not needed. Higher levels are more accurate and may lead to more economic solutions, but require more effort.

This system will also be implemented in this thesis to differentiate various methods with regard to their needed effort and assumed accuracy. The Model Code gives a figure to illustrate LoA, given in Figure 4.1.

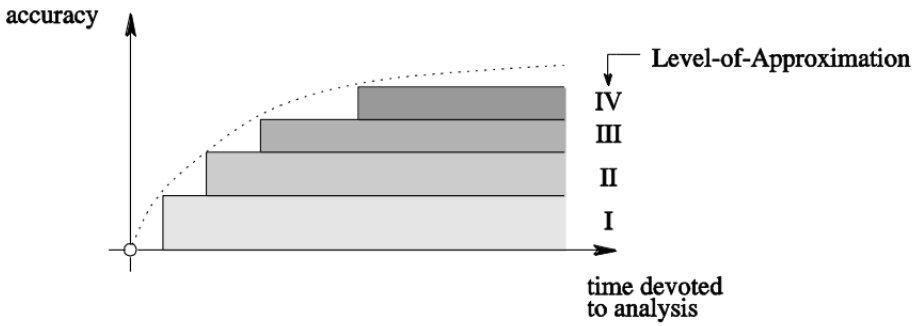

Figure 4.1: Illustration of Levels-of-Approximation [4]

By gradually increasing the LoA mistakes are more easily detected, since the more detailed calculations always can be compared to the simpler ones. Simple calculations are generally more conservative, so by including more detailing the result should be less conservative.

4.2 Design Capacities

Eurocode 2 suggests three different methods for calculation of axially loaded slender columns subjected to buckling. The methods found in Eurocode 2-1-1 (EC2-1-1) and Eurocode 2-2 (EC2-2) are:

- The nominal stiffness method (EC2-1-1, 5.8.7)
- The nominal curvature method (EC2-1-1, 5.8.8)
- The General method (5.8.6 of both EC2-1-1 and EC2-2)

The stiffness and curvature methods both estimate the nominal second order moment based on the curvature of the column. The curvature method estimates the curvature directly while the stiffness method estimates the curvature from a reduced nominal stiffness [10]. The curvature method seems to have the highest degree of mechanics implemented, as the stiffness method tends to be more based on empirical equations obtained from curve fitting. The Partial safety factor (PSF) method is the safety format applied in both methods.

Since the Eurocode is constructed to be conservative, including more detail is expected to *increase* the design capacity. In the LoA-approach described in Section 4.1, the General method is categorized as the highest level as it applied NLFEA. The simplest calculations were done first, and successively more detailing was added as seen in the following list.

1. Nominal stiffness and curvature with constant concrete stress distribution
2. Nominal stiffness and curvature with parabolic concrete stress distribution
3. NLFEA applied to the General method

It is a reasonable assumption that the columns are considered slender after the criteria given in EC2-1-1, 5.8.3.1. No information found in the National Annex was used in the following calculations. In all calculations, the self-weight of the columns was neglected. The design capacities by the nominal stiffness and nominal curvature methods were calculated with Matlab, and the scripts can be seen in the digitally attached appendices. The axial capacity was found at the point where the work diagram of the stiffness/curvature method intersected with the MN-diagram.

4.2.1 Construction of MN-diagrams

As mentioned above, MN-diagrams were needed to determine the capacities from the nominal stiffness- and curvature methods. Two different MN-diagrams with different levels of approximation were constructed.

The cross-sectional resistance for a given axial force and moment is calculated by assuming a strain state in the cross section and demanding strain compatibility and force equilibrium over the entire cross section. This was done in Matlab and the codes can be seen in the digitally attached appendices.

According to EC2-1-1 Section 3.1.7(3), a rectangular stress-strain distribution for concrete

may be used as an approximation to the actual compressive stress distribution. For a first level of approximation design, this was implemented. Furthermore, the tensile capacity of the concrete was neglected. Perfect bonding between the concrete and reinforcement was assumed. Figure 4.2 shows the assumptions made for the cross sectional strains, stresses and forces for an arbitrary cross section.

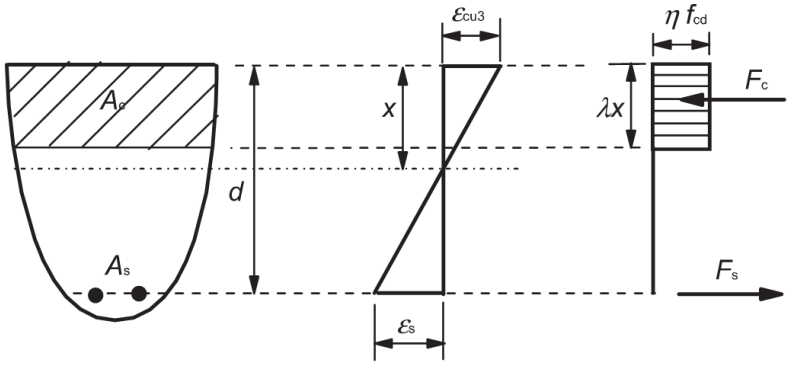

Figure 4.2: Compressive stress distribution approximated by a constant stress block [2]

In Figure 4.2, d is the effective cross sectional height, A_s is the reinforcement area, A_c is the concrete area assumed in compression, x is the distance to the neutral axis from the end of the compression zone, ε_{cu3} is the concrete strain limit, ε_s is the reinforcement strain, λ defines the effective compression zone height, η defines the effective concrete strength, F_c is the compressive force resultant, and F_s is the resultant force from the reinforcement.

As a higher level of approximation, a non-linear representation of the concrete cross sectional stresses was wanted. The parabolic relation in Equation (3.1), shown in Figure 3.1b, was implemented. Figure 4.3 illustrates the parabolic stress distribution over a rectangular cross section for a given strain profile.

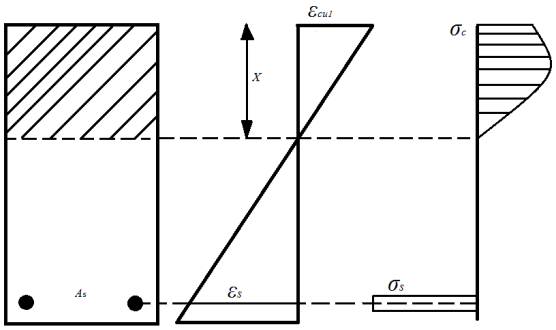

Figure 4.3: Compressive stress distribution approximated by a parabolic function

In Figure 4.3, σ_c is the compressive stress and σ_s is the reinforcement stress.

4.2.2 Method of nominal stiffness

The method based on nominal stiffness increases the design moment and second order moment, using a factor dependent on the nominal stiffness of the slender compression member. There is a simplified approach not applied in this thesis, that uses linear 2^{nd} order analysis while including a reduced stiffness to account for cracking, creep and material non-linearity. The method of nominal stiffness shows good agreement with the exact solution when considering a structure subject to constant first order bending moment, while slightly unsafe results may appear when considering e.g. parabolic moment distributions [10].

4.2.3 Method of nominal curvature

In the method of nominal curvature, a nominal second order moment, M_2, is added to the first order moment, M_{0Ed}. The secondary moment, which is the difference between cross section resistance and the first order moment, is found through the second order deflection e_2. The deflection is dependent upon the curvature $1/r$ and the effective length [10].

4.2.4 The General method

The General method is expected to give the most accurate design capacity as it includes both geometric and material non-linearity. The General method is to be used with an FEA solver running a non-linear analysis. The assumptions made are the following [10]:

- Linear strain distribution
- Equal strains in reinforcement and concrete at the same level
- Stress-strain relationships for concrete and steel

These assumptions seem to be a good approximation to the real behavior when using perfect bond between reinforcement and concrete, as shown in Appendix C. The General method uses the non-linear stress-strain relations for concrete and bi-linear reinforcement relation with post-yielding hardening shown in Figures 3.1b and 3.1c.

The general rules for the non-linear methods are given both in chapter 5.8.6 of EC2-1-1 and EC2-2. These two methods differ in use of safety format:

- Eurocode 2-1-1: Partial safety factor (PSF) method
- Eurocode 2.2: Global resistance factor method (GRFM)

The safety format used in Eurocode 2-1-1 [2] accounts for all types of uncertainties by reducing the material parameters with partial safety factors. They were originally developed for component checks, but can according to the Eurocode 2 also be applied to non-linear analyses. EC2 defines resistance as

$$R = \Theta X_G X_f R_n, \tag{4.1}$$

where Θ, X_G and X_f are random variables of model, geometric and material uncertainties and R_n is the nominal resistance. Hence the variation of resistance becomes

$$V_R = \sqrt{{V_\Theta}^2 + {V_G}^2 + {V_f}^2},$$

where V_Θ, V_G and V_f are the coefficient of variation of model, geometric and material uncertainties respectively.

The values of the partial safety factors are derived according to Equation (4.2) for steel and Equation (4.3) for concrete. The additional factor of 1.15 for concrete accounts for the uncertainty arising from the concrete being tested with specially cured cylinder specimens [10].

$$\gamma_s = e^{(3.04V_R - 1.64V_f)} \tag{4.2}$$

$$\gamma_c = 1.15e^{(3.04V_R - 1.64V_f)} \tag{4.3}$$

By applying the assumed coefficients of variation listed in Table 4.1, the equations result in $\gamma_s = 1.15$ and $\gamma_c = 1.50$. The method is only applicable to calculate the capacity of sections subjected to bending moments and normal forces [10].

	Assumed coefficient of variation	
Type of uncertainty	Steel	Concrete
Model	$V_\Theta = 2.5\%$	$V_m = 5.0\%$
Geometry	$V_G = 5.0\%$	$V_G = 5.0\%$
Material	$V_f = 4.0\%$	$V_f = 15.0\%$

Table 4.1: Coefficients of variation for steel and concrete as recommended in EC2

The design resistance can be calculated as in Equation (4.4). Schlune et al. [15] suggest that this approach leads to use of low material parameters, which might result in unrealistic load

distribution and too conservative design for structures where 2nd order effects influence the structure.

$$R_d = R\left(\frac{f_{ck}}{\gamma_c}, \frac{f_{yk}}{\gamma_s}, a_{nom}\right) \tag{4.4}$$

The safety format of PSF corresponds to the design material set described in Section 3.1.1. Using design values as input to the analysis is assumed to result in the design value of the ultimate load as output. The PSF method satisfies the last of the two basic criteria for a safety format in non-linear analysis [10].

1. It should be possible to use the same set of material parameters in all parts of the member to avoid discontinuities and computational problems.
2. The safety format should be compatible with the general design format based on partial safety factors.

Eurocode 2-2 [16] modifies the safety format used in EC2-1-1. The method is called Global resistance factor method (GRFM), and introduces an overall safety factor. This allows for more realistic material parameters as input to the non-linear calculations [15]. Still, the method is only applicable to cross-sections subjected to bending moment and normal force. Modified values of the yield strength and concrete strength, $\tilde{f}_y$ and $\tilde{f}_c$, as seen in Equations (4.5) and (4.6) should be applied.

$$\tilde{f}_y = 1.1 f_{yk} = 1.27 f_{yd} \tag{4.5}$$

$$\tilde{f}_c = 1.1 \frac{\gamma_s}{\gamma_c} \alpha_{cc} f_{ck} = 1.27 f_{cd} \tag{4.6}$$

The design resistance is found by dividing the resistance by an overall safety factor, γ_O, as shown in Equation (4.7). The factor can be set to 1.27 if model uncertainties are not considered explicitly in the analysis [16].

$$R_d = \frac{R(\tilde{f}_y, \tilde{f}_c, a_{nom})}{\gamma_O} \tag{4.7}$$

4.3 Best estimate evaluation

The goal of a *Best estimate* is to describe the column capacity as realistically as possible, to predict the actual load where the column fails. No conservative assumptions are made in these types of calculations. The calculations of the best estimate were organized after the level of approximation as well, where the most simplified calculations were done first. More detailing

was added gradually. In addition, another aspect called *Level of Knowledge* is relevant to these calculations, as a comparison to some actual realizations of the capacities in the IABSE experiments was possible.

The methods used to calculate the best estimates were like those described in Section 4.2 to calculate the design capacities, though the input was changed from design values to more realistic, expected values. Several new sets of relevant material parameters were proposed, and they are described in Section 3.1.2. Thus, best estimates were created with the EC2 hand calculation methods with nominal stiffness and curvature, as well as a NLFEA solution with DIANA FEA.

4.3.1 Column A

A best estimate for Column A was calculated prior to the calculations of the best estimate of Column B. The MN-diagram using a linear stress distribution, combined with the work diagrams of nominal curvature/stiffness gave a first estimate of the Column A capacity. Secondly the work diagrams were combined with an MN-diagram with non-linear material relations. Then, as for the design calculations, the column was analyzed in DIANA FEA with the three sets of material combinations introduced in Section 3.1.2. The estimates of Column A were done with information only found in codes and with the use of best engineering practice. No conservative assumptions were made, which means the conservative Eurocode methods had to be interpreted extensively.

4.3.2 Column B

Column B was calculated with the same methods as Column A. The difference in these estimates was that the test results of Column A was known, which provided some additional information about the model weaknesses that was used in the analyses of Column B.

The Fib Model Code has the advantage of being applicable to concrete grades up to C120, which also covers the concrete grade of Column B. This is not the case for Eurocode 2, which only covers concrete grades up to C90. The Eurocode material parameters were applied on Column B in material set A and B, by extrapolating equations listed for each parameter. It should be noted that the material equations are quite similar in FIB and in the Eurocode, so using Eurocode 2 material parameters on Column B is assumed to be adequate.

Some remedies were made to give a better estimate of Column B. The following experimental

results of Column B would have said something about the influence of knowledge in such calculations and analyses.

4.4 Non-linear finite element modelling

A non-linear finite element model of the problem was developed through an extensive parametric study using DIANA FEA. For more detailed information about the study the reader is referred to Appendix B. The objective of the study was to create a model that was applicable to the EC2-1-1 General method design and a best estimate of the column response. Furthermore, a model describing a satisfying response with minimum use of CPU costs was established for the probabilistic representation of the problem.

4.4.1 Constitutive model

The constitutive model chosen for concrete was a total strain based crack model, also preferred by the Guidelines for NLFEA [11]. The cracks are continuously rotating with the principal directions of the strain vector, which is a well suited approach for reinforced concrete structures [5]. The crack-bandwidth was determined using the projection method provided by Govindjee [17]. This method takes into account the element size, element aspect ratio and crack orientation.

The recommended tensile behavior was defined by an exponential softening diagram based on the tensile strength and fracture energy, illustrated in Figure 4.4a. This diagram would lead to more localized cracks and consequently avoid large areas of diffuse cracking [11]. Since the Poisson effect of a material disappears when the concrete is in a cracked state, it was reduced by applying a damage based reduction model for the tensile behavior.

For the compressive behavior, the parabolic model in DIANA [18], shown in Figure 4.4b, was applied to achieve the best estimate. The EC2-1-1 [2] parabolic model was used for the General method results, shown in Figure 4.4c. Both models are dependent on the compressive strength and a limit for which the strain softening starts. In the EC2-1-1 model the limit appears at a set strain value, while the other model is based on fracture energy. The softening behavior may lead to a localization of deformations consequently creating a strong mesh dependency. The parabolic model in DIANA avoids this effect by relating the constitutive model to a fracture energy, G_c, and to the geometry of the finite element mesh through an equivalent length, h_{eq}.

This model was the natural choice for a best estimate model. The Poisson ratio and Young's modulus were the basis for the isotropic linear-elastic material model.

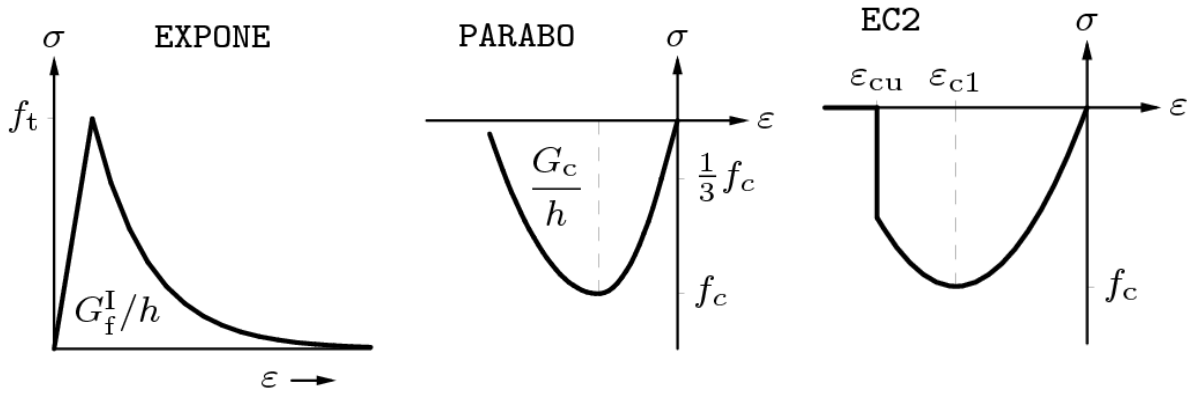

(a) Tensile behavior *(b) Parabolic comp. behavior* *(c) EC2-1-1 comp. behavior*

Figure 4.4: Concrete constitutive model in tension and compression [5]

The compressive strength in cracked concrete is reduced by large tensile strains perpendicular to the principal compressive direction. The model was therefore applied the relation defined by Vecchio and Collins [19] to reduce the strength due to lateral cracking. To avoid excessive reduction that results in an unrealistic response, the minimum reduction coefficient β_σ^{min} was set to 0.4, as recommended in fib Model Code 2010 [4]. The stirrups embedded in the concrete may lead to an increasing lateral confinement and consequently an increase in concrete strength. This effect was neglected in the EC2-1-1 model which was a conservative assumption. Seeking the best estimate, this effect was included to fully understand the non-linear behavior of concrete.

Embedded reinforcement was chosen for both longitudinal reinforcement and stirrups, and Von-Mises plasticity model for reinforcement yielding was applied. A linear elastic model with isotropic hardening, as illustrated in Figure 3.1c, was used. Perfect bond between reinforcement and concrete was assumed in the model. For the platens, a simple linear elastic model for steel was applied.

4.4.2 Geometric model

In total, three basis models of different element types were developed and compared, a 3D structural solid model, a 2D plane stress model and a 2D beam element model. The basis

models were constructed based on experience and available research and recommendations. The measurements coincide with the dimensions shown in Section 2.1. The center of area of the stirrups were assumed to coincide with the center of area of the longitudinal reinforcement where the stirrups and the longitudinal reinforcement intersect. As perfect bond between reinforcement and concrete was assumed, the simplification was considered appropriate.

The 3D structural solid model was built with three solid blocks; one for the column and two for the platens, along with lines describing the longitudinal reinforcement and stirrups. The 3D solid model is illustrated in Figure 4.5a.

The 2D plane stress model included a total of three parts; one to represent the column, and two to represent the loading platens. The parts were assigned a thickness out of the plane To best describe the most likely failure mode of the column, it was assumed that large mid span displacement normal to the weak axis of the cross section was the largest contributor to the column failure, and the shortest cross-sectional edge was therefore the basis of the model. The reinforcement was represented by lines with assigned cross-sectional areas corresponding to the sum of the areas of the reinforcements over the width of the column at a given point on the 2D-plane. The model is shown in Figure 4.5b.

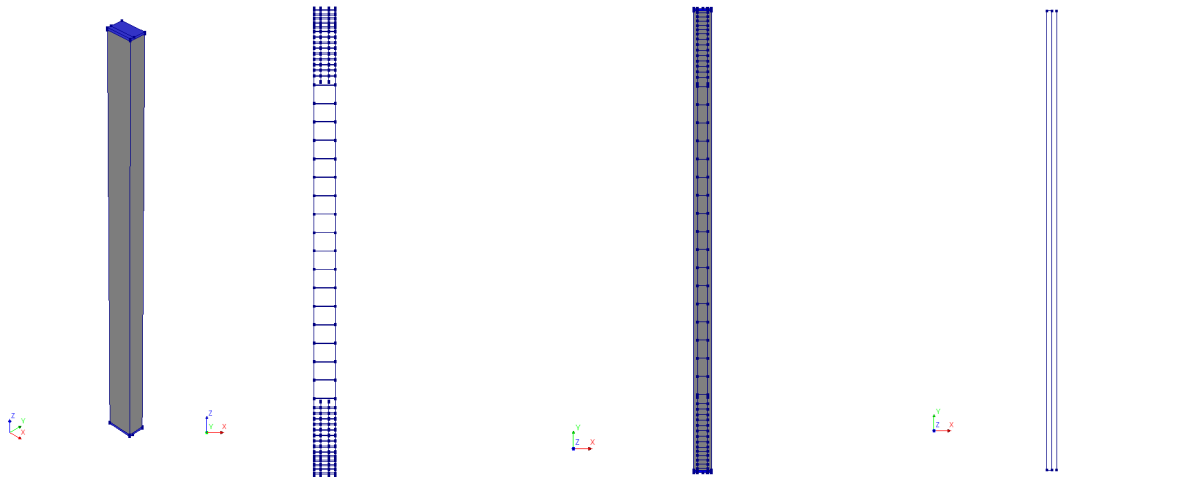

(a) 3D solid model *(b) 2D plane stress model* *(c) 2D beam model*

Figure 4.5: Geometric models for the NLFEA

The 2D beam model consisted of five lines; one at the centroid of the cross section to represent the concrete column, two to represent the reinforcement bars and two lines assigned beam elements, connected to the column line to represent the eccentricity to which the boundary con-

ditions and load were applied. As a simplification, no shear reinforcement was modelled and the inner longitudinal reinforcement bars at the top and bottom of the column were neglected. The lines representing the reinforcement were assigned a cross-sectional area corresponding to the sum of the areas of the reinforcements over the width of the column. A sketch of the model is presented in Figure 4.5c.

4.4.3 Finite element discretization

According to Guidelines of NLFEA [11], elements with quadratic interpolation of the displacement field should be used, and this recommendation was applied to all three basis models. The 3D solid model used twenty-node isoparametric solid brick elements, CHX60, for the concrete and platens. The CHX60 element is based on quadratic interpolation and Gauss integration [5]. Quadratic regular plane stress elements, CQ16M, with a 2x2 integration scheme were chosen for the 2D plane stress model. The beam element chosen was a two-dimensional class-III beam element, CL9BE, with 3x3 integration points in the cross-section. Composed elements CL3CM were utilized to extract bending moments from the column cross section and CQ48I was used for the interface element between two planes in the three-dimensional configuration. All models used embedded reinforcement, which implies that the reinforcement does not have degrees of freedom of its own.

The element size was adapted and tested to increase the accuracy of the models. To avoid a snap-back in the stress-strain relationship of the constitutive model, the maximum element size should be approximately half of the maximum equivalent length [11], which is defined as

$$h_{eq} < \frac{EG_F}{{f_{ct}}^2}.$$

According to Guidelines for NLFEA [11], to achieve a relatively smooth stress field, the maximum element size of a beam structure should be limited by Equation (4.8).

$$h_{max} = min\Big(\frac{l}{50}, \frac{h}{5}, \frac{b}{5}\Big) \tag{4.8}$$

4.4.4 Boundary conditions and load application

In Section 2.2, it was shown that the support and load was applied as a line along the width of the column with an eccentricity of 40 mm. To model this, a line load was applied as well

as a line of support to the 3D model. The load was replaced by an equivalent prescribed displacement of 10 mm to use the method of displacement control instead of force control. This is considered a more stable method and is applicable for problems with only one acting load.

The load and support were applied on the steel platens at each end of the column. To reduce the local stress concentrations, a no-tension interface between the concrete and platens was applied. The purpose of the interface was to simulate possible gaping between column and platen. To achieve a stiff interface the normal stiffness, D_{SN}, was set as in Equation (4.9), dependent on the elastic modulus and concrete element size, h_c. The stiffness was completely reduced if an opening was detected.

$$D_{SN} = 1000\frac{E_c}{h_c} \tag{4.9}$$

As mentioned in Section 2.1, the inner longitudinal reinforcement of 600 mm was welded to the platens. This effect was simulated by dividing the interface surface such that the areas around these bars were fully embedded to the plate and not affected by the interface properties. A simple tension test of the model was done to verify the behavior of the column-platen interaction by detecting gaping at all areas affected by the interface. The results of the tension test can be found in Appendix B. In the beam and plane stress models, there was no interface, and the load was modelled as a point force.

To reduce the finite element model, exploiting the symmetry of the problem and the load application was considered. A model with one symmetry plane at mid-length of the column was compared to the total model. The use of a symmetry model may reduce the computational costs, but requires a symmetric failure mode and must be carefully investigated [11].

4.4.5 Analysis

A structural non-linear analysis was run with non-linear elasticity, plasticity, total strain based cracking and interface non-linear behavior. Geometric non-linearity was included adopting a Total Lagrange description where strain and stress measures are defined with reference to the undeformed geometry. The system of equations was solved using Sparse-Cholseky.

The load step size was defined explicitly and kept constant throughout the analysis. The parametric study resulted in a load step size of 0.003 with a total of 180 steps giving a total load

factor of 0.54 or a 5.4 mm prescribed deformation. Regular Newton-Raphson iteration was applied to solve the equilibrium equations, an effective method that may exhibit a quadratic rate of convergence [20]. Still, the process can be time consuming since the decomposition of the stiffness matrix must be performed at every iteration. To avoid a large number of iterations, but still achieving convergence at roughly all steps, a maximum of 50 iterations was set. As mentioned previously, displacement control was a proper choice for this type of problem. Therefore, a convergence norm based on displacement with a criterion of 0.001 was applied to stop the iteration process if the results were satisfactory. Furthermore, a displacement-norm should not be used alone [11], so an energy-norm with a relatively strict criterion of 0.0001 was added as well.

The two translations extracted from the analyses were the longitudinal displacement at the top of the column and the lateral displacement at mid-length. The forces were collected and summed at the support to project the axial force in the column. The bending moment was collected from the composed line for the 2D plane stress and 3D models.

5 Structural reliability methods

A probabilistic representation of the problem was developed and a study was performed using several reliability analysis methods. These methods were tested for different sensitivities to find weaknesses and limitations. The reliability analyses were initially assessed analytically before non-linear finite element reliability analyses were conducted.

The Eurocode reliability level was tested through the various reliability methods. In this context, testing the safety format in EC2 means checking whether the capacity found in EC2 results in $\beta > 3.8$. The EC2 capacity was set as the nominal curvature capacity described in Section 4.2, divided by the partial safety factor for dominating self-weight.

The design methods in Section 4.2 were done with a semi-probabilistic approach where the reliability level is not explicitly dealt with. To find the design points where the reliability index is exactly 3.8, an inverse approach was made. The value of 3.8 is the 50-year reliability index [14], and is the *target reliability index* for inverse analyses. This was done by varying the mean value of the load until the reliability index was sufficiently close to the target reliability index, β_T. A target β within the interval $\beta_t \pm 0.05$ was assumed to be sufficiently accurate for the NLFEA assessments. For the analytic assessments, the target β was found within $\beta_t \pm 0.005$

First the reliability studies were focused on Column A and B. Later the studies were extended to include several column setups, with ambition to spot trends in the design points and safety factors for a given safety level.

5.1 The limit state

The main objective of a reliability analysis in structural engineering is to ensure that the estimated probability of failure of the structure is below a certain target value. The classic solution to this problem is to define a Limit state function (LSF) given as $G = R - S$, where R is the resistance and S is the load action. The variables R and S are uncertain, and are often assigned appropriate probability density functions. Once these functions are known, the probability of failure, $P(G \leqslant 0)$, can be calculated. In many real-life engineering problems, however, the LSF may not be explicitly defined, and approximate methods are needed.

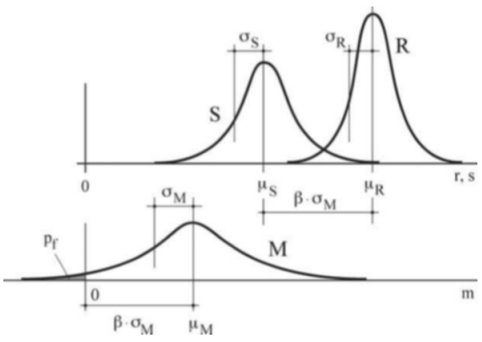

Figure 5.1: Probability density function of resistance, load and safety margin [6]

The limit state can also be expressed as the safety margin $M = R - S$, as shown in Figure 5.1. The method developed by Basler [21] and presented in the notation of Cornell [22], can be used to find the exact probability of failure assuming the variables are normally distributed. If the resistance and load are normally distributed, so is the safety margin, and all variables can be introduced by their mean and standard deviation only. The mean and standard deviation of the safety margin, μ_M and σ_M, can now be represented by the mean and standard deviation of the resistance, μ_R and σ_R, and load, μ_S and σ_S, as in Equations (5.1) and (5.2). In these equations, it is assumed that R and S are uncorrelated.

$$\mu_M = \mu_R - \mu_S \tag{5.1}$$

$$\sigma_M = \sqrt{{\sigma_R}^2 + {\sigma_S}^2} \tag{5.2}$$

The reliability index, β, is determined as in Equation (5.3), and the probability of failure, P_f, can be read from standard normal distribution tables as in Equation (5.4).

$$\beta = \frac{\mu_M}{\sigma_M} \tag{5.3}$$

$$P_f = \Phi(-\beta) \tag{5.4}$$

Furthermore, Hasofer and Lind [23] suggest transforming the basic variables and the limit state to the standard normal space, and define the reliability index as

$$\beta = min_{g=0}\sqrt{\mathbf{u}^T\mathbf{u}},$$

where u is the realization of the random variable U, in standard normal space. The results from this method can be shown to be invariant to the definition of the LSF. The random variables representing the column resistance, f_c, f_y and E_c, were assumed to be lognormally distributed. They would require a transformation to the standard normal space as suggested in the

Hasofer/Lind method to follow the procedures suggested by Basler/Cornell mentioned earlier. The transformation between lognormal and standard normal space are shown in Equations (5.5) and (5.6).

$$U(x) = \frac{ln(x) - \mu_{ln}}{\sigma_{ln}} \tag{5.5}$$

$$X(u) = exp(u\sigma_{ln} + \mu_{ln}) \tag{5.6}$$

where the lognormal mean, μ_{ln}, and lognormal standard deviation, σ_{ln}, are given as

$$\mu_{ln} = ln\left(\mu_x{}^2\sqrt{\frac{1}{\sigma_x{}^2 + \mu_x^2}}\right), \qquad \sigma_{ln} = \sqrt{ln(V_x{}^2 + 1)}$$

The random variables representing the load, e and N, were assumed to have normal distributions. The transformation between normal space and standard normal space are given by Equations (5.7) and (5.8).

$$U(x) = \frac{x - \mu_x}{\sigma_x} \tag{5.7}$$

$$X(u) = u\sigma_x + \mu_x \tag{5.8}$$

5.2 Reliability methods

Several reliability methods were tested to evaluate the different methods abilities to ensure a sufficient estimation of the safety level. The accuracy of the reliability analysis is considered to increase by adding more random variables. Introducing a random variable to the problem introduces more uncertainty to the analysis, but increases the confidence in the results. All reliability methods tested in this thesis started off with only two random variables, then the random variables were introduced in turn to verify the assumption of increasing accuracy.

5.2.1 Monte Carlo

The Monte Carlo (MC) method is considered the most accurate of the methods that will be presented, given that the physical model of the problem is accurate. The Monte Carlo simulation technique is based on a series of analyses, each with random realizations of the stochastic variables **X**. The probability of failure is simply the number of failures divided by the number

of simulations. The coefficient of variation of the failure probability, V_{Pf}, can be approximated by

$$V_{Pf} \approx \frac{1}{\sqrt{zP_f}},$$

where z is the number of simulations and P_f is the probability of failure [6]. The reliability index was calculated using the inverse of the normal cumulative distribution $\beta = \Phi^{-1}(P_f)$.

In structural reliability problems, where low probabilities of failure and coefficients of variation are sought, a large number of simulations are needed to cover the tail region of the distributions. Running 10^7 simulations is considered enough to achieve this accuracy [6].

5.2.2 FORM

The First order reliability method (FORM) used in this thesis is an extension of the Hasofer/Lind method which includes several variables and non-linear limit state functions. The Limit state function is linearized by using only the linear terms in a Taylor series expansion around a certain point x_i. The LSF will then be on the form

$$G = a_0 + \sum_{i=1}^{n} a_i X_i, \tag{5.9}$$

where n is the number of random variables and a_i is a set of constants. The further iteration process is as follows:

1. Approximate the limit state function $G = G(X_1, X_2, ..X_n)$ by Equation (5.9).
2. Determine $a_i = \frac{\partial G}{\partial X_i}|*$ and $a_0 = G(x_i*) - \sum_{i=1}^{n} a_i x_i*$
3. Estimate x_i^*.
4. Calculate the mean and standard deviation of G.
5. Calculate the sensitivity factors α_i, the reliability index, β, and the next design point.
6. Control convergence by $\varepsilon_{FORM} = \sqrt{\sum_{i=1}^{n}(x_{i,j} - x_{i,j-1})^2}$, where j is the iteration number.
7. Calculate P_f if convergence is reached, else return to 3 with the new design point.

* refers to the design point. A more detailed explanation of the FORM iterative scheme is found in Schneider [6].

5.2.3 SORM

In the Second order reliability method (SORM) second order terms are included in the Taylor expansion used to approximate the LSF. This provides a second order adaption to the limit state, which can be necessary when the limit state is highly non-linear.

The design points and reliability index are found through the same iteration process as described for FORM. The difference occurs when extracting the probability of failure. For one variable, the probability of failure is defined as the filled area in the density function separated by the design point, as seen in Figure 5.2a. Expanding to more variables, it is slightly more complex. The difference between FORM and SORM can be illustrated for two stochastic variables. The probability of failure will in this case be the volume of the joint density function separated by the limit state function in Figure 5.2b. The SORM probability of failure is shown with hatching, which can be seen adjusts better to the limit state than FORM.

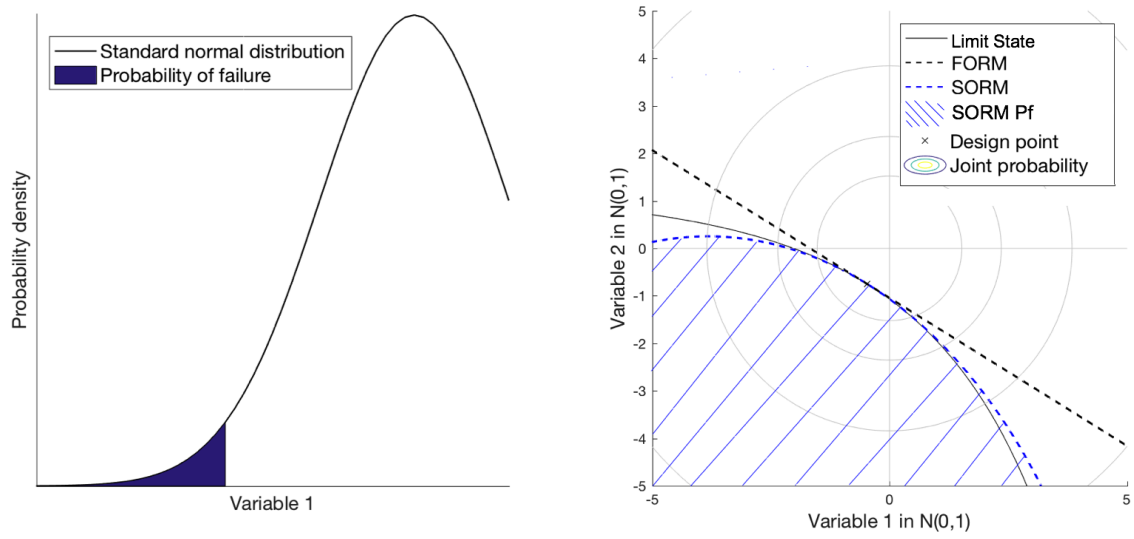

(a) One random variable *(b) Two random variables*

Figure 5.2: Graphic illustration of probability of failure-estimates for FORM and SORM

SORM adapts slightly better to non-linear limit states, and is expected to give a somewhat more precise probability of failure than FORM. There can still appear situations where this is not the case. As seen in Figure 5.3, the FORM adaption may lead to a more accurate approximation than SORM due to the highly alternating LS.

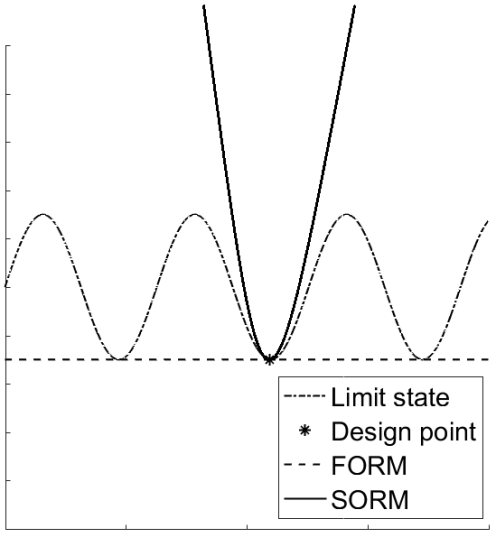

Figure 5.3: FORM and SORM adaption to highly alternating limit state

There exists an exact formula to calculate the SORM probability of failure based on a reliability index from FORM, but due to time limitations a simplified method was implemented, valid for small probabilities of failure. In this approach, $\Phi(-\beta)$ is multiplied by a SORM-factor, ζ [24], which is shown in Equation (5.10) below.

$$\zeta = \prod_{i=1}^{n}(1-\beta\kappa_i)^{-\frac{1}{2}} = (\det[(\mathbf{I}_n - \mathbf{P})\widetilde{\boldsymbol{H}}(\mathbf{I}_n - \mathbf{P}) + \mathbf{P}])^{-\frac{1}{2}} \tag{5.10}$$

where n is the number of random variables, $\mathbf{I}_n$ is an n-by-n identity matrix, κ_i is the curvature, and $\mathbf{P}$ and $\widetilde{\boldsymbol{H}}$ are defined in terms of the gradient $\nabla g(\mathbf{u}^*)$ and the Hessian $\nabla^2 g(\mathbf{u}^*)$ by

$$\mathbf{P} = \frac{\nabla g(\mathbf{u}^*)\nabla g(\mathbf{u}^*)^T}{|\nabla g(\mathbf{u}^*)|^2} \qquad\qquad \widetilde{\boldsymbol{H}} = \mathbf{I}_n + \beta\frac{\nabla^2 g(\mathbf{u}^*)}{|\nabla g(\mathbf{u}^*)|}.$$

The final probability of failure from SORM is shown in Equation (5.11). For simplicity when reporting the results, an equivalent reliability index, β_{eq}, is back calculated from the probability of failure as shown in Equation (5.12).

$$P_f = \Phi(-\beta)\zeta \tag{5.11}$$

$$\beta_{eq} = \Phi^{-1}(P_f) \tag{5.12}$$

To show how the SORM solution adapts to the limit state, second order terms are added to the FORM LSF approximation given in Equation (5.9):

$$G \approx G(x_i{}^*) - \sum_{i=1}^{n} x_i{}^* \frac{\partial G}{\partial X_i}|^* + \sum_{i=1}^{n} X_i \frac{\partial G}{\partial X_i}|^* + \frac{1}{2}\sum_{i=1}^{n} (X_i - x_i{}^*)^2 \frac{\partial^2 G}{\partial X_i^2}|^*$$

where * refers to the design point. Introducing and collecting constants

$$a_i = \frac{\partial G}{\partial X_i}|^*, \qquad b_i = \frac{1}{2}\frac{\partial^2 G}{\partial X_i^2}|^*, \qquad a_0 = G(x_i{}^*) - \sum_{i=1}^{n} x_i{}^* a_i + \sum_{i=1}^{n} x_i{}^{*2} b_i,$$

yields the SORM LSF as

$$G = a_0 + \sum_{i=1}^{n} X_i a_i - 2\sum_{i=1}^{n} X_i x_i{}^* b_i + \sum_{i=1}^{n} X_i^2 b_i.$$

The FORM- and SORM-algorithms were implemented in Matlab scripts. To validate the algorithms, they were tested against the commercial software COMREL, which is a program in the STRUREL software package [25], for several limit state functions with varying number of random variables. The results are given in Appendix D.

5.2.4 RSM

The Response surface method (RSM) approximates the limit state function $g(\mathbf{x})$ by a polynomial function $\widetilde{g}(\mathbf{x})$, dependent on the stochastic variables $\mathbf{X}$ under consideration. The method is effective in problems where a closed-form mechanical model of the response is unavailable. An example of such a situation can be when considering a numerical NLFE model. Several sample points that are realizations of the stochastic variables $\mathbf{X}$ are used as input in e.g. a finite element code, which generates the response for a certain set of realizations of $\mathbf{X}$. The classic RSM-approach suggested by Bucher and Bourgund [26] is based on a second order polynomial without cross terms given as

$$\widetilde{g}(\mathbf{x}) = a + \sum_{i=1}^{n} b_i x_i + \sum_{i=1}^{n} c_i x_i^2, \tag{5.13}$$

where n is the number of random variables. When using matrix notation, Equation (5.13) becomes

$$\widetilde{g}(\mathbf{x}) = \mathbf{Ab},$$

where $\mathbf{A} = [1, x_1, x_2, x_1^2, x_2^2]$ and the vector of undetermined coefficients is $\mathbf{b}^T = [a, b_1, b_2, c_1, c_2]$ when considering only 2 stochastic variables. To obtain the constants, $2n+1$ experiments have to be conducted [27].

The accuracy of the Response surface (RS) may be improved by introducing cross-terms [26] as follows,

$$\widetilde{g}(\mathbf{x}) = a + \sum_{i=1}^{n} b_i x_i + \sum_{i=1}^{n} \sum_{j \geq i=1}^{n} c_{ij} x_i x_j. \tag{5.14}$$

This increase of accuracy requires the number of experiments to rise to $0.5(n+1)(n+2)$.

The sampling points x_i should according to Bucher and Bourgund be chosen to be the mean values $\bar{x}_i$ and $x_i = \bar{x}_i \pm f_i \sigma_i$, where f_i is an arbitrary factor. When the sample space is saturated, that is when the number of sample points equals the number of paramaters in the response surface, the undetermined coefficients are found by $\mathbf{b} = \mathbf{A}^{-1}\mathbf{g}$. Where $\mathbf{g}$ is a vector containing realizations of the capacity/limit state. For an over-saturated sample space, a least squares approach may be used to find $\mathbf{b}$ by Equation (5.15) [28].

$$\mathbf{b} = (\mathbf{A}^T\mathbf{A})^{-1}\mathbf{A}^T\mathbf{g} \tag{5.15}$$

Lack of correlation added to the parameters of the $\mathbf{b}$-vector, may result in a highly sensitive RS. The correlation of the parameters of the $\mathbf{b}$-vector was not added in this thesis, but could have been considered in the analysis by modifying the polynomial form of the RS by a correction factor. Instead of using a polynomial based on only the spatial averages of the parameters in the $\mathbf{b}$-vector, a polynomial which includes both spatial average and global deviations can be used such that the correlations are included [29].

5.2.5 RSM-FORM/SORM

The RSM was used in conjunction with FORM and SORM to form an iterative response surface approach. The iterative procedure was as follows:

1. A RS is generated based on the initial starting points for the random variables
2. Design points and β are found using FORM and SORM with the RS as input.
3. Check for convergence: $\varepsilon_{RSM} = \sqrt{\beta_{i+1}^2 - \beta_i^2}$
4. If convergence is achieved, the RSM-iterations are stopped, else the updated design points are used as the centre of the sampling grid in the generation of the next RS.

The iteration scheme aims at moving the design points closer and closer to the actual limit state $g(\mathbf{x}) = 0$ for every RSM-iteration. The combination of the RSM and FORM/SORM were used in both analytic and NLFEA reliability assessment.

The convergence criterion was set to 0.01 for the RSM, while the convergence criteria for analytic FORM and FORM with NLFEA were set to 10^{-6} and 10^{-4} respectively. The probability of failure was calculated using both FORM and SORM when the RSM-iterations converged. The cross terms were included using Equation (5.14) when two random variables were considered. Due to the increase in number of analyses when using cross terms, a second order response surface *without* cross terms, Equation (5.13), was adopted when more than two random variables were considered.

5.3 Reliability assessment methods with an analytic approach

Analytic solutions to the reliability problem were found to verify the methods and their accuracy, as well to give an indication of the expected design point of the NLFEA solution. The comparison between the analytic and NLFEA methods were in addition expected to give a hint of the necessity of NLFEA assessment.

Until this point, the analytic response capacities have been determined as the intersection point between the MN-diagram and work-diagram, both developed through an iterative scheme with interpolation between points. This approach is only compatible with the methods of MC, RSM-FORM and RSM-SORM. It should be mentioned that only the constant concrete stress-strain definition given in Section 4.2.1 was used as this decreased computation time dramatically. For consistency in the reliability methods, the work diagram was changed to an equation based on the governing differential equation that can be used both iteratively and in a closed-form solution. The difference between this solution and the nominal stiffness and curvature methods is shown in Figure 5.4. It resulted in a slightly higher capacity, but was considered acceptable.

The Monte Carlo method was only used as a reference point to the correct P_f for the analytic assessments. Simulations were run with both 2 and 5 random variables. When using the Monte Carlo method, the resistance with respect to the axial force in the column was recorded for all the analyses and stored in a response vector. The resistances in the response vector were then compared to the load N, and the number of failures were counted.

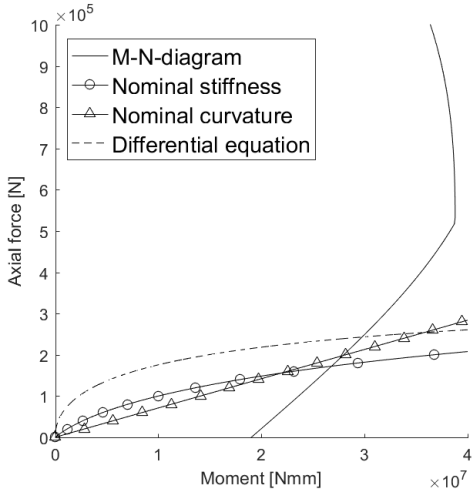

Figure 5.4: Closed form work diagram compared to nominal stiffness and curvature

To simply apply the FORM and SORM analysis, a closed-form limit state equation is required. For this case study, two limit state equations can be developed, distinguishing between the two expected failure modes of the column. The development of these two limit states is intricate and requires the use of Matlab's solve-function in conjunction with symbolic functions. This process is computationally demanding and therefore not applicable to MC simulations. The development of the closed-form limit states is further described in Section 5.3.1.

Another interesting aspect was the effect on the reliability when introducing more random variables. Analyses with both FORM and RSM-FORM for 2, 3, 4 and 5 random variables were conducted.

5.3.1 Closed-form limit state

The failure of columns is mainly governed by two failure modes; yielding of the reinforcement combined with buckling, and compression failure of the concrete. For slender columns, the second order effects are large, and the failure mode is usually governed by yielding of the reinforcement combined with buckling, further referred to as yield failure. For non-slender columns however, the second order moment in the column is small compared to the axial force and first order moment, and the failure is governed by concrete compressive failure. Two limit states, one for compression failure and one for yield failure, were developed to fully represent the problem. The MN-diagram was divided into one equation for each failure mode, then combined with the work-diagram to find two intersection points representing the limit states, illustrated in Figure 5.5.

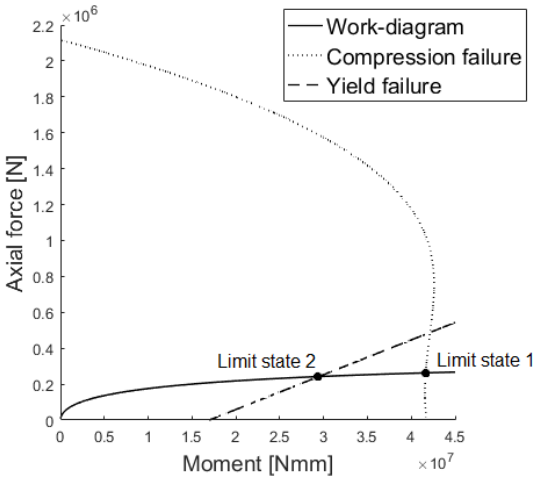

Figure 5.5: Work diagram and divided MN-diagram for the closed-form analytic solution

The work diagram was found through the governing differential equation for Euler buckling (5.16) with an additional moment due to eccentricity.

$$EI\frac{d^2u_2}{dx^2} + Nu_2 = 0 \tag{5.16}$$

The resulting horizontal displacement of the column as a function of the position, x, is shown in Equation (5.17). Further derivation can be found in Appendix E.

$$u_2 = \left(\frac{1 - cos\sqrt{\frac{N}{EI}}l}{sin\sqrt{\frac{N}{EI}}l} sin\sqrt{\frac{N}{EI}}x + cos\sqrt{\frac{N}{EI}}x - 1\right)e \tag{5.17}$$

The bending moment could now be expressed as a function of the axial force $M_{work} = Nu_2$.

The expression representing the compression failure in the MN-diagram was developed under the assumption that the strain at the top of the cross-section was constant and set as the ultimate strain, ε_{cu3}, defined by EC2-1-1. Equations for the bending moment and axial force, Equations (5.18) and (5.19), were developed as functions of the strain in the bottom reinforcement using Figure 5.6. It was assumed no yielding of the reinforcement, even if the reinforcement strain was larger than the yield strain.

$$N(\varepsilon_{s2}) = N_c + N_{s1} + N_{s2} = 0.8\alpha d b f_c + \varepsilon_{cu3}\frac{\alpha d - c}{\alpha d}\frac{E_s A_s}{2} + \varepsilon_{s2}\frac{E_s A_s}{2} \tag{5.18}$$

$$M(\varepsilon_{s2}) = N_c\left(\frac{h}{2} - \frac{0.8\alpha d}{2}\right) + (N_{s1} - N_{s2})\frac{h'}{2} \tag{5.19}$$

where

$$\alpha = \frac{\varepsilon_{cu3}}{\varepsilon_{cu3} - \varepsilon_{s2}}.$$

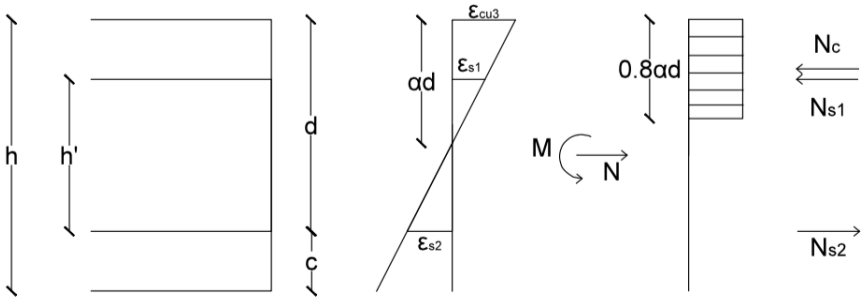

Figure 5.6: Strain state for compression part of the MN-diagram

Solving Equation (5.18) for the strain in the bottom reinforcement, ε_{s2}, and substituting ε_{s2} into Equation (5.19), gives an expression for the bending moment as a function of the axial force, $M_{comp} = M_{comp}(N)$.

A simplification was made for the part of the MN-diagram representing the yield failure. The curve was assumed to be linear, running through the point of full tension in the cross-section and the point of compression failure combined with double yield strain in the bottom reinforcement, see Figure 5.7. In the first point, there is no bending moment present and the axial force can be represented as $N_1 = -f_y A_s$. The axial force and bending moment in the second point are defined as in Equations (5.20) and (5.21).

$$N_2 = N_c + N_{s1} + N_{s2} = 0.8\alpha d b f_c + \varepsilon_{cu3}\frac{\alpha d - c}{\alpha d}\frac{E_s A_s}{2} - \frac{fyA_s}{2} \tag{5.20}$$

$$M_2 = N_c\left(\frac{h}{2} - \frac{0.8\alpha d}{2}\right) + (N_{s1} - N_{s2})\frac{h'}{2} \tag{5.21}$$

where

$$\alpha = \frac{\varepsilon_{cu3}}{\varepsilon_{cu3} - 2\varepsilon_y}.$$

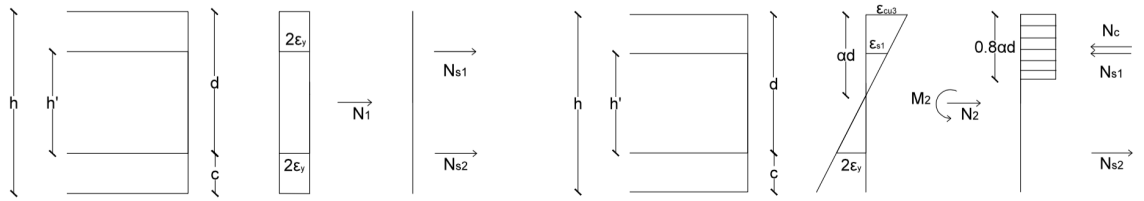

(a) First point of yield curve *(b) Second point of yield curve*

Figure 5.7: Strain states for the yield part of the MN-diagram

The resulting yield curve becomes

$$M_{yield} = \frac{N - N_1}{N_2 - N_1} M_2.$$

The two limit state functions defined by the intersection points of the MN-diagram and work diagram were then represented by $G_1 = M_{comp} - M_{work} = 0$ and $G_2 = M_{yield} - M_{work} = 0$.

5.3.2 RS limit state

When computing the RSM-FORM and RSM-SORM results, care was taken to find a RS that sufficiently described both closed-form limit states. This was more easily controlled when using only 2 random variables, f_c and f_y, as they are the governing parameters regarding the failure modes. The RSM methods were tested for load levels expected to result in either yield or compression failure. The RS was expected to be highly sensitive to changes in the sample points, both in the choice of starting point and f-factor. A study taking these two aspects into account was conducted with RSM-FORM. Another reason for the sensitivity might be the lack of added correlation between the parameters in the **b**-vector, as mentioned in Section 5.2.4, but was not studied further in this thesis.

The exact position of the transition between yield failure and compression failure is uncertain. Using a well-guessed sample point with a small f-factor may be necessary to avoid one failure mode affecting the other, as illustrated in Figure 5.8. In this case, the load applied yields compression failure. As seen, this is only achieved in a satisfying manner when the intial sample points are moved closer to the assumed design point.

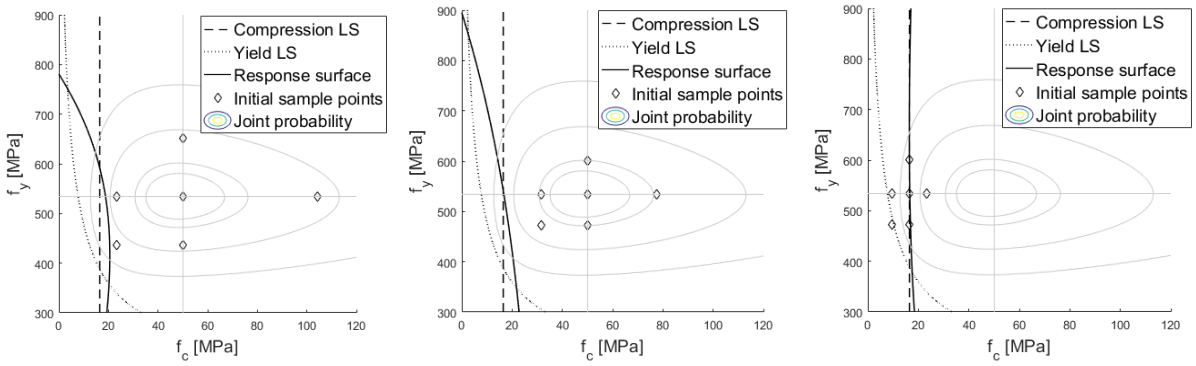

(a) Mean sample points and f=5.0

(b) Mean sample points and f=3.0

(c) Adjusted sample points and f=3.0

Figure 5.8: RS sensitivity due to choice of initial sample points

5.3.3 System reliability

In the case of the closed-form analytic assessment of the problem, two limit states were developed and system reliability needed to be considered. As the column will fail when either of the two limit state functions given from the two failure modes are smaller than zero, it is a series system. The failure domain of a series system, Ω_F, is given by Equation (5.22). The probability of failure, P_{fsys}, can be approximated by Eq. (5.23), where Φ_n is the n-dimensional cumulative standard normal distribution, **B** is a vector with the βs for the two limit state functions calculated from FORM, and **R** is the correlation coefficient matrix. The correlation coefficients in **R** can be approximated by Eq. (5.24), where $\mathbf{A}_i$ is a vector with the sensitivity factors from the FORM analysis for limit state i and n is the number of limit states under consideration. This correlation is then an approximation of the correlation between component failure events [30].

$$\Omega_F = \bigcup_{i=1}^{n} \{g_i(\mathbf{x}) \leqslant 0\} \tag{5.22}$$

$$P_{fsys} = 1 - \Phi_n(\mathbf{B}, \mathbf{R}) \tag{5.23}$$

$$\rho_{ij} = \mathbf{A}_i \mathbf{A}_j^T, i = 1, 2, ..., n; j = 1, 2, ..., n \tag{5.24}$$

To compare the closed form analytic assessments to the other methods in terms of β, a system reliability index, β_{sys}, was back calculated from the system probability of failure as

$$\beta_{sys} = \Phi^{-1}(P_{fsys}).$$

5.4 Reliabilty assessment methods with NLFEA

The NLFEA solution has some drawbacks compared to the analytic solutions. An explicit distinction between yield failure and compression failure mode is difficult to find, and each finite element analysis is time consuming. The LSF needs to be approximated through an efficient reliability method that is flexible towards non-linearities and requires as few analyses as possible. The method considered to be the most adequate was the Response surface method in combination with FORM and SORM. The inverse NLFEA assessments were only performed with RSM-FORM. A full Monte Carlo simulation was not possible due to computational time, and FORM alone was not possible due to the requirement of a closed form solution. However, to validate the Response Surface from non-linear reliability assessments, a small sample Monte

Carlo analysis was performed around the response surface close to the design points. A probability of failure could not be attained from these analyses, only the pattern of the RS could be compared.

For each RSM iteration, one NLFEA was run in each of the sample points. The final solution uses all sample points to interpolate the limit state, which means picking adequate starting points both reduced computational time and increased the quality of the RS-shape. The capacity sensitivity factors were expected to be positive, while the load sensitivity factors were expected to be negative. This information combined with engineering judgment was used to pick good starting points.

A good and efficient NLFE model was needed to find the response surface. The reader is referred to Section 4.4 and Appendix B for the development of these models. The 2D plane stress model was implemented with a few adjustments. Due to the total eccentricity being a random variable, the loading platen had to be extended to have a mesh to connect the load to in the cases where the total eccentricity exceeded the physical cross-section of the column. The stiffness of the platen was also increased by a factor of five to avoid excessive deformation at the point of load application. The load step size was increased to reduce analysis time.

The DIANA model was implemented with material set A, which is the insitu-adjusted 50%-fractile values described in 3.1.2 and summarized in Table 3.2. The axial capacities were extracted at the maximum force that could be applied to the column, rather than the maximum moment. The reason for this is that failure of columns is dependent on the axial load, and the moment is present only because of the axial force. The failure criterion is illustrated in Figure 5.9. Figure 5.9a shows the extracted capacity when a descending branch is present, which is the case for Column A with material set A. Figure 5.9b shows how the capacity is extracted without a descending branch, which is a likely case in the inverse analyses where the eccentricity is increased and the concrete stiffness decreased. This first case deviates from the analytic assessments, where the ultimate capacities were extracted at the intersection between the work diagram and the MN-diagram.

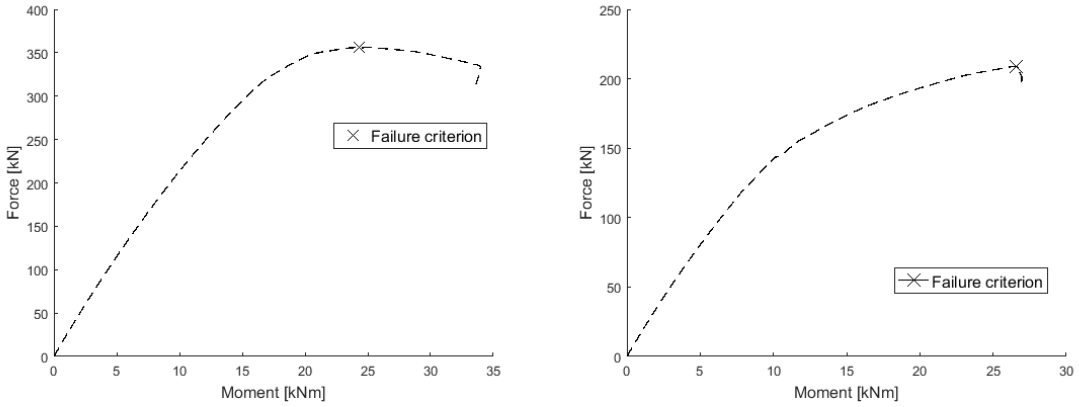

(a) Descending branch and failure criterion

(b) No descending branch and failure criterion

Figure 5.9: Failure criterion used in NLFEA

To increase the extent of the reliability study, analyses were run on a wider range of columns. These studies were run inversely to find the design points for the target reliability index, as well as directly to check the validity of the EC2 safety format for the different column setups. The nominal curvature capacity was used for all new column setups when the EC2 safety format was checked.

5.4.1 Concrete grade study

Several other concrete grades were tested to investigate the effect of the concrete grade. Analyses of C20, C30, (C45), C60, C80 and (C100) were conducted, where the concrete grades in parentheses correspond to Column A and B. The same column geometry and reinforcement layout was used.

Strauss et al. [31] found that for concrete grades lower than or equal to C30 the correlation coefficient between f_c and E_c can be assumed as 0.4, while it is assumed 0 for grades higher than C30. Correlation in f_c and E_c was therefore included for C20 and C30. As a side study, the effect of correlation was investigated. C20 and C30 were analyzed using no correlation, and a study testing the effect of including a correlation coefficient of 0.4 between f_c and E_c to all the concrete grades was performed.

Correlated random variables were first standardized to a space referred to as Y-space, by Equation (5.5) or (5.7), and were further transformed to a standard space in which the variables are uncorrelated, called U-space, by Equation (5.25). The transformation matrix to Y-space is

given by Equation (5.26). **Y** is a vector of the standardized variables in Y-space and $\boldsymbol{\rho}$ is the correlation coefficient matrix. **T** is found by Cholesky factorization [32].

$$\mathbf{Y} = \mathbf{TU} \tag{5.25}$$

$$\mathbf{TT}^T = \boldsymbol{\rho} \tag{5.26}$$

5.4.2 Slenderness study

A slenderness study was done by varying the length of the column. The cross section and reinforcement layout was not changed, and the concrete grade was set to C45. Table 5.1 shows the lengths that were included, and the corresponding slenderness ratios, λ. The slenderness ratio is calculated as

$$\lambda = \frac{\sqrt{12}l}{h},$$

where l is the column length and h is the shortest cross sectional edge [2].

Length [mm]	1500	2000	2500	3000	3500	4000	4500
λ	34.6	46.2	57.7	69.3	80.8	92.4	103.9

Table 5.1: Column lengths and corresponding slenderness ratios for the slenderness study

The standard deviation of the eccentricity is dependent on the column length. The total eccentricity used to find the design load was changed as the column lengths were changed. For the reliability assessments, the mean of the eccentricity was unchanged, but the standard deviation was increased with increasing column length.

5.5 Method for deriving PSF

Using the design points, f_{cd}, f_{yd}, E_{cd} and N_d, found through the inverse analyses, new safety factors were proposed. Since the reference for the safety factor calculations vary, they are listed in Table 5.2 with the safety factor abbreviations, how they were calculated and the value given in the Eurocode. Since the load was entirely assumed to originate from self-weight, the safety factor is calculated from the nominal load value, which is assumed to correspond to a mean value of the load. The nominal load is thus corresponding to the mean capacity from the inverse analyses. Note that material set A is used in the reliability analyses, and therefore the $E_{cm,is}$ from Table 3.2 is used.

	Concrete Strength	Yield Strength	Youngs Modulus	Axial Capacity
Abbreviation	γ_c	γ_s	γ_{CE}	γ_G
Reference	Characteristic	Characteristic	Mean	Nominal
Calculation	f_{ck}/f_{cd}	f_{yk}/f_{yd}	$E_{cm,is}/E_{cd}$	N_{Ed}/N_{Nom}
EC2 value	1.50	1.15	1.20	1.35

Table 5.2: Approach to calculate PSFs for the random variables

The eccentricity was included as a basic variable as well, but the corresponding PSF was not calculated. The eccentricity variable includes different geometry effects, with different standard deviations. There does not exist any mean- or characteristic value in EC2 to use as a reference, nor a safety factor. However, the final design point of the eccentricity can be compared with the value calculated from the effects of imperfections in Section 3.2.1 for Eurocode validation.

5.6 Approach to the Model Uncertainty

Accurately quantifying model uncertainty is still an unresolved matter in structural reliability. In current state of the research, different suggestions have been made for the mean and standard deviation of a model uncertainty variable, Θ. A proposal of how to find the model uncertainty was made in this project, but due to the time span and lack of experimental work it was not quantified. It is hard to quantify the model uncertainty without any interference from the other uncertainties [33], because geometry and material properties that are used in experiments are never 100% certain.

Given adequate distributions for the experiments and the non-linear model, the mean of the model uncertainty could be expressed as Equation (5.27), and the standard deviation is suggested expressed by Haugens quotients estimator [34] as in Equation (5.28).

$$\mu_\Theta = \frac{\mu_{exp}}{\mu_{NLFEA}} \tag{5.27}$$

$$\sigma_\Theta = \frac{1}{\mu_{NLFEA}} \left(\frac{\mu_{NLFEA}^2 \sigma_{exp}^2 + \mu_{exp}^2 \sigma_{NLFEA}^2}{\mu_{NLFEA}^2 \sigma_{NLFEA}^2} \right)^{1/2} \tag{5.28}$$

where μ_Θ and σ_Θ are the model mean and standard deviation, μ_{exp} and σ_{exp} are the experimental mean and standard deviation, and μ_{NLFEA} and σ_{NLFEA} are the mean and standard deviation of the modelled capacity.

To find the distribution of the modelled capacity, the load was considered a deterministic variable and RSM-FORM was run with several load levels. Ensuring the resulting probabilities of failure roughly covered the whole range from zero to one, a lognormal Cumulative density function (CDF) was fitted to the model results, and μ_{NLFEA} and σ_{NLFEA} were extracted. The scripts that execute this procedure is digitally attached.

The distribution of the experimental results was assumed lognormally distributed. Due to the few samples, statistical uncertainty should be included, but this was not done. The mean and standard deviation of the sample statistics were calculated as in Eq. (5.29) and (5.30) [35],

$$m_Y = \frac{1}{n}\sum_{i=1}^{n} y_i \tag{5.29}$$

$$s_Y = \sqrt{\frac{1}{n-1}\sum_{i=1}^{n}(y_i - m_Y)^2} \tag{5.30}$$

where n is the number of samples, y_i is the logarithm of experimental outcome i, and m_Y and s_Y are the two moments of the sample statistics. Further it was assumed that the experimental results follow a lognormal distribution and that $m_Y = \mu_{exp}$; $s_Y = \sigma_{exp}$, which are the distribution mean and standard deviation.

6 Results

6.1 Design capacities with increasing LOA

The preliminary estimate of the design capacities using EC2 methods will be presented in this section for both Column A and B.

6.1.1 Column A

The design capacities according to the methods presented in Eurocode 2 for Column A are given in Table 6.1 and shown in Figure 6.1. Capacities related to the first Level-of-Approximation, using linear stress distribution and analytic formulas with design parameters, are shown in Figure 6.1a. The second LoA are represented by the nominal stiffness method and nominal curvature method using a parabolic stress distribution as shown in Figure 6.1b. In the same diagram the highest-order LoA is represented by the non-linear finite element solution of the General method and PSF safety format. Figure 6.1c shows the General method with the GRFM.

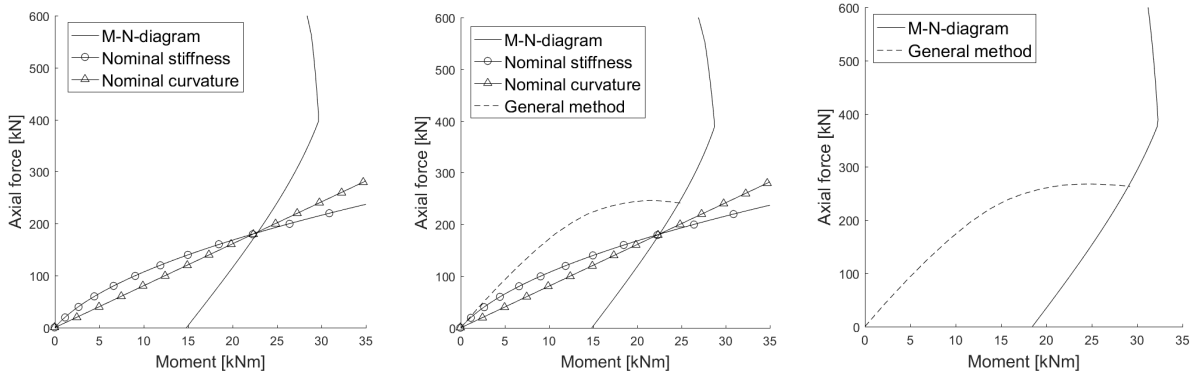

(a) Linear stress dist. and PSF format

(b) Parabolic stress dist. and PSF format

(c) Parabolic stress dist. and GRF format

Figure 6.1: Design capacity methods for Column A according to Eurocode 2

Material / Method	Linear stress dist.	Parabolic stress dist.	
	PSF	PSF	GRF
Nominal stiffness	183 kN (I)	181 kN (II)	-
Nominal curvature	184 kN (I)	182 kN (II)	-
General method	-	242 kN (IV)	208 kN (IV)

Table 6.1: Eurocode 2 axial design capacities for Column A, with LoA shown in parenthesis

6.1.2 Column B

The design capacities according to the methods presented in Eurocode 2 for Column B are given in Table 6.2 and Figure 6.2. Since the work-diagram of EC2-2 in Figure 6.2c never intersects the MN-diagram, the capacity was set to the axial force at maximum bending moment. As mentioned for Column A, this capacity was divided by the overall safety factor as well.

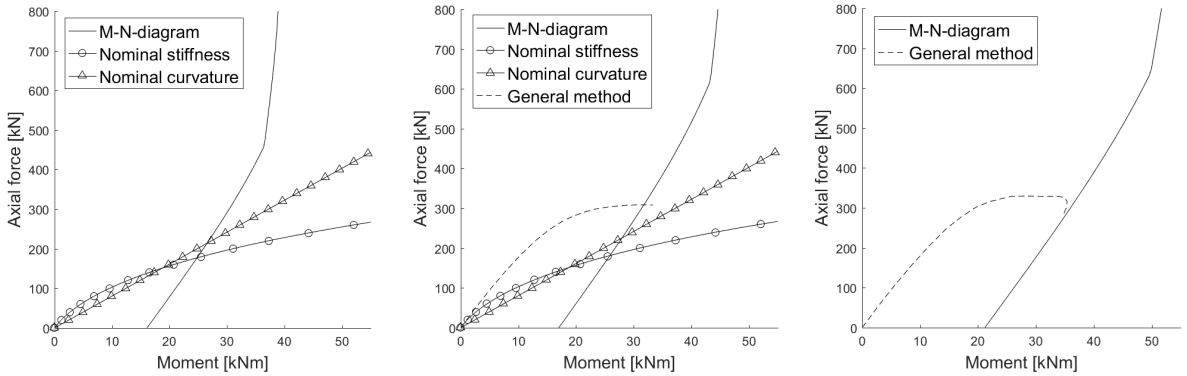

(a) Linear stress dist. and PSF format

(b) Parabolic stress dist. and PSF format

(c) Parabolic stress dist. and GRF format

Figure 6.2: Design capacity methods for Column B according to Eurocode 2

Material / Method	Linear stress dist.	Parabolic stress dist.	
	PSF	PSF	GRF
Nominal stiffness	177 kN (I)	181 kN (II)	-
Nominal curvature	214 kN (I)	226 kN (II)	-
General method	-	309 kN (IV)	249 kN (IV)

Table 6.2: Eurocode 2 axial design capacities for Column B, with LoA shown in parenthesis

6.2 Best Estimate and Round-Robin study

The configuration of the best estimate solution went through several stages with increasing level of approximation to reach the final result. In the following sections the results of these stages are summarized for Column A and B. An important factor to keep in mind is the increased level of knowledge from the experimental results of Column A before starting the estimations of Column B.

6.2.1 Column A

The results of the methods of nominal stiffness and nominal curvature for Column A with adapted material sets given in Section 3.1.2, are shown in Figure 6.3 and Table 6.3.

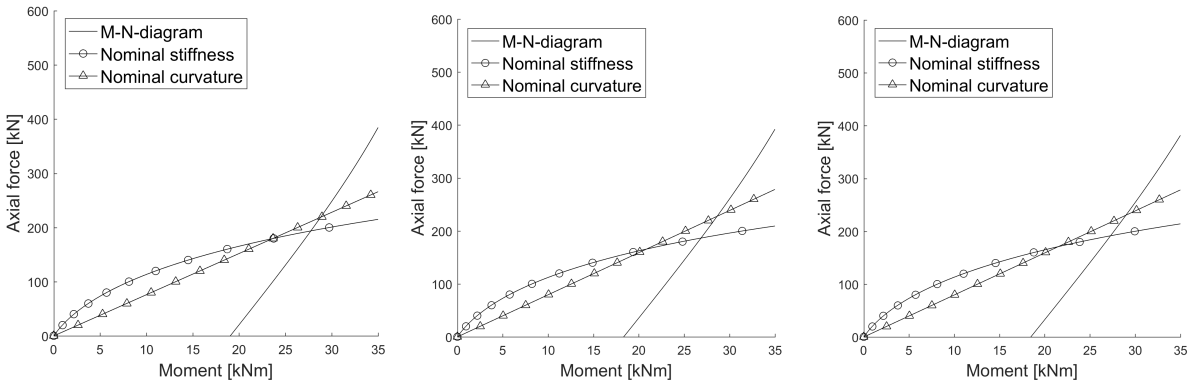

(a) Material set A *(b) Material set B* *(c) Material set C*

Figure 6.3: Capacities using EC2 hand-calculations and mean materials for Column A

	Material set A	Material set B	Material set C
Nominal stiffness	194 kN	187 kN	192 kN
Nominal curvature	219 kN	228 kN	231 kN

Table 6.3: Axial capacities using EC2 hand-calculations and mean materials for Column A

The NLFEA used to determine the best estimate for Column A was tested with the three material sets all based on realistic mean values. The results from the 3D model with varying material sets are shown in Figure 6.4.

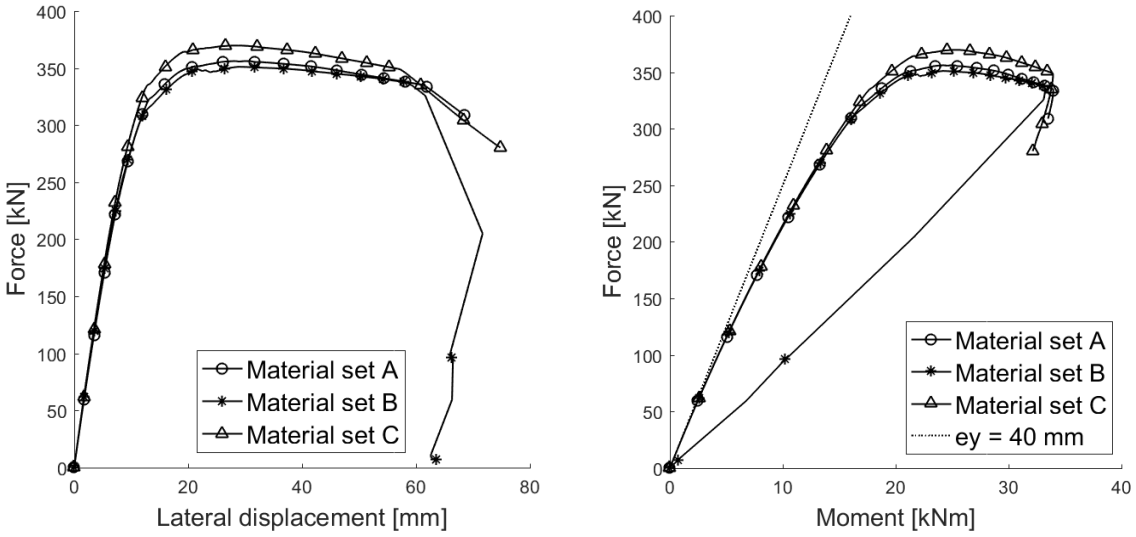

(a) Load-displacement curve *(b) Moment and axial force relation*

Figure 6.4: Results of NLFEA with mean material sets for Column A

The material model using insitu mean parameters was assumed to result in more accurate results, and was used in the results handed in to IABSE. A comparison between the results from all institutions participating in the Round-Robin study can be found in Table 6.4.

Institution	Software	N [kN]	u_y [mm]	M [kNm]
1	SCIA	325.5	49.5	29.1
2	Metóda C	342.0	44.0	28.0
3	Metóda A	344.4	35.5	26.0
4	Dlubal	363.0	30.3	25.5
5	Stab2nl	336.8	26.4	22.4
6	Atena	357.8	20.9	21.8
7	Atena	396.6	38.7	31.2
8	Atena	323.0	18.9	19.0
This report	DIANA	356.2	28.3	24.3

Table 6.4: Results of Round-Robin test provided by IABSE [1] and best estimate of this report

The results from the experimental testing done by IABSE are shown in Figure 6.5a together with the best estimate model found in this report using NLFEA. The best estimate found in this thesis is plotted together with the results from other institutions in Figure 6.5b.

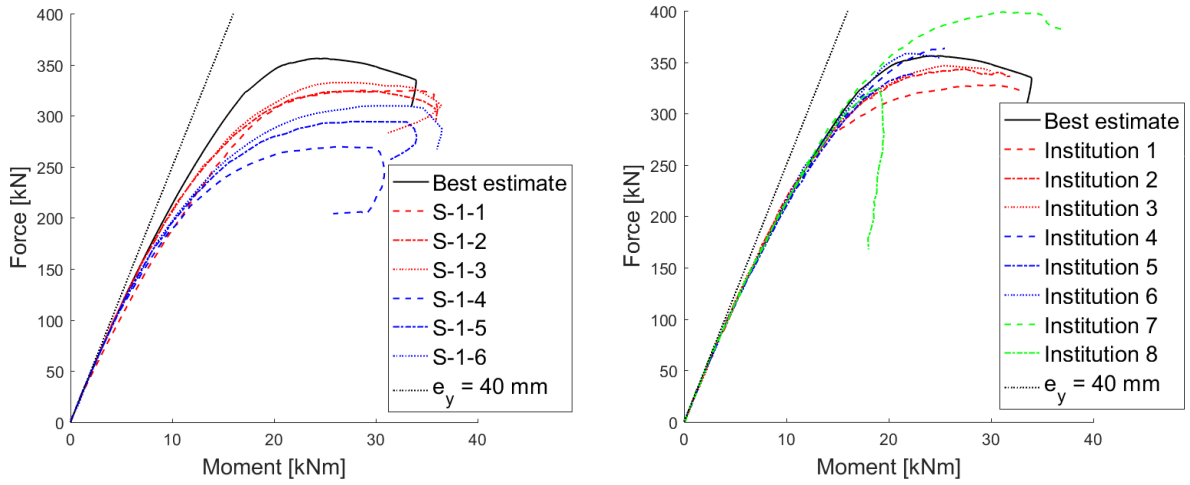

(a) Experimental results and best estimate *(b) NLFE modelling findings and best estimate*

Figure 6.5: Results of Round-Robin test provided by IABSE [1] and best estimate for Column A

6.2.2 Column B

The results of nominal stiffness and nominal curvature for Column B with adapted material sets given in Section 3.1.2, are shown in Figure 6.6 and Table 6.5.

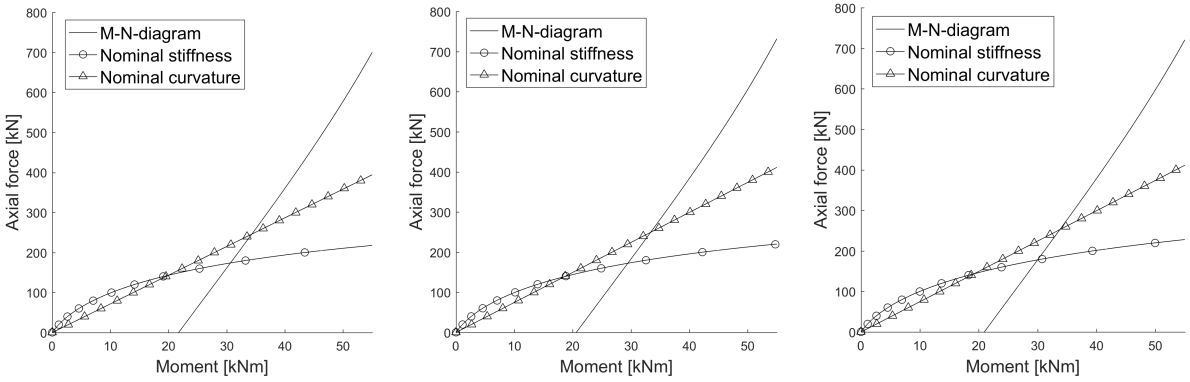

(a) Material set A *(b) Material set B* *(c) Material set C*

Figure 6.6: Capacities using EC2 hand-calculations and mean materials for Column B

	Material set A	Material set B	Material set C
Nominal stiffness	174 kN	172 kN	178 kN
Nominal curvature	246 kN	250 kN	253 kN

Table 6.5: Axial capacities using EC2 hand-calculations and mean materials for Column B

As done for Column A, Column B was simulated with Material set A for the best estimate. Two results were collected, one with the initial eccentricity set to 40 mm and one with 48 mm. The results can be seen in Figure 6.7

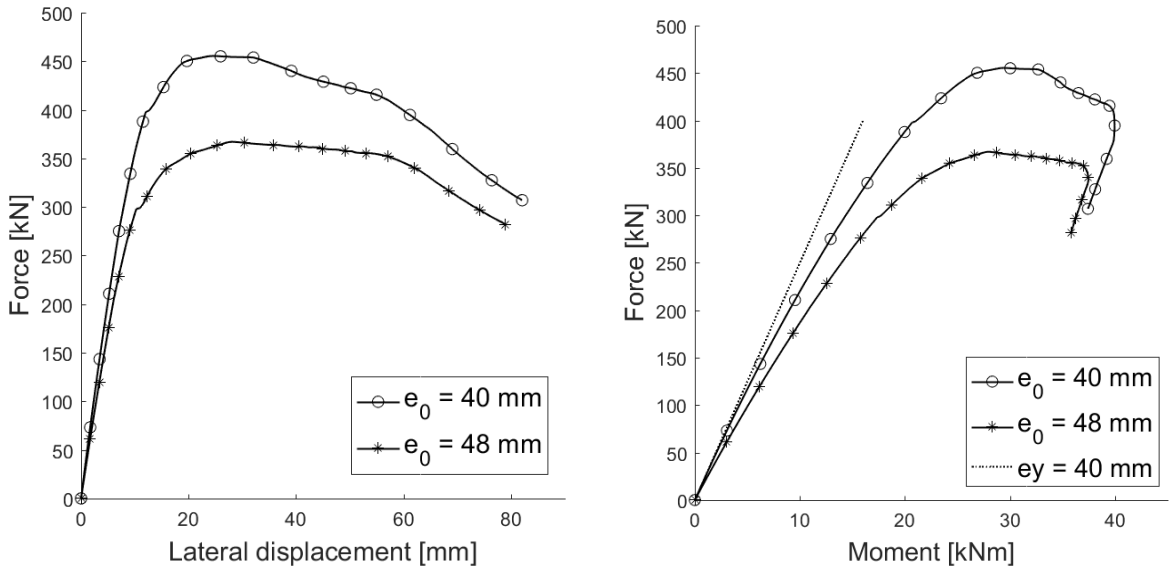

(a) Load-displacement curve *(b) Moment and axial force relation*

Figure 6.7: Results of NLFEA with different initial eccentricities for Column B

6.3 Reliability level Eurocode 2

The results of the reliability studies using the design capacity found in Eurocode 2 calculations are presented in this section. A summary of the results comparing the different reliability methods will be shown first. Further details of each method will follow.

The β resulting from each method were compared to the reliability index achieved by Monte Carlo as shown in Table 6.6 for five random variables. Note that the assessments with NLFEA are fundamentally different from the analytic, and not directly comparable to the results of the analytic Monte Carlo.

		Column A		Column B	
LSFE	Method	β	β-difference [%]	β	β-difference [%]
Analytic	Monte Carlo	4.19	-	3.56	-
Analytic	FORM	4.08	-2.65	3.38	-5.12
Analytic	RSM-FORM	4.16	-0.80	3.56	-0.17
Analytic	SORM	4.10	-2.14	3.39	-4.80
Analytic	RSM-SORM	4.17	-0.34	3.57	0.28
NLFEA	RSM-FORM	5.29	26.27	5.31	49.07
NLFEA	RSM-SORM	5.26	25.62	5.29	48.51

Table 6.6: Results of reliability methods using EC2 Design load and five random variables

The corresponding limit states used in analytic FORM, analytic RSM-FORM and RSM-FORM with NLFEA are plotted together with the simulated realizations of the analytic Monte Carlo in Figure 6.8. In Figure 6.8a, concrete strength is plotted against reinforcement yield strength, while the rest of the random variables are fixed at design point. Figure 6.8b shows the axial force plotted against the concrete stiffness. Note that the figures illustrate results of *all* simulations in the Monte Carlo and not a two-dimensional cut in the five-dimensional space.

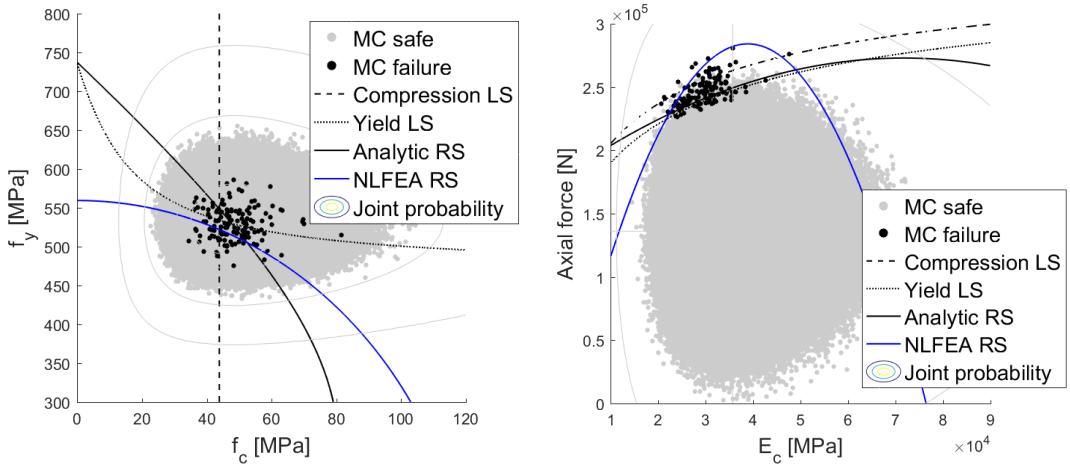

(a) Concrete strength - Reinforcement yield strength

(b) Concrete stiffness - Axial force

Figure 6.8: LS for all reliability methods using five random variables applied to Column A

6.3.1 Monte Carlo

Running Monte Carlo with 10^7 simulations using two random variables, f_c and f_y, resulted in zero failures when applying a load level below 226 kN. Hence, the EC2 design capacity could not be checked. To still be able to compare Monte Carlo with other methods for two variables, the probability of failure for two different load levels applied to Column A were found. The results can be found in Table 6.7 and Figure 6.9.

Load Level [kN]	230.0	240.0
P_f	2.18E-04	1.42E-01
V_{P_f}	0.0214	0.0008
β	3.52	1.07

Table 6.7: Results of Monte Carlo using two random variables on Column A

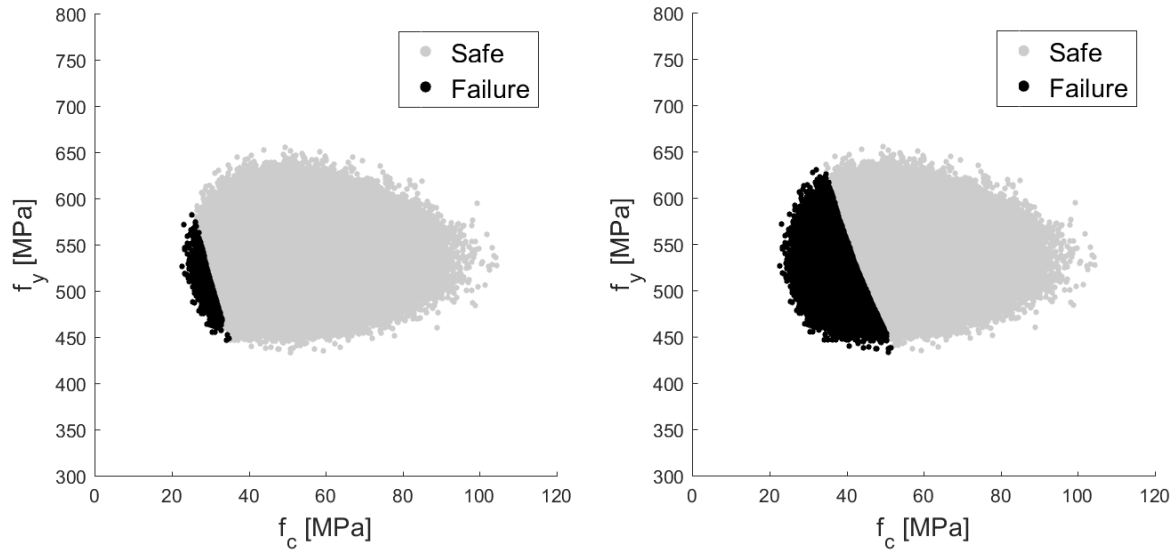

(a) F = 230 kN *(b) F = 240 kN*

Figure 6.9: Results of Monte Carlo using two random variables for Column A

Monte Carlo with five random variables were run with the mean capacities, and the results are shown in Table 6.8 for Column A and B. Figures 6.10 and 6.11 shows all 10 million simulations and the simulations where the limit state was exceeded are marked with a black dot.

	Column A	Column B
Mean Capacity [kN]	136.0	159.0
P_f	1.40E-05	1.84E-05
V_{P_f}	0.0845	0.0233
β	4.189	3.562

Table 6.8: Results of Monte Carlo using five random variables

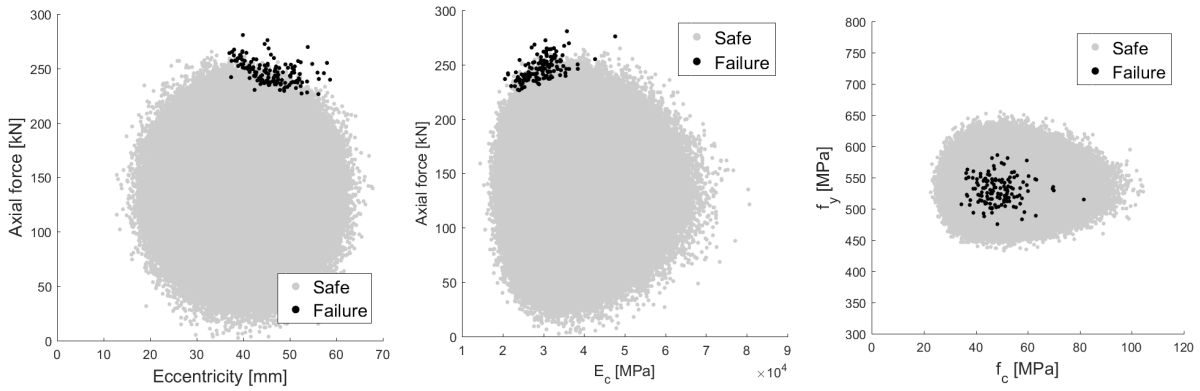

(a) Eccentricity-Axial force *(b) Concrete stiffness-Axial force* *(c) Concrete strength-Yield strength*

Figure 6.10: Results of Monte Carlo using five random variables for Column A

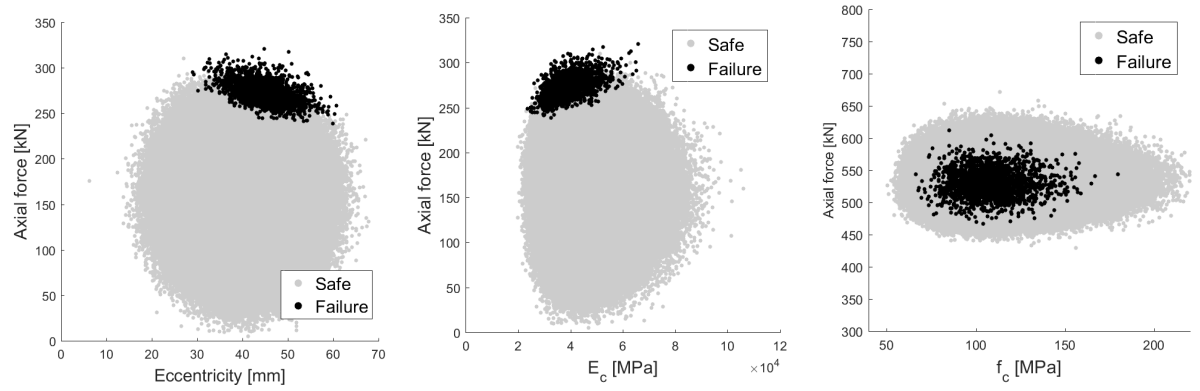

(a) Eccentricity-Axial force *(b) Concrete stiffness-Axial force* *(c) Concrete strength-Yield strength*

Figure 6.11: Results of Monte Carlo using five random variables for Column B

6.3.2 FORM and SORM

The FORM and SORM iterations were performed in the standard normal space. In Figure 6.12a, the first and last FORM iteration for both limit states are presented. The transformation

to real space can be seen in Figure 6.12b. The last FORM iteration for compression failure lies directly on the limit state.

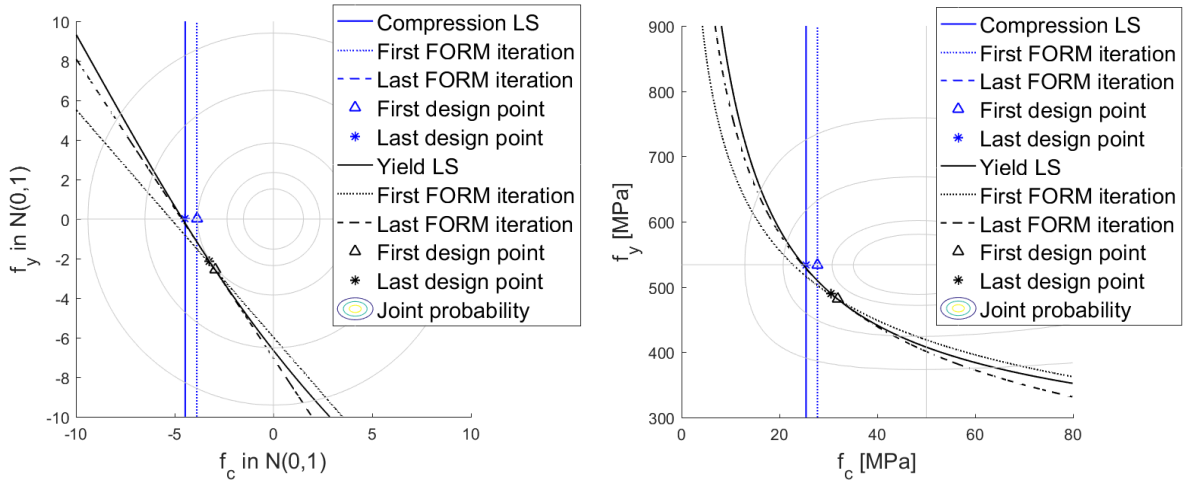

(a) Standard normal space *(b) Real space*

Figure 6.12: First and last FORM iteration for Column A subject to N=230 kN

In the implemented SORM-algorithm, the design points and sensitivity factors are obtained equally as in the FORM analysis. Still, the SORM limit state approximation is of second order, and differs from the first order FORM limit state. The difference in standard normal space and in real space can be seen in Figure 6.13 for the load level of 230 kN when using 2 random variables.

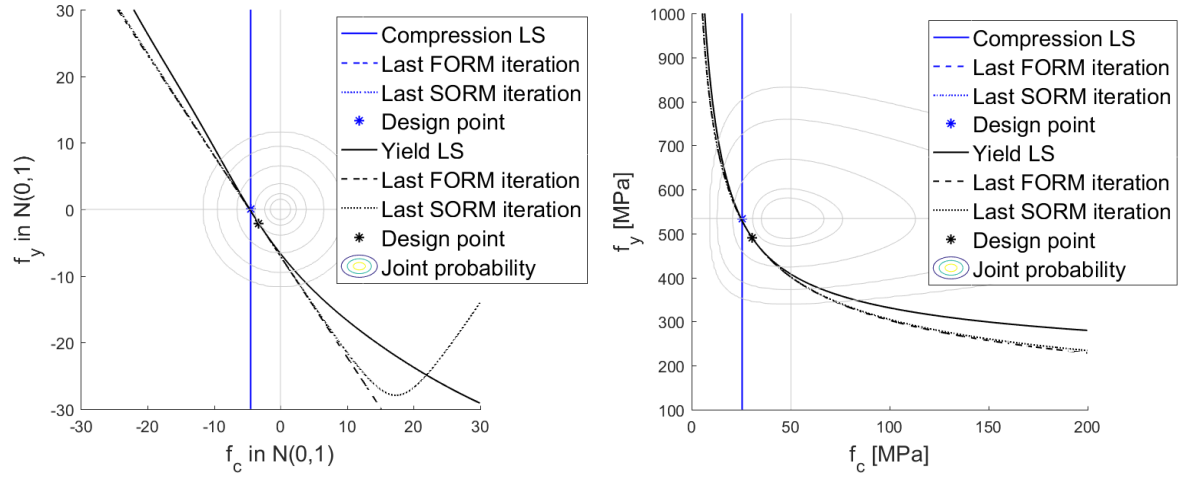

(a) Standard normal space *(b) Real space*

Figure 6.13: FORM and SORM approximations to the LS for Column A subject to N=230 kN

The results of analytic FORM and SORM using 5 random variables with both Column A and B subject to the design capacity found through the EC2-1-1 can be seen in Table 6.9. The capacity and load sensitivity factors, α_R and α_S, are shown in the curly brackets.

	Column A		Column B	
EC2 capacity [kN]	136.0		159.0	
$\beta_{sysFORM}$	4.08		3.38	
$\beta_{sysSORM}$	4.10		3.39	
Failure mode	Comp.	Yield	Comp.	Yield
β_{FORM}	4.69	4.09	4.35	3.38
β_{eqSORM}	4.70	4.10	4.36	3.39
α_{fc}	0.173	0.021	0.136	0.014
α_{fy}	0.000 } 0.298	0.059 } 0.252	0.000 } 0.272	0.053 } 0.222
α_E	0.242	0.245	0.235	0.215
α_e	-0.221 } -0.955	-0.260 } -0.968	-0.189 } -0.962	-0.243 } -0.975
α_N	-0.929	-0.932	-0.944	-0.944
f_{cd} [MPa]	43.88	48.91	100.75	109.27
f_{yd} [MPa]	53.58	528.49	533.58	529.79
E_{cd} [GPa]	29.47	30.11	38.13	39.93
e_d [mm]	45.6	45.7	44.4	44.4
N_d [kN]	254.5	239.6	289.5	260.5

Table 6.9: Results of analytic FORM and SORM using EC2-1-1 capacity load

6.3.3 RSM-FORM and RSM-SORM

The results of analytic RSM-FORM and RSM-SORM using 5 variables with both Column A and B subject to the design capacity found through the EC2-1-1 can be seen in Table 6.10. Recall that these two methods only differ in the probability of failure and consequently the equivalent reliability index. The force has a mean value, equal to the design capacity calculated from EC2, divided by the partial safety factor for dominating self weight of 1.35. All five random variables were included. The sensitivity factors, α_i, are summed for the load and resistance to find α_R and α_S in the curly brackets.

	Column A		Column B	
EC2 Capacity [kN]	136.0		159.0	
β_{FORM}	4.15		3.56	
$\beta_{eq,SORM}$	4.17		3.57	
α_{fc}	0.064	0.256	0.054	0.229
α_{fy}	0.039		0.032	
α_E	0.245		0.221	
α_e	-0.254	-0.967	-0.234	-0.945
α_N	-0.933		-0.945	
f_{cd} [MPa]	47.59		106.96	
f_{yd} [MPa]	530.17		531.16	
E_{cd} [GPa]	30.03		39.57	
e_d [mm]	45.7		44.5	
N_d [kN]	241.4		265.8	

Table 6.10: Results of analytic RSM-FORM and RSM-SORM using EC2 capacity load

The difference between the FORM and SORM adaption to the RS is shown in Figure 6.14 for both real and standard normal space for Column A. Only the two random variables of N and E_c are shown, while the three other variables are kept constant at their final design point.

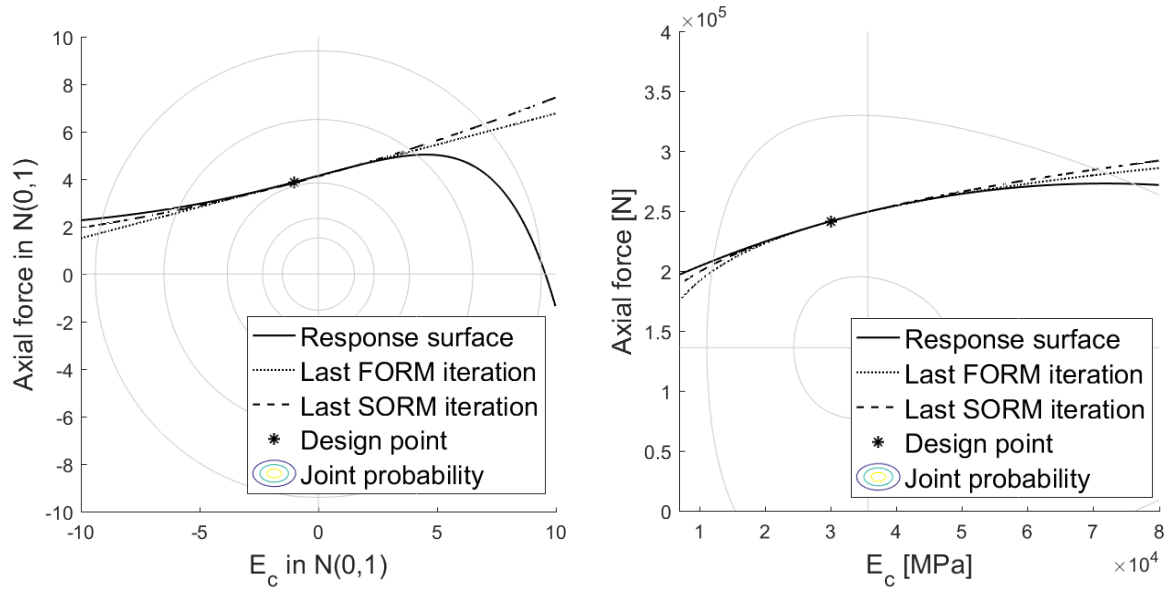

(a) Standard normal space *(b) Real space*

Figure 6.14: Last FORM and SORM iteration compared to the analytic RS for Column A

Table 6.11 shows the result of the reliability assessment of Column A and Column B using RSM-FORM and RSM-SORM with NLFEA. In Figure 6.15, the basic variables with highest sensitivity factors are shown in a joint probability plot for standard and real space.

	Column A		Column B	
EC2 Capacity [kN]	136.0		159.0	
β_{FORM}	5.29		5.31	
$\beta_{eq,SORM}$	5.28		5.29	
α_{fc}	0.089	0.578	0.031	0.588
α_{fy}	0.142		0.144	
α_E	0.553		0.569	
α_e	-0.503	-0.816	-0.521	-0.809
α_N	-0.643		-0.619	
f_{cd} [MPa]	46.18		107.4	
f_{yd} [MPa]	517.78		517.52	
E_{cd} [GPa]	22.25		27.85	
e_d [mm]	54.3		54.9	
N_d [kN]	228.5		263.5	

Table 6.11: Results of RSM-FORM and RSM-SORM with NLFEA using EC2 capacity load

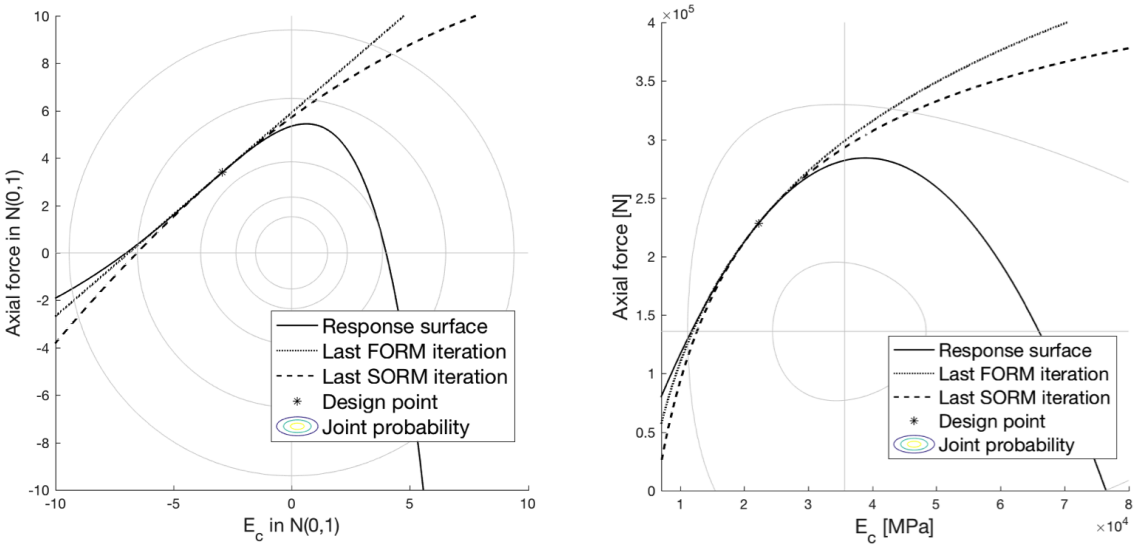

(a) Standard normal space *(b) Real space*

Figure 6.15: Last FORM and SORM iteration compared to the NLFEA RS for Column A

To validate the RSM with NLFEA, a small sample of NLFEA were run around the area of failure seen from Figure 6.15b. The results are plotted in Figure 6.16.

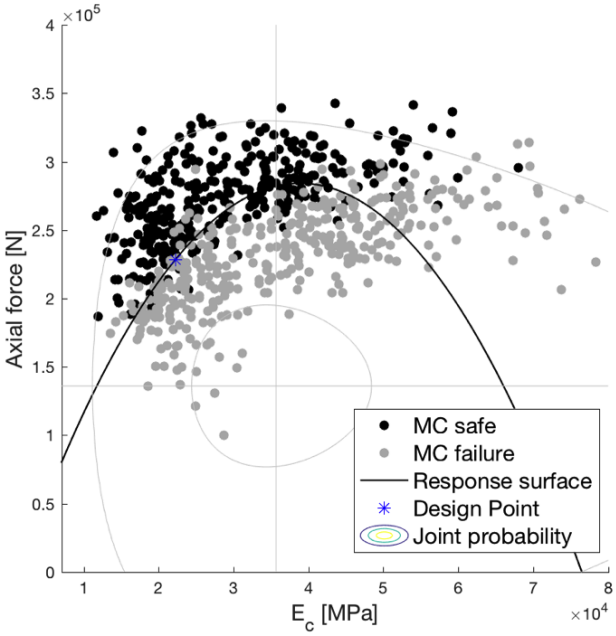

Figure 6.16: RSM with NLFEA compared to Monte Carlo realizations around failure

6.4 Inverse analysis and PSF

Inverse analyses were performed on each method except NLFEA RSM-SORM, to determine the design point corresponding to the target reliability defined in EC2, $\beta_T = 3.8$. The following section lists the design value found for each random variable when target reliability was achieved. The applied mean load, μ_N, necessary to achieve this index will also be shown.

The resulting design points achieved by each method are summarized in Table 6.12 for Column A and Table 6.13 for Column B. RSM-FORM with NLFEA is considered most accurate of the listed methods.

LSFE	Method	f_{cd} [MPa]	f_{yd} [MPa]	E_{cd} [GPa]	e_d [mm]	N_d [kN]
Analytic	FORM	48.97	529.00	30.57	45.2	241.0
Analytic	RSM-FORM	47.81	530.58	30.60	45.1	243.2
Analytic	SORM	48.97	529.02	30.59	45.2	241.1
Analytic	RSM-SORM	47.82	530.60	30.63	45.0	243.3
NLFEA	RSM-FORM	47.36	526.94	26.89	50.5	267.8

Table 6.12: Result of inverse analysis of Column A for all reliability methods

LSFE	Method	f_{cd} [MPa]	f_{yd} [MPa]	E_{cd} [MPa]	e_d [mm]	N_d [kN]
Analytic	FORM	109.13	529.10	39.13	45.1	258.4
Analytic	RSM-FORM	106.66	530.92	39.10	44.9	264.6
Analytic	SORM	109.14	529.12	39.15	45.1	258.4
Analytic	RSM-SORM	106.68	530.93	39.13	44.8	264.7
NLFEA	RSM-FORM	109.47	527.07	33.60	51.0	314.0

Table 6.13: Result of inverse analysis of Column B for all reliability methods

6.4.1 FORM and SORM

The results of the inverse FORM and SORM analyses with $\beta_T = 3.8$ are presented in Table 6.14 for Column A and Column B. Note that the reliability index listed for SORM is an equivalent reliability index as mentioned in Section 5.2.3.

	Column A				Column B			
	FORM		SORM		FORM		SORM	
μ_N [kN]	140.9		141.1		150.7		150.9	
Failure mode	Comp.	Yield	Comp.	Yield	Comp.	Yield	Comp.	Yield
β	4.39	3.80	4.39	3.80	4.82	3.80	4.82	3.80
f_{cd} [MPa]	44.37	48.97	44.39	48.97	99.30	109.13	99.33	109.14
f_{yd} [MPa]	533.58	529.00	533.58	529.02	533.58	529.10	533.58	529.12
E_{cd} [GPa]	29.95	30.57	29.97	30.59	37.16	39.13	37.19	39.15
e_d [mm]	45.1	45.2	45.1	45.2	45.1	45.1	45.1	45.1
N_d [kN]	256.2	241.0	256.2	241.1	287.0	258.4	287.1	258.4

Table 6.14: Inverse analytic FORM and SORM for Column A and B

6.4.2 RSM-FORM and RSM-SORM

The results of the inverse analytic RSM-FORM and RSM-SORM analysis with $\beta_T = 3.8$ are presented in Tables 6.15 and 6.16 for Column A and Column B.

	Column A		Column B	
μ_N [kN]	142.1		154.2	
Random variable	Design	PSF	Design	PSF
f_c [MPa]	47.81	0.94	106.66	0.94
f_y [MPa]	530.58	0.94	530.92	0.94
E_c [GPa]	30.60	1.17	39.10	1.16
e [mm]	45.1	-	44.9	-
N [kN]	243.2	1.71	264.6	1.72

Table 6.15: Inverse analytic RSM-FORM for Column A and B with $\beta_T = 3.8$

	Column A		Column B	
μ_N [kN]	142.4		154.5	
Random variable	Design	PSF	Design	PSF
f_c [MPa]	47.82	0.94	106.68	0.94
f_y [MPa]	530.60	0.94	530.93	0.94
E_c [GPa]	30.63	1.16	39.13	1.16
e [mm]	45.0	-	44.8	-
N [kN]	243.3	1.71	264.7	1.71

Table 6.16: Inverse analytic RSM-SORM for Column A and B with $\beta_T = 3.8$

The inverse analytic RSM-FORM and SORM showed negligible difference in the final design points as seen in Tables 6.15 and 6.16. Therefore, the inverse RSM-SORM was not performed using NLFEA. The results of inverse RSM-FORM using NLFEA are shown in Figure 6.17.

	Column A		Column B	
μ_N	173.5		206.5	
Random variable	Design	PSF	Design	PSF
f_c [MPa]	47.36	0.95	109.47	0.91
f_y [MPa]	526.94	0.95	527.07	0.95
E_c [GPa]	26.89	1.33	33.60	1.35
e [mm]	50.5	-	51.0	-
N [kN]	267.8	1.54	314.0	1.52

Table 6.17: Inverse RSM-FORM with NLFEA for Column A and B

6.5 Limit state and response surface sensitivity

The limit states used in analytic FORM, analytic RSM-FORM and RSM-FORM with NLFEA are plotted together with the simulated realizations of the analytic Monte Carlo for two variables in Figure 6.17. The load level in this case is set to 230 kN for better illustration of Monte Carlo.

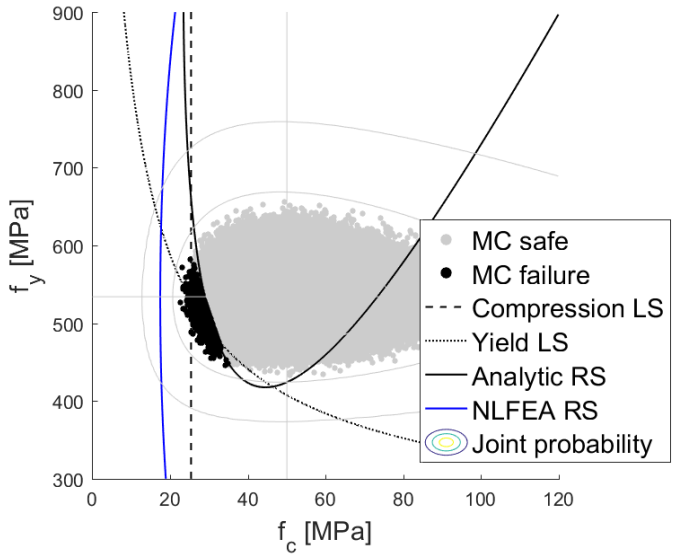

Figure 6.17: Approximations to the LS for all reliability methods using two random variables

6.5.1 Closed-form limit state

The results of the analytic FORM simulations for different load levels using only two random variables, f_c and f_y, can be found in Table 6.18.

Load Level [kN]	210.0		220.0		230.0		240.0	
β_{sys}	7.38		5.90		3.88		0.69	
P_f	7.83E-14		1.77E-09		5.30E-05		2.46E-01	
Failure mode	Comp.	Yield	Comp.	Yield	Comp.	Yield	Comp.	Yield
β	7.38	10.54	5.90	7.15	4.48	3.88	3.08	0.69
α_{fc}	1.000	0.843	1.000	0.841	1.000	0.834	1.000	0.823
α_{fy}	0.000	0.538	0.000	0.541	0.000	0.552	0.000	0.568
f_{cd} [MPa]	16.47	13.16	20.53	20.19	25.40	30.54	31.28	45.52
f_{yd} [MPa]	533.58	425.28	533.58	457.09	533.58	489.77	533.58	525.31

Table 6.18: Results of analytic FORM using different load levels for Column A

The two limit states representing compression and yield failure can be seen in Figure 6.18. Two cases are represented, one load level where compression is the dominating failure mode, and one load level where yielding dominates. The last FORM approximation is presented for both failure modes. The FORM approximation for compression failure cannot be seen, as it lies directly below the limit state.

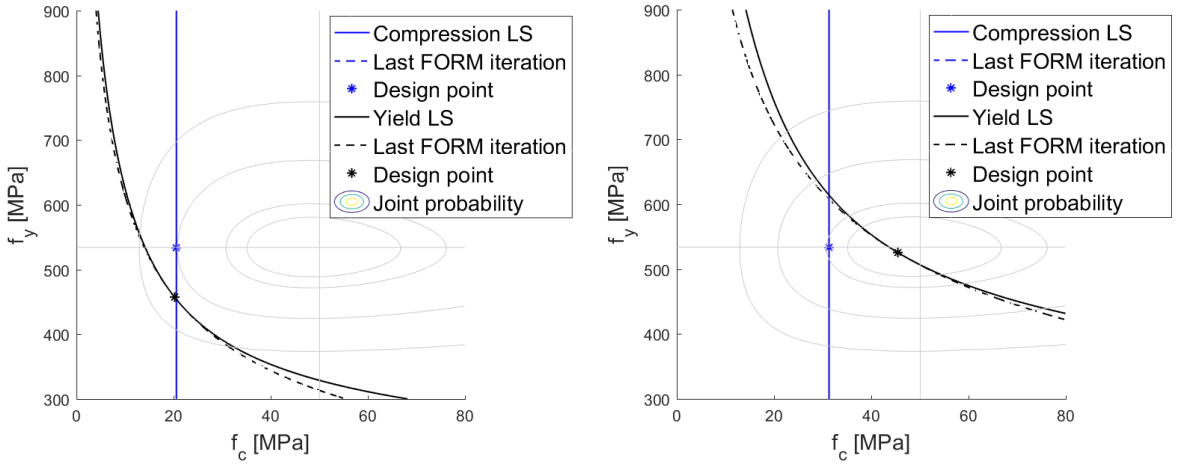

(a) Compression failure F =220 kN *(b) Yield failure F= 240 kN*

Figure 6.18: Limit states for compression and yield failure for Column A

6.5.2 RS sensitivity study

By narrowing the search area with an f-factor of 0.5 and making a qualified guess of a starting point close to the design point, response surfaces for both yield failure and compression failure were found for analytic RSM-FORM. A study on the choice of initial sample points was conducted where the β values were compared to β=4.19 found through Monte Carlo. The analyses were run with 5 variables and the change in the centre value of the initial sample points are shown in Table 6.19.

Random variable	Original sample point	Modified sample point
f_c [MPa]	50.08	45.00
f_y [MPa]	534.01	530.00
E_c [GPa]	35.67	30.00
e [MPa]	40.0	45.0
N [kN]	136.0	240.0

Table 6.19: Change in initial sample point for the RS sensitivity study

The results of the study are listed in Table 6.20, and the change in f-factor is illustrated in Figure 6.19.

	Original sample point			Modified sample point		
f	β	P_f	β-error [%]	β	P_f	β-error[%]
0.5	4.15	1.63E-05	0.82	4.16	1.62E-05	0.80
1.0	4.15	1.64E-05	0.87	4.16	1.62E-05	0.80
1.5	4.15	1.66E-05	0.94	4.16	1.62E-05	0.80
2.0	4.15	1.69E-05	1.03	4.16	1.62E-05	0.80
2.5	4.14	1.73E-05	1.14	4.16	1.62E-05	0.80
3.0	4.14	1.77E-05	1.28	4.16	1.62E-05	0.80
3.5	4.13	1.83E-05	1.46	4.16	1.62E-05	0.80
4.0	4.12	1.90E-05	1.68	4.16	1.63E-05	0.81
4.5	4.11	2.00E-05	1.96	4.16	1.62E-05	0.79
5.0	4.09	2.13E-05	2.30	4.16	1.61E-05	0.77

Table 6.20: Change in P_f and β due to varying initial sample point for analytic RSM-FORM

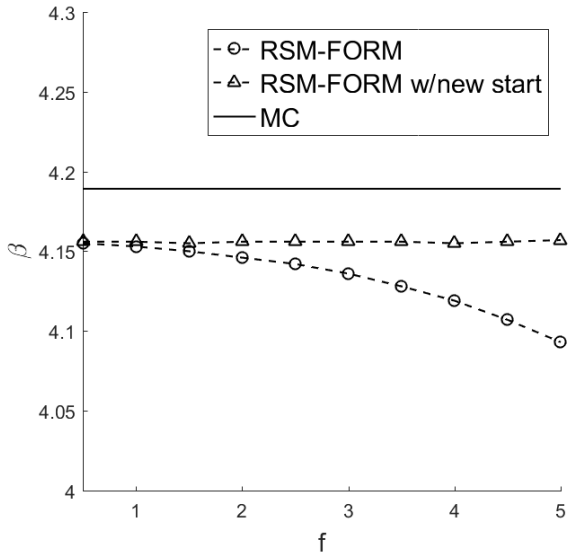

Figure 6.19: Change in β due to varying f-factor for analytic RSM-FORM

According to the results in Table 6.18, a design load of 210 kN should generate compression failure, and a design load of 240 kN should result in yield failure when using 2 random variables. The limit states used in the FORM analysis and the response surface of the RSM-FORM analysis are plotted together in Figure 6.20.

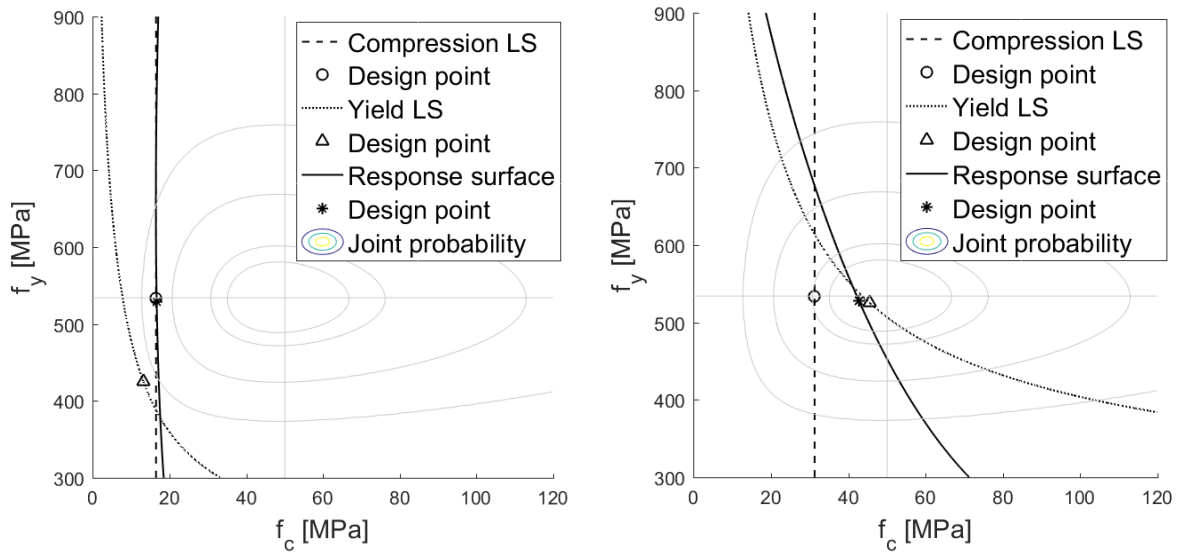

(a) Compression failure *(b) Yield failure*

Figure 6.20: FORM LS and RSM-FORM RS for compression and yield failure in Column A

6.5.3 Effect of introducing more random variables

The accuracy of all reliability methods was increased by adding three more random variables to the analyses. The effects of introducing the random variables one by one to the analytic FORM can be seen in Table 6.21. The random variables used in each analysis are the following.

- 2 variables: f_c and f_y
- 3 variables: f_c, f_y and E_c
- 4 variables: f_c, f_y, E_c and e
- 5 variables: f_c, f_y, E_c, e and N

	2 variables		3 variables		4 variables		5 variables	
EC2 Capacity [kN]	184.0		184.0		184.0		136.0	
β_{sys}	Inf		8.21		7.62		4.09	
Failure mode	Comp.	Yield	Comp.	Yield	Comp.	Yield	Comp.	Yield
β	11.65	20.36	9.79	8.25	9.24	7.62	4.69	4.09

Table 6.21: Change in β when introducing random variables in analytic FORM

The change in the sensitivity factors when introducing more random variables is illustrated in Figure 6.21 for both failure modes.

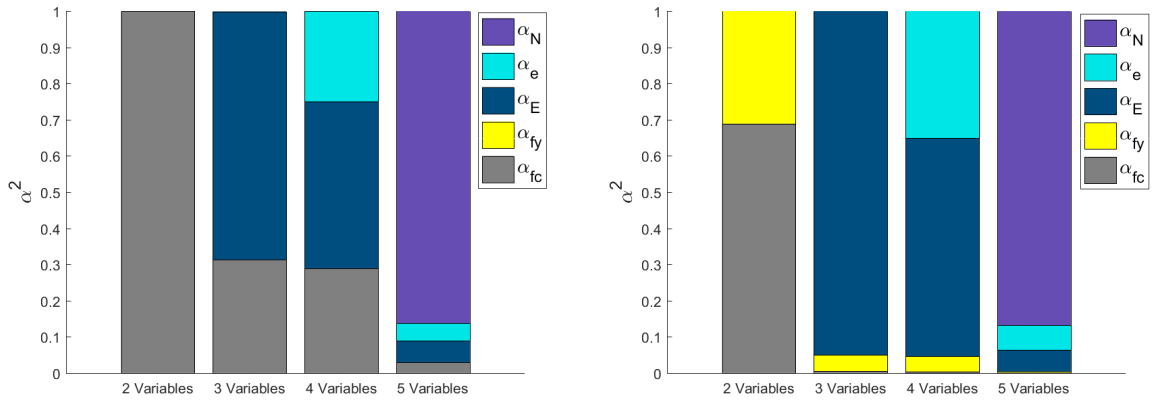

(a) Compression failure *(b) Yield failure*

Figure 6.21: Change in α_i^2 when introducing random variables in analytic FORM

The effects of introducing the random variables one by one to the analytic RSM-FORM can be seen in Table 6.22. The change in the sensitivity factors when introducing more random variables is illustrated in Figure 6.22.

	2 variables	3 variables	4 variables	5 variables
EC2 Capacity [kN]	184.0	184.0	184.0	136.0
β	11.64	8.31	7.75	4.14

Table 6.22: Change in β when introducing random variables in analytic RSM-FORM

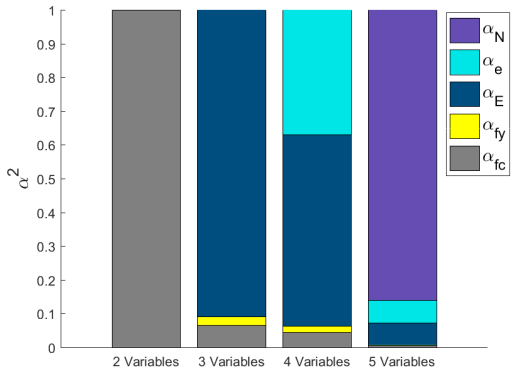

Figure 6.22: Change in α_i^2 when introducing random variables in analytic RSM-FORM

The effect of introducing more random variables in the RSM-FORM NLFEA is presented in Table 6.23 and Figure 6.23.

	2 variables	3 variables	4 variables	5 variables
EC2 Capacity [kN]	184	184	184	136
β_{FORM}	7.54	7.55	5.86	5.29

Table 6.23: Change in β when introducing random variables in RSM-FORM using NLFEA

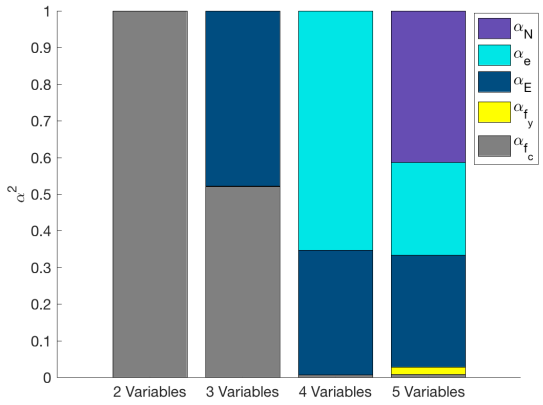

Figure 6.23: Change in α_i^2 when introducing random variables in RSM-FORM using NLFEA

Figure 6.24 illustrates how the failure mode changes from compressive failure to yield failure when including more stochastic variables into the NLFEA.

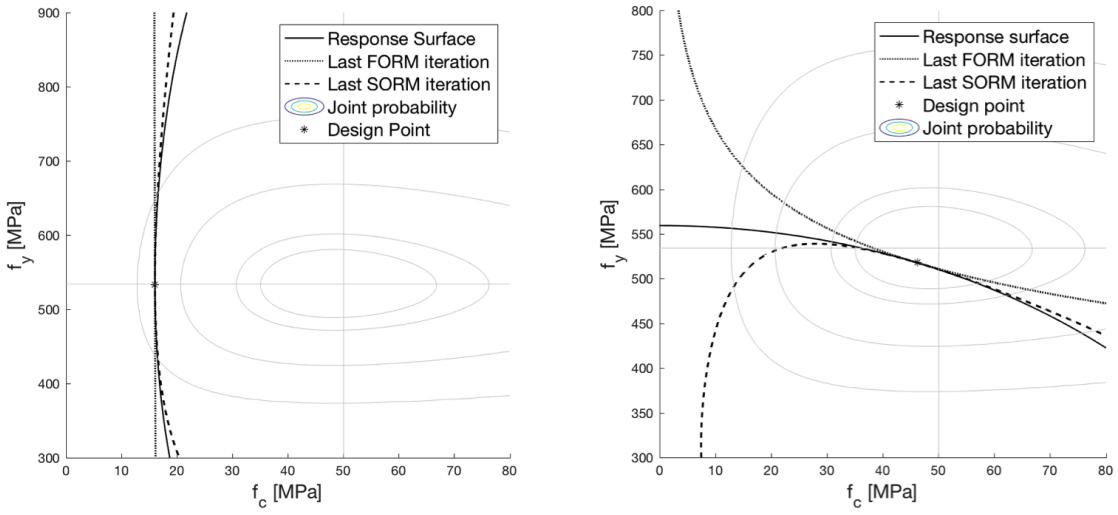

(a) Two variables, Real space *(b) Five variables, Real space*

Figure 6.24: Change in failure mode when including more random variables in the NLFEA

6.6 Concrete grade study

The results of the concrete grade study will be presented in the following sections. First, the results of the analyses using the Eurocode 2 design capacity will be shown. Then, the results of the inverse analysis and found PSFs are presented. Finally, a further study on the topic of correlation is shown.

6.6.1 Reliability level Eurocode 2

Table 6.24 shows the resulting reliability index, and the equivalent reliability index obtained from RSM-FORM and RSM-SORM using NLFEA for varying concrete grades.

	C20	C30	C45	C60	C80	C100
Correlation	Yes	Yes	-	-	-	-
EC2 Capacity [kN]	108.9	120.0	136.0	145.9	157.0	159.0
β	4.57	5.10	5.29	5.22	5.10	5.31
β_{eq}	4.60	5.06	5.28	5.24	5.10	5.29

Table 6.24: Results of RSM-FORM/SORM with NLFEA and EC2 capacity load for varying concrete grade

6.6.2 Inverse analysis and PSF

All resulting design points and partial safety factors of the inverse analysis for different concrete grades are presented in Tables 6.25 and 6.26.

Grade	C20	C30	C45	C60	C80	C100
μ_N [kN]	124.7	154.0	173.5	186.0	197.0	206.5
Correlation	Yes	Yes	-	-	-	-
f_{cd} [MPa]	17.64	27.34	47.36	64.49	86.98	109.47
f_{yd} [MPa]	525.15	526.26	526.94	527.21	527.05	527.07
E_{cd} [GPa]	21.33	23.71	26.89	29.05	31.47	33.60
e_d [mm]	49.1	49.6	50.5	50.8	50.9	51.0
N_d [kN]	194.2	230.8	267.8	286.0	301.8	314.0

Table 6.25: Design points of inverse RSM-FORM with NLFEA for varying concrete grade

Grade	C20	C30	C45	C60	C80	C100
μ_N	124.7	154.0	173.5	186.0	197.0	206.5
Correlation	Yes	Yes	-	-	-	-
γ_c [MPa]	1.13	1.10	0.95	0.93	0.92	0.91
γ_s [MPa]	0.95	0.95	0.95	0.95	0.95	0.95
γ_{cE} [GPa]	1.31	1.33	1.33	1.34	1.34	1.35
γ_G [kN]	1.56	1.50	1.54	1.54	1.52	1.52

Table 6.26: PSFs from inverse RSM-FORM with NLFEA for varying concrete grade

To get a better picture of possible trends in the partial safety factors and sensitivity factors, trend plots from the concrete grade study are presented. Figure 6.25 shows the sensitivities of resistance and load found in this study compared to the given sensitivities of Eurocode 2.

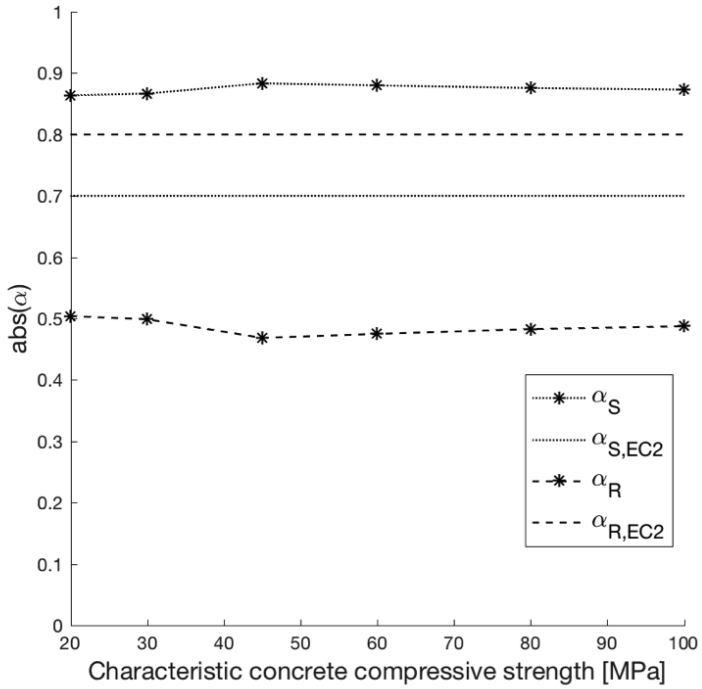

Figure 6.25: Trend in α_R and α_S for varying concrete grade

Figure 6.26a and Figure 6.26b presents the change in sensitivity factors and PSFs of each random variable respectively.

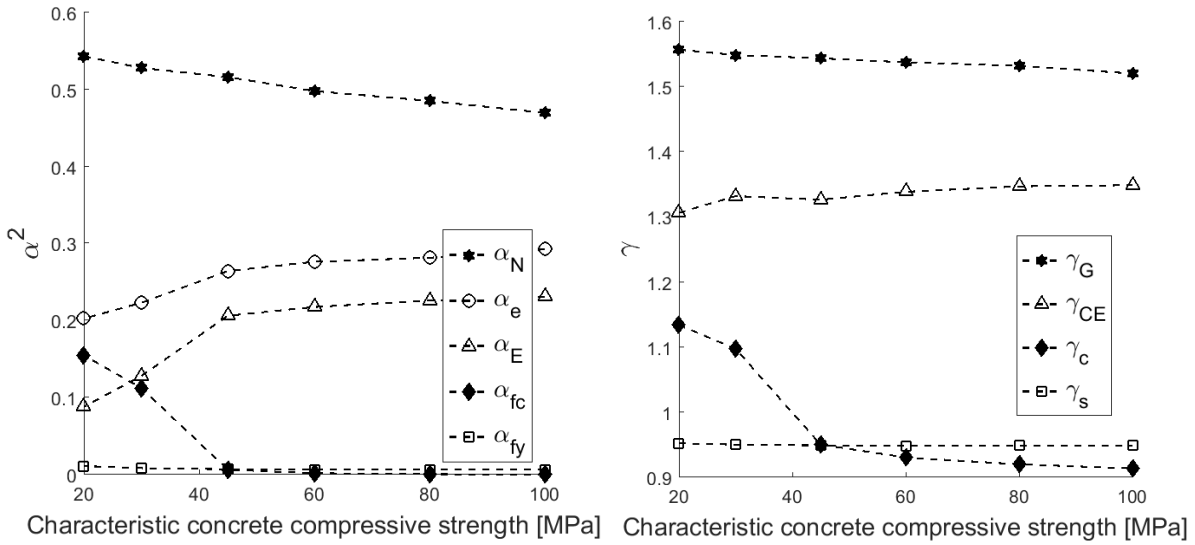

(a) Sensitivity factors *(b) Partial safety factors*

Figure 6.26: Trends for each random variable with varying concrete grade

The resulting work-diagram of the NLFEA for each concrete grade, using the final design point values of the RSM-FORM as input, can be seen in Figure 6.27. Note the descending branch for the concrete grades C20 and C30.

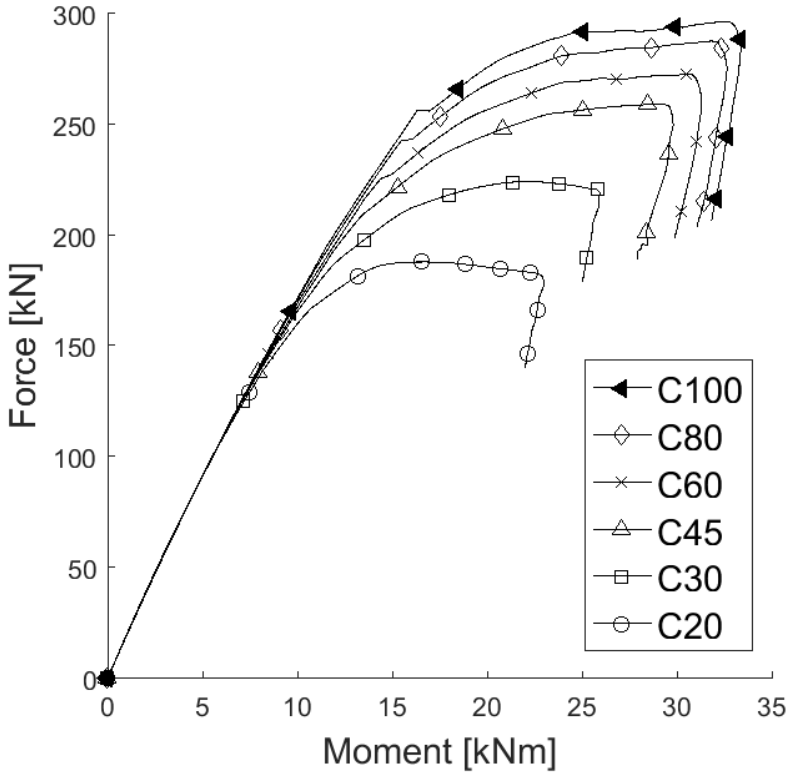

Figure 6.27: Work diagram for varying concrete grade using design values from inverse RSM-FORM with NLFEA

6.6.3 Effect of correlation

The effect of including correlation between the concrete strength and stiffness was investigated. A range of different concrete grades were analyzed using RSM-FORM with NLFEA, and the sensitivity factors are shown in Figures 6.28a and 6.28b.

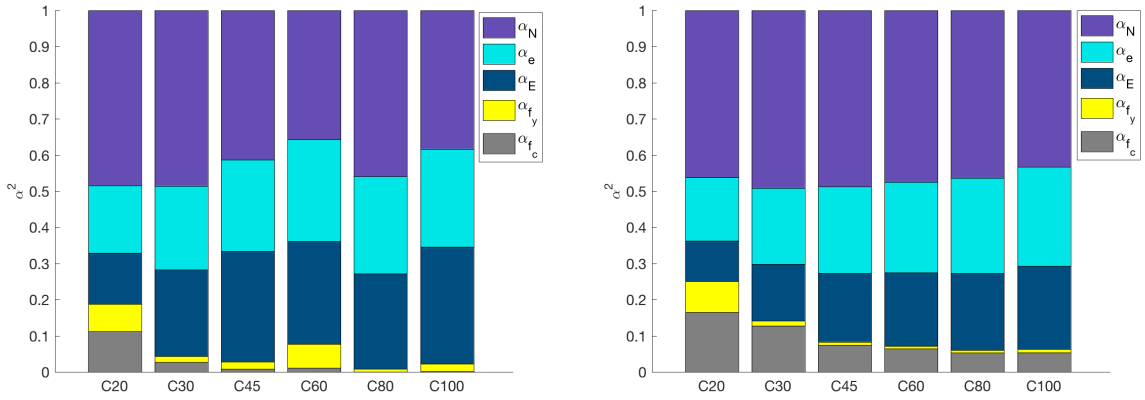

(a) No correlation *(b) With correlation*

Figure 6.28: Effect of correlation on sensitivity factors in the concrete grade analyses

Figure 6.29 shows how the resistance and load sensitivity factors vary with the concrete strength.

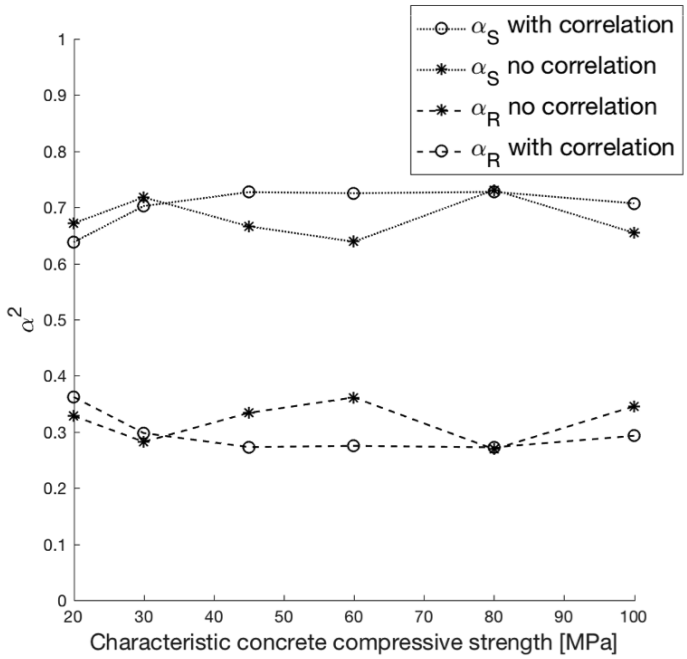

Figure 6.29: Effect of correlation among f_c and Ec on α_R and α_S for varying concrete grade

6.7 Column slenderness study

The results of the column slenderness study will be presented in the following section. First, the results of the analyses using the Eurocode 2 design capacity will be shown. Then the results of the inverse analysis and found PSFs are presented.

6.7.1 Reliability level Eurocode 2

Table 6.27 shows the resulting reliability index, and the equivalent reliability index obtained from RSM-FORM and RSM-SORM using NLFEA for varying column slenderness.

Length, l [m]	1.5	2	2.5	3	3.5	4	4.5
Slenderness, λ	34.6	46.2	57.7	69.3	80.8	92.4	103.9
Design eccentricity EC2 [mm]	43.8	45.0	46.3	47.5	48.8	50	51.3
EC2 Capacity [kN]	354.8	299.3	251.9	201.5	155.6	121.5	97.8
β	5.09	5.23	4.86	4.88	5.26	5.66	5.87
β_{eq}	5.13	5.27	4.81	4.92	5.22	5.58	5.90

Table 6.27: Results of RSM-FORM/SORM with NLFEA and EC2 capacity load for varying slenderness

6.7.2 Inverse analysis and PSF

All resulting design points and partial safety factors of the inverse analysis for different column slenderness are presented in Tables 6.28 and 6.29.

Length [m]	1.5	2.0	2.5	3.0	3.5	4.0	4.5
μ_N [kN]	430.0	364.3	295.5	241.5	195.2	162.0	136.0
f_{cd} [MPa]	36.08	38.49	40.93	44.10	46.47	47.73	48.34
f_{yd} [MPa]	521.07	522.22	523.01	524.57	525.61	525.92	526.74
E_{cd} [GPa]	31.30	30.04	28.39	27.43	26.90	27.02	27.08
e_d [mm]	40.9	42.7	44.9	46.8	49.0	50.9	52.8
N_d [kN]	685.8	584.7	472.6	383.2	306.0	251.9	210.3

Table 6.28: Design points of inverse RSM-FORM with NLFEA for varying slenderness

Length [m]	1.5	2.0	2.5	3.0	3.5	4.0	4.5
μ_N [kN]	430.0	364.3	295.5	241.5	195.2	162.0	136.0
γ_c [MPa]	1.25	1.17	1.10	1.02	0.97	0.94	0.93
γ_s [MPa]	0.96	0.96	0.96	0.95	0.95	0.95	0.95
γ_{cE} [GPa]	1.14	1.19	1.26	1.30	1.33	1.32	1.32
γ_G [kN]	1.59	1.60	1.60	1.59	1.57	1.55	1.55

Table 6.29: PSFs from inverse RSM-FORM with NLFEA for varying slenderness

Possible trends in the partial safety factors and sensitivity factors in the slenderness study are presented next. Figure 6.30 shows the sensitivities of resistance and load found in this study compared to the given sensitivities of Eurocode 2.

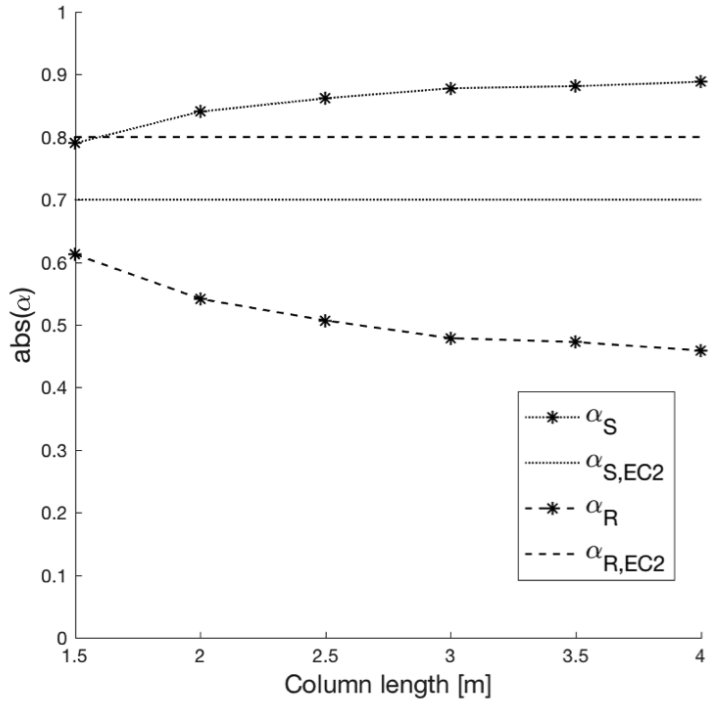

Figure 6.30: Trend in α_R and α_S for varying column slenderness

Figure 6.31a and Figure 6.31b presents the change in sensitivity factors and PSFs of each random variable respectively.

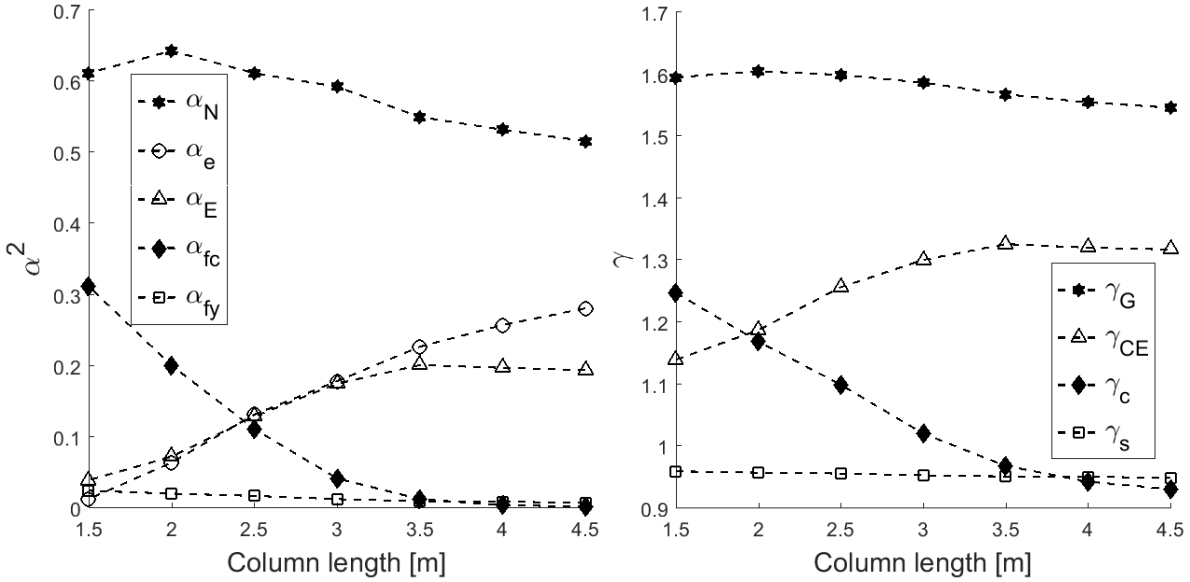

(a) Sensitivity factors *(b) Partial safety factors*

Figure 6.31: Trends for each random variable with varying column slenderness

The resulting work-diagram of the NLFEA for each slenderness, using the final design point values of the inverse RSM-FORM as input, can be seen in Figure 6.32.

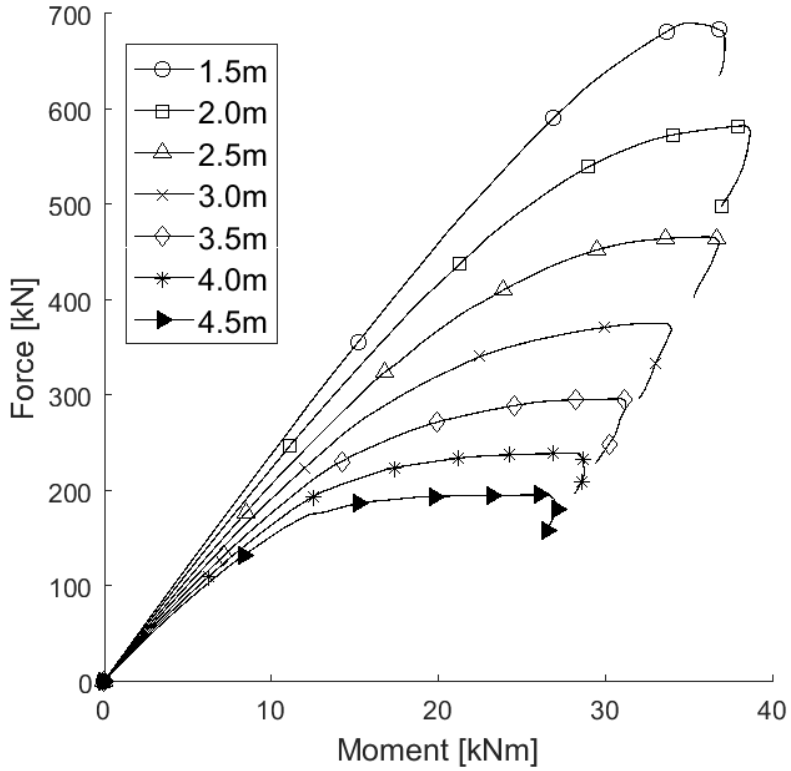

Figure 6.32: Work diagram for varying column slenderness using design values from inverse RSM-FORM with NLFE

6.8 Capacity distribution and model uncertainty

The model uncertainty was not explicitly quantified, but parts of what is needed to quantify the model uncertainty was found.

The probability of failure for the different load levels is plotted with the lognormal CDF fit in Figure 6.33a. The corresponding PDF is plotted in Figure 6.33b, which represent the distribution of the capacity achieved through NLFEA. The assumed density function of the experimental results is plotted as well, and the statistical properties of the distributions are given in Table 6.30.

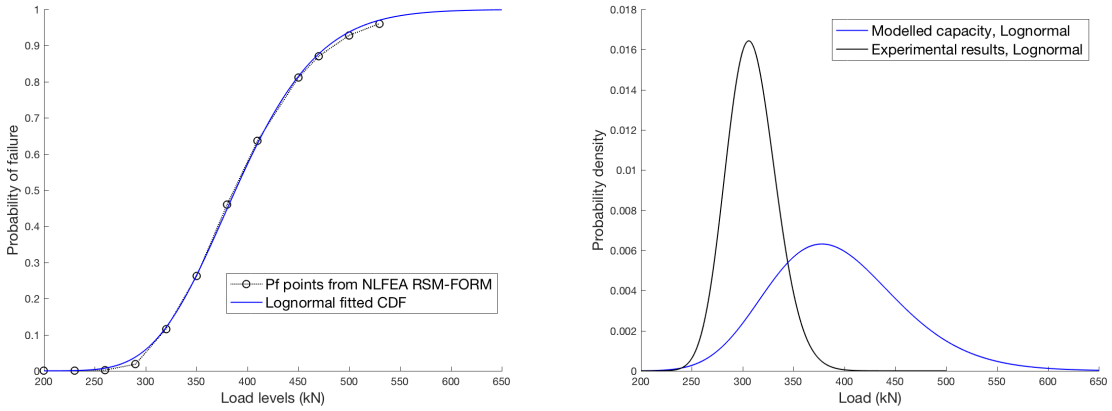

(a) Cumulative load distribution *(b) Probability density distributions*

Figure 6.33: Distributions of experimental and NLFEA capacities

	Mean	Standard deviation	Coefficient of variation
NLFEA	393.6kN	65.3kN	0.166
Experiments	308.9kN	24.5kN	0.079

Table 6.30: Statistical properties of the capacity from the experiments and NLFEA

7 Discussion

A discussion of the most important findings of the results is given in this section. The various design methods in the Eurocode and how the level of approximation affects the design capacity are reviewed first. Following, the best estimates and how both level of approximation and level of knowledge influence the estimates are discussed. A discussion of the various reliability methods will then be presented. A comparison between the methods is done first, and then the estimated reliability of Column A and B as well as different column setups is discussed. Some proposals for code revisions are also presented. Finally, the uncertainties that were included and left out in the reliability assessments, and how they influence the results is discussed.

7.1 Eurocode design capacity

The hand-calculations of Column A, as seen in Table 6.1, result in similar results for both the nominal curvature method and the nominal stiffness method. Looking at Figure 6.1, the two curves intersect at the point where they also meet the MN-diagram, hence the similar results. The same consistency in results is not as apparent when considering Column B. Larger deviations between the nominal curvature and nominal stiffness methods can be detected in Figure 6.2 and Table 6.2. The method of nominal stiffness results in an equal or lower capacity for Column B than Column A, an unrealistic result as column B is made of high strength concrete.

In Section 4.2 it was stated that the method of nominal stiffness was to an extent based on empirical curve fitted relations. These curve-fitted relations cannot be expected to fit concrete grades higher than the scope of the Eurocode, and thus the results of nominal stiffness applied to Column B are doubtfully accurate. Also, the concrete grade of Column B lies outside of the Eurocode 2 material scope, which might explain some of the variation in the results of Column B. Care should be taken when applying EC2 methods to concrete strengths higher than C90, though the nominal curvature method is considered most reliable of the two due to the more mechanical relations.

The level-of-approximation was increased in the design calculations by introducing a parabolic stress distribution instead of a linear stress distribution. This had just a slight impact on the results of Column A, and the assumption of constant stress in the compression zone seems to

be most feasible. For Column B, the difference between a linear and parabolic stress distribution was more apparent. This may be a result of the reduction factor η in the compression zone for higher strength concrete when assuming constant stress. Still, the small increase of capacity suggests that using more time to increase the accuracy of the stress distribution might be redundant, and that the assumption to use linear distribution in the reliability assessment is acceptable in this particular case.

The General method is of a higher LoA and generates higher capacities for both columns. The General method is expected to yield more accurate results than the hand calculation methods, and looking at the results in Section 6.1 it is apparent that the nominal stiffness and curvature methods are conservative estimations. The General method in EC2-2, GRFM, gives a more conservative capacity than the General method in EC2-1-1, PSF method, for both columns. This could be explained with the second basic criterion of safety formats in non-linear analyses, which the GRFM does not satisfy [10]. The second criterion requires that design safety formats are compatible with use of partial safety factors, which allows to place the material and geometric uncertainties where they are largest. GRFM rather divides the resulting capacity with an overall safety factor, γ_O. This reduction can be overly conservative since the material and geometric uncertainty is spread across *all* parts of the model, and is according to the EC2 commentary equivalent to dividing all parameters by a factor of γ_O. This results in a too severe reduction of the reinforcement strength and stiffness especially [10]. The proposal of Engen et al. [9] of allowing the analyst to distinguish the different sources of uncertainties to avoid too conservative estimates with a global resistance factor seems more appropriate.

The Eurocode 2 commentary [10] implies that the PSF method of EC2-1-1 is a better choice of safety format. The results found for the case handled in this thesis verifies these observations. However, when examining larger structural systems, NLFEA with the PSF safety format could be expected to increase the possibility of finding the wrong failure mode, because the relation between input material parameters are unrealistically scaled. This statement is supported in studies performed on larger concrete structures [15, 36], where a global safety format where the overall safety factor is calculated for each particular case is the preferred safety format.

Since the columns investigated in this thesis were statically determined and well fit with PSF method, a further study could be to fix the rotational degree of freedom to the bottom support

and see how the failure mode is affected. The PSF format is traditionally used on local member level checks, and it can be discussed whether PSF method is applicable to global checks when static redundancy is exploited through the NLFEA.

7.2 Best estimate

In Section 6.2, the results of the steps leading to the best estimate indicate a large increase in axial force capacity with increasing LoA. The estimated capacity, listed as "This report" in Table 6.4, is almost doubled compared to the design capacity found using EC2 hand-calculations. The increase in capacity is mainly found when transferring from hand-calculations to NLFEA. Applying mean values will also increase the capacity, but to a smaller degree as seen in Table 6.3 and Figure 6.3 for Column A, and Table 6.5 and Figure 6.6 for Column B. The difference between the three mean material sets is close to negligible for both hand-calculations and NLFEA. However, it is observed in Figure 6.4 that material sets with the highest concrete stiffness result in the highest capacities, which is as expected.

The results of the six experiments conducted by IABSE are shown in Figure 6.5a. The best estimate found in this thesis clearly overestimates the axial capacity determined by the experiments, while a better fit for the bending moment capacity is found. The non-linear finite element solution for the best estimate experiences a peak in the MN-curve before softening occurs until maximum bending moment is reached. This trend is not found in the experimental results. The experimental results deviate from the linear curve of $e_y = 40mm$ at an earlier stage than the best estimate found using NLFEA, indicating that there were more second order effects present than what is included in the estimate. From the material sensitivity study in Appendix B, Figure B.5, a similar work diagram to the experimental results could be achieved by lowering the concrete stiffness. The same effect was found by increasing the expected eccentricity, which could be done in compliance with the JCSS model.

Table 5.1-6 in the fib model code 2010 gives the qualitative change in the modulus of elasticity for different types of aggregate [4]. It lists lower E_c than used in this report for certain types of aggregate. A report made by the Norwegian Public Roads Administration (NPRA), addresses the high correlation between aggregates and the elastic modulus of concrete. The report concludes that the aggregate has a large effect on the concrete stiffness, with a difference up to 17 GPa after 90 days [37]. In the article by Strauss et al. [31], the statistical parameters for the

modulus of elasticity determined by experimental testing indicates lower E_c for C40 and C50 for 28 days than the value given in the EC2-1-1. As the aggregate type used in the experiments conducted by IABSE is unknown, direct conclusions are difficult to draw, but reducing the elastic modulus in simulations may result in more accurate results.

The eccentricity was adjusted to also take imperfections into account for Column B in order to reduce the overestimation of the capacity. This is recommended by the JCSS model code [3]. The difference between using $e = 40mm$ and $e = 48mm$ on Column B is shown in Figure 6.7. The difference in capacity and reduction of the softening branch is significant. This alteration could lead to a more accurate estimate of the Column B capacity, and a comparison with the experimental results would have been an interesting aspect regarding the Level-of-Knowledge concept. A Round-Robin study by van Mier and Ulfkjær [38] from 2000 was performed on high- and normal strength concrete beams. They found that the coefficient of variation of the calculated failure loads were 10% for the normal strength concrete beams, and much higher for the high-strength concrete. They concluded that improved constitutive models were needed with improved predictive qualities for these *new* high strength materials. Since Column B is of a high-strength concrete grade, the results may be expected to deviate a lot based on the above mentioned study. Further, as the current Round-Robin study by IABSE is performed on slender columns, even higher variations might be expected.

A comparison between the non-linear findings of other institutions compared to the findings of this thesis imply that most institutions overestimated the capacities as well. In Table 6.4 and Figure 6.5b the differences can be observed. The bending moment experiences a max deviation of 39.1% from the mean of all the results. The displacement differs up to 61.8% from the mean, while the axial force deviates with 18.6%. The results may be considered alarming, both in the non-conservative estimation of the capacity, and in the different capacity achieved by institutions possessing same precondition and knowledge of the problem. A similar Round-Robin study was conducted by Strauss et al. in 2015 [39], where the participants also overestimated the capacity. These findings show that when allowing for non-linear modelling in structural design, the model uncertainty must be in mind when reviewing the results. The large scatter in NLFEA results may indicate that the existing codes are difficult to interpret when trying to estimate realistic mean values of the material parameters.

7.3 Reliability

Reviewing the approximations to the limit state using five random variables in Figure 6.8, it is important to recall that no exact formulation of the limit states was computed. However, since the closed form limit state explicitly differentiates the two failure modes in an expected manner, they are used as guidance when judging how the other methods estimate the failure modes. As is shown in Figures 6.21, 6.22 and 6.23, the sensitivities of f_c and f_y when five variables are included are rather low, hence the random plot in Figure 6.8a. While in Figure 6.8b, where the random variables plotted have larger sensitivities, the analytic limit states and response surface seem to be approximated well to the MC results.

Taking a closer look at the results of the MC run with 5 random variables, seen in Figures 6.10 and 6.11, one can detect differences in probabilities of failure for Column A and B subject to the EC2 capacity load. As seen in Table 6.8, Column B does not have a reliability index higher than $\beta_T = 3.8$, and is considered unsafe. This may substantiate the mentioned caution necessary when considering concrete grades outside of the EC2 scope.

Since the MC method is based on the same iterative development of the MN-diagram as the analytic RS, their good fit is assumed to be no coincidence and serve as a satisfying validation of the RSM. The closed form LS differ from the analytic RS formulations in the way the yield failure is simplified, which may explain why it gives a slightly smaller failure area than MC. All analytic methods fit well to the Monte Carlo results in the proximity of the design point as shown in Table 6.6. The RS for RSM-FORM with NLFEA in Figure 6.16 fits well around the design point when compared to small sample MC, indicating that the RSM works as intended also when used with NLFEA. There are considerable differences in the analytic and NLFEA assessments, that will be discussed later, which means a direct comparison of the two methods is not particularly useful.

An important choice in reliability assessments is which parameters that should be regarded as stochastic variables, since neglecting important variables means leaving out significant sources of uncertainty. The most important trends when increasing the number of variables in the analyses are:

- Decreasing reliability β for RSM-FORM both analytic and with NLFEA as seen in Tables 6.22 and 6.23. This is caused by the introduction of more uncertainty with each variable.

- The failure mode tends to change from compression failure to yield failure, as seen in Figure 6.24, when variables connected to second order effects are included. This can be seen from the system reliability indexes in Table 6.21, where β is lowest for compression failure for two variables, but changes to yield failure when the concrete stiffness is added as a variable. From the FORM and RSM-FORM sensitivity factors displayed in Figures 6.21, 6.22 and 6.23 the random variables representing the second order effects govern the sensitivity when they are included, which substantiate the change to yield failure.

When doing reliability assessments on slender structures, it seems crucial to include probabilistic representations of parameters that are connected to second order effects.

When using only f_c and f_y as random variables, Figure 6.18 shows that the dominating failure mode could easily be altered by changing the design load. The analytic FORM and SORM are series systems, with a system reliability dependent on both failure limit states. In Table 6.18 one can see that the system reliability index equals the lowest reliability index of the two failure modes. A change between failure modes appears between 220 kN and 240 kN in this case. It appears that choosing the lowest β of the two failure modes is not introducing significant errors compared to finding a system reliability. However, it should be noted that errors might arise when the design points of the two limit states are closer together, since both limit states would affect the system probability of failure. This relate to the situation where probable failure occurs near the *balance point*, in the transition between compression and yield failure. This means that conducting reliability assessments with NLFEA without concerning the system reliability is acceptable when failure far from the balance point is expected.

Figure 6.20 shows that the analytic RSM was able to distinguish between the two failure modes as well, if adapted properly. As shown in Figure 5.8, great care was necessary to force the RS to fit the different failure modes. The RS presented in Figure 6.20a, showing compression failure, was only found by choosing an initial sample point closer to the actual design point. The study of the f-factor and initial sample point shown in Table 6.20 and Figure 6.19 confirms the larger errors in β is expected when using a large f-factor and an initial sample point far from the design point. The results also suggest that moving the initial sample point closer to the expected design point yields the same effect as reducing the f-factor. Still, when no information of the design point is known, a better approximation may be to reduce the f-factor.

Further, if the initial sample point is too close to the design point, in combination with a small f-factor and highly non-linear response, the resulting response surface *could* become incorrect. In extreme cases choosing mean values as starting points may be so far away from the design points that the RSM-algorithm does not converge. To solve these problems a qualified guess must be made, where the starting points should be in the correct quadrant of the design points.

As mentioned in Section 5.2.3, it was expected that SORM would result in more accurate results than FORM. Table 6.6 somewhat confirms these assumptions, since the difference in β compared to MC is less using analytic RSM-SORM than RSM-FORM for Column A. The FORM and SORM adaptions to the limit states and RS seen in Figures 6.13, 6.14 and 6.15 are quite similar. The RS and LS in standard normal space found for each method appear close to linear in the proximity of the design points. By comparing the inverse analytic RSM-FORM and RSM-SORM seen in Tables 6.15 and 6.16, a negligible difference in final design point is found between the two methods. In this case study, the difference in FORM and SORM was minor, and the use of SORM may be unnecessary. When RSM is used in conjunction with SORM, the errors of wrong curvature may become large. SORM takes the curvature of the response surface into account when calculating the probability of failure. This effect is magnified when the RS is highly non-linear and wrongly curved. This indicates that when the RS curvature is in any way uncertain, FORM is a safer choice. On the other hand, when the RS is curved correctly as in Figure 6.13, SORM fits the RS better and will give a more accurate probability of failure. As it is impossible to know a priori whether the curvature of the RS is correct, FORM in conjunction with RSM might be a more robust choice.

Table 6.11 shows that the RSM-FORM with NLFEA, when using design values from Eurocode 2, resulted in a reliability index of 5.28 and 5.31 for Column A and B respectively. The Eurocode design format is thus safe with this model. Compared to the analytic reliability assessments seen in Tables 6.9 and 6.10, the non-linear results indicate a significantly safer structure. There can be several possible reasons to this, and it is worth pointing out that the reliability assessments were run with the design load achieved from the *hand calculations*. These methods have proved to be more conservative than the non-linear assessments, and the design load that was compared was significantly lower than the design load of the non-linear analyses. When running the non-linear reliability assessments, the design load was on the safe side, which means a higher reliability index than from the analytic assessment should be expected. What

these calculations do is to control how reliable the hand calculation methods are, but by using a more realistic model to assess the reliability. The analytic reliability assessments use a more conservative model to assess the reliability, thus yielding a lower safety level. The reliability indexes from the concrete grade and slenderness study run with NLFEA were larger than the target reliability, as seen in Tables 6.24 and 6.27. This indicates that with the model used to validate the Eurocode safety format, the safety level seems adequate for a range of different setups. Still, the target reliability varies both regarding concrete strength and concrete stiffness.

An attempt at locating the source of the conservative capacity estimates in the analytic methods was made. A study of the MN-diagram is given in Appendix F, and concludes that for slender columns resulting in large second order effects combined with reinforcement yielding, the MN-diagram and NLFEA are in agreement. As the columns analyzed in this thesis mostly failed due to large second order effects, the MN-diagram does not seem to be the source of the conservative estimates. This suggests that the analytic definitions of the work diagram may be the source of the difference between the analytic and the non-linear finite element solutions.

The inverse analyses for Columns A and B are shown in Tables 6.12 and 6.13 for the different methods. These results show that the analytic assessments do not return as conservative results for the eccentricity, concrete stiffness and load as the NLFEA assessments. To fully capture the second order effects, non-linear models seems to be necessary. The inverse analytic FORM and SORM seen in Table 6.14, result in a reliability index of 3.8 for yield failure while the index for compression failure is slightly higher. This may indicate that buckling in combination with yielding in the reinforcement is the dominating failure mode in this study.

The inverse concrete grade study gave further insight to the sensitivity factors and partial safety factors. Figure 6.26 illustrates that for the lower concrete grades the sensitivity factor for f_c is significantly higher than for the higher concrete grades. At first it was suspected that this might have been a result of the correlation between f_c and E_c, but as Figures 6.28 and 6.29 show, the same trend can be observed when neglecting correlation. This suggests that the failure mode may be different for the lower concrete grades. As the concrete grade gets higher, the failure mode is transitioning from compression failure to yield failure. As a result of this, the safety factor for f_c is significantly larger for C20 and C30, while the other safety factors remain more or less constant across the concrete grades, as illustrated in Figure 6.26. The results of the

PSFs from the concrete grade study in Table 6.26 suggest that EC2 is conservative with regard to material parameters that govern the cross sectional resistance. The variables governing the second order effects on the other hand, are non-conservative.

The slenderness study revealed more non-linear trends in sensitivity factors and partial safety factors, as seen in Figure 6.31 and Table 6.29. For lower slenderness ratios the resistance parameters governing cross-sectional resistance are more important than the ones governing the second order effects. This is regarded as a logical outcome of the analyses. It can also be seen in Figure 6.32 that the the failure of the shorter columns are determined by cross sectional failure. The trends in partial safety factors are changing for column lengths longer than 3.5 m, indicating a transitioning from non-slender to slender columns. The second order effects are more dominant for these columns and the failure mode is yielding. For the columns that are 3.5 m and longer, the safety factors are stabilizing. It is possible that for even shorter columns, the safety factors would stabilize too. This provides one set of partial safety factors for non-slender columns, one set for slender columns, and a transition zone between the two. Based on these results, a new set of safety factors for slender columns are proposed in Table 7.1.

γ_G	γ_{CE}	γ_c	γ_s
1.60	1.35	1.00	1.00

Table 7.1: Proposed set of safety factors for slender columns

It should be emphasized that this proposal is only valid for the most slender columns, and a new slenderness limit should be defined. Table 7.1 is found based on concrete grade C45, but looking at Figure 6.26b, it may seem like changing the grade to high strength concrete would not effect the set of safety factors proposed. It is also important to keep in mind that these proposals may only be valid for this case study.

The sensitivities on the action- and resistance side shown in Figure 6.25 are deviating from the 0.8 and -0.7 given in the Eurocode [2], as the inverse concrete grade study yielded average values of 0.49 and -0.87 across the grades. This is also the case for different slenderness ratios, as shown in Figure 6.30. For the most slender columns, the load action sensitivity is even more on the unsafe side. The values set in the Eurocode are conservative approximations that need to cover a vast number of cases [40]. It was not expected that load and resistance sensitivities

would be exactly as in the Eurocode, since the squared sum of them do not add up to one, but one should expect to be on the safe side.

As explained in Section 5.5, no partial safety factor was calculated for the eccentricity. Still, the design point of inverse RSM-FORM with NLFEA present an eccentricity of 50 mm for both Column A and B, which corresponds well to the values calculated for imperfections in the Eurocode. Considering this modelled case, the Eurocode appears to cover the geometric uncertainties well. Extending the scope by considering several different column lengths, this conclusion does not change. The design eccentricities from inverse RSM-FORM given in Table 6.28 are close to the design eccentricities from EC2-1-1, presented in Table 6.27. The Eurocode is however slightly conservative for the shorter columns, and slightly non-conservative for the longer columns. Considering different concrete grades in Table 6.25, the same conclusion is drawn as the design eccentricity is close to the 50 mm in EC2-1-1.

It should be noted that the fixed number of load steps that was used for the NLFEA does not guarantee that the column is loaded to failure for extreme realizations of the material variables. It introduces some inconsistencies in the RSM-iterations since the capacity might be extracted at different points in the work diagram for different sampling points. As seen in Figures 6.27 and 6.32, the effect of stopping the NLFEA too early will not have a dramatic effect on the capacity for the more slender columns, because the slope in the work diagram is close to zero at the end of the analyses. The error will however increase when second order effects are smaller, that is for the shorter columns, low realizations of the eccentricity or high realizations of the concrete stiffness. Stopping the analysis early will be conservative, but might affect the distribution of the sensitivity factors. The risk of stopping the analyses prematurely for the shorter columns is small, as the number of load steps required to reach failure is much smaller than for the longer columns. A more robust solution strategy for the finite element analyses, ensuring that the column is loaded to failure for all realizations of the stochastic variables would have been beneficial. It would have to be accurate and stable in order to be applicable to probabilistic analysis. One possibility would have been to continue the analysis until some failure criterion is reached, e.g. when yielding occurs.

It was suspected that the descending branch in the work diagrams had an impact on the sensitivities of f_c and f_y. As the steel does not yield prior to the top point in the work diagram, see

Figure C.1, the capacity is to a greater extent governed by f_c when the descending branch is present. The parametric study in Appendix B showed that by reducing the concrete stiffness, the descending branch was reduced. Increasing the eccentricity had similar effect. As E_c is reduced and the eccentricity is increased through the RSM-FORM iterations, the descending branch may be reduced or even removed at some of the sampling points. If so, the sensitivity factor of the steel is increased. The same trend cannot be seen for the analytic solution, as the failure criterion in this case is given by the intersection of the MN-diagram and work diagram. In Figure 6.17 the difference in failure mode of non-linear and analytic solutions is shown for 2 variables, where the analytic methods get more affected by the yield failure mode. Had the failure criterion in the non-linear analyses been chosen differently, i.e. as the axial force at the point of maximum moment, these differences in the analytic and non-linear solution might have been less significant. Defining the failure criterion at the point of maximum axial force, and not at the point of maximum moment, is legitimate since moment is only a secondary effect dependent on the axial force. This is a model choice that should be addressed when reviewing and comparing the results, especially since the analytic assessments have a different criterion.

7.4 Uncertainties

There are large uncertainties involved when conducting the aforementioned analyses, and it is important to acknowledge that these results were only a product of the models that were used and the choices and assumptions that were made. Other analysts' estimates did not give the same results, as illustrated in Figure 6.5b. The large scatter in the non-linear finite element estimates of all institutions points to large modelling uncertainty across the different models. Note that the modelling uncertainty across different models should not be mixed with the model uncertainty within each model.

The best estimates that were presented in this report were not exact estimates, and could not be exact either, because the capacity is a random variable as well. The experimental results were only six realizations of this variable, as illustrated in Figures 6.5a and 6.33.

The sources of uncertainty from non-linear analyses is often divided into three parts; material, geometric and model uncertainty. The first two sources of uncertainty are assumed included by using the concrete strength and stiffness, the yield strength and the eccentricity as basic variables, where the eccentricity carries the geometric uncertainty. The model uncertainty is

more complex [33], and was not included in the probabilistic model. This may be an important reason as to why the non-linear assessments resulted in high reliability indexes.

Since the finite element program seemed to overestimate the capacity of the column, a systematic error is introduced in the probabilistic model, resulting in a biased result. Similarly, the analytic calculations underestimated the column capacity. To alleviate this bias, it would be appropriate to take model uncertainty into account.

A procedure to calculate the statistical properties of the model uncertainty, Θ, was proposed in Section 5.6. This procedure turned out to be inadequate due to the distributions shown in Figure 6.33b. The model uncertainty parameter is supposed to be a scaling to make the NLFEA distribution fit the experimental distribution. However, as seen in Table 6.30, the experimental standard deviation is less than for NLFEA in this study, so a scaling to make the NLFEA curve fit the experimental curve is currently not possible.

The reason why there is such a difference in standard deviations can be investigated by considering the basic variables in the probabilistic model. When the experiments were conducted, it is likely that the same batch of concrete was used, and that the reinforcement originated from the same manufacturer. It is also likely that the same formwork was used and that the load application was done almost identically for all columns. This reduces the variations in the experiments drastically. Reviewing the results in Figure 6.5a more closely, the main reason that there is scatter in the experimental capacities is the casting direction.

If the model uncertainty is to be assessed for this case, the insitu material properties should be measured and implemented in the probabilistic model, and only variation within a batch should be included if that is the case. The coefficient of variation for concrete used in this model was the recommended value from the Eurocode, which also covers other uncertainties than variation within a batch. In addition, the variation in the eccentricity was probably significantly larger than in the experimental setup. In principle, all uncertainties but the model uncertainty should be attempted reduced when finding a model uncertainty parameter. This is difficult because there is always variations such as in the concrete strength within a batch. Still, when IABSE publishes the material sample tests and more information about the setup, a suggestion to the model uncertainty may be assessed in the future. This matter is relevant in structural reliability and is presented as a suggestion for Further Work.

8 Conclusion

The main objective of this thesis was to investigate how reliable the Eurocode methods are when applied on slender structures, with the use of NLFEA. These results were further used to give proposals to changes in design of slender structures. To reach this goal, defining material properties, creating a reliable finite element model and implementing good and efficient reliability assessment procedures were some important milestones. Since the scope of this project was comprehensive, several conclusions can be made in the different steps of achieving the final goal.

The hand-calculation methods proposed for calculation of slender columns in EC2-1-1, called nominal stiffness and nominal curvature, are highly conservative methods. Although the lowest levels of approximations by principle should be conservative, usage of these methods may lead to a lot costlier design than necessary. When the scope of the Eurocode is near being exceeded, the method of nominal curvature is recommended since it is the less empirically founded method of the two.

Since the new proposals of safety formats in non-linear analyses tend to involve applying mean parameters as input, and divide the output resistance by a global safety factor, some clear guidelines as to how to extract mean parameters are needed. Today the designer must interpret the codes individually to convert design parameters and relations to a corresponding mean. The individual interpretations lead to, in combination with other model choices, a large scatter in final estimates from different institutions in the case of the Round-Robin study.

In the post-processing of the model used to give a best estimate, that also was used in the reliability assessments, some other weaknesses to the Eurocode unfolded. With a model that is based on mean values, EC2 does not explicitly account for imperfections. If the Eurocode is to be used with a global resistance factor format, imperfections are left out of the calculations. Another possible source of bias caused by the Eurocode was the concrete stiffness value. Several sources [37, 4, 31], state that the modulus of elasticity of concrete is over-estimated in the Eurocode. The findings in this project supports that the concrete stiffness may be lower than what is stated in the Eurocode, since the model accuracy increased when the stiffness was reduced. Reexamining the concrete stiffness should be a priority in the construction of new codes, especially for slender structures where the stiffness has a large impact.

The Response Surface Method is a convenient method to evaluate the limit state when NLFEA is necessary in reliability assessments. Still, the computational time of the finite element model should be sufficiently short, and optimizing the process to the specific case regarding sampling and inclusion of polynomial terms is beneficial. There were spotted some drawbacks in the method's sensitivity which indicate that the RSM is the *weakest link* of the assessment procedure. Having a physical understanding of the limit state beforehand is crucial. If the RS is highly non-linear, the f-factor should be relatively large to avoid spurious distortions of the RS. In such a case, it could be advantageous that the initial sampling points are farther from the design points to cover the overall trend of the curve.

When there are several relevant failure modes, it is beneficial to have an idea of which is the relevant one for the case studied. The initial sampling points and f-factor can then be chosen in such a way that the RS does not get affected by the other failure modes, to avoid influence that may cause the RS to curve wrongly. Using a smaller f-factor and initial sample points closer to the design point is consequently a good strategy in these cases. This last point is particularly important when RSM is used in conjunction with SORM, since SORM takes the RS curvature into account when evaluating the probability of failure. If the analyst is unsure about the curvature of the RS, FORM is the safer reliability method.

Regarding the considerable modelling uncertainty that was left out of the reliability assessments, a general conclusion should not be drawn as to whether the Eurocode reliability level is sufficient. Nevertheless, the results given no modelling uncertainty can be used to spot trends and weaknesses in the design format that is used today.

In general, it is seen that when second order effects are present, the Eurocode may allocate too much sensitivity to the resistance, and too little to the action effects. It seems evident that for slender columns, it is advantageous to propose a new set of safety factors that are calibrated to consider the second order effects. In general, safety factors associated to second order effects should be increased, and safety factors associated to the cross-sectional resistance may be decreased or set to one.

9 Further work

When examining the different safety formats of the General Method in Eurocode 2, it was suggested that the PSF method of EC2-1-1 could yield wrong failure mode in NLFEA for undetermined structures because static redundancy can be treated wrongly with unrealistic material parameters. For further work, the rotational degree of freedom in the bottom support could be fixed and investigate whether the failure mode of the PSF method and GRFM would differ. An approach to the problem could be to find a range of lengths where the failure mode differs in the two safety formats for an undetermined structure. An extended approach could be to address larger structures such as a frame.

The model uncertainty, Θ, was not included in the reliability analyses due to time constraints. It is recommended to incorporate the model uncertainty as a random variable in similar work in the future, since it is suspected to be an influential parameter. The response surface would then be on the form $\mathbf{R} = \Theta\mathbf{Ab}$. The mean and standard deviation of the model uncertainty could either be retrieved from literature, or calculated as proposed in this thesis if the necessary information about the uncertain parameters are given. It is important that the model uncertainty is implemented adequately. If an unsuitable Θ is used, one may experience the unwanted event that an advanced method gives a more conservative result than a simpler method.

Another aspect of interest for further work is to reduce the RS sensitivity by including an error term, ε, to the RS definition. The error term is a stochastic variable that can be expressed by two moments. The RS will then be defined as $\mathbf{R} = \Theta[\mathbf{Ab} + \varepsilon]$, when the model uncertainty also is included.

Although neglecting system reliability seemed to have negligible effect on the failure probability in this thesis, it is a relevant study for further work to implement a solution strategy for NLFEA that takes system reliability into account. The finite element program would need to be altered such that the different failure modes are imposed, and then assess each respective probability of failure through reliability methods.

10 References

[1] A Strauss and V Benko. *Safety Formats RC columns design based on stochastic simulations*, 2017.

[2] CEN. *Eurocode 2: Design of concrete structures — Part 1-1: General rules and rules for buildings*, April 2004.

[3] Joint Committee on Structural Safety. *JCSS Probabilistic Model Code*. Technical University of Denmark, 2015.

[4] fib. *Model Code 2010*. The International Federation for Structural Concrete, 2012.

[5] Jonna Manie. *DIANA-10.1 User's Manual*. DIANA FEA BV, 2015.

[6] Jörg Schneider. *Introduction to safety and reliability of structures*. IABSE-AIPC-IVBH, 2006.

[7] Paul. A. Lagace. Unit m4.7, the column and buckling. Lecture note - Unified Engineering, 2009. Department of Aeronautics and Astronautics, MIT.

[8] Svein Ivar Sørensen. *Betongkonstruksjoner - Beregning og dimensjonering etter Eurocode 2*. Akademika forlag, 2013.

[9] Morten Engen, Max A.N. Hendriks, Jan Arve Øverli, and Erik Ålstedt. Reliability assessment of a large concrete structure making use of nonlinear finite element analysis. *Proceedings from the 2nd Concrete Innovation Conference, Tromsø, Norway*, 2017.

[10] JP Jacobs. *Eurocode 2 Commentary*. European Concrete Platform ASBL, June 2008.

[11] M.A.N Hendriks, J.A. den Uijl, A. de Boer, P.H. Feenstra, B. Belletti, and C. Damoni. *Guidelines for Nonlinear Finite Element Analysis of Concrete Structures*. Rijkswaterstaat Centre for Infrastructure, May 2012.

[12] R. J. Torrent. The log-normal distribution: A better fitness for the results of mechanical testing of materials. *Materiaux et Constructions*, 11(64), 1978.

[13] MathWorks. Half-normal distribution, May 2017.

[14] CEN. *Eurocode: Basis of structural design*, April 2010.

[15] Hendrik Schlune, Mario Plos, and Kent Gylloft. Safety formats for non-linear analysis of concrete structures. *Magazine of Concrete Research*, 64(7):563–574, 2012.

[16] CEN. *Eurocode 2: Design of concrete structures — Part 2: Concrete bridges — Design and detailing rules*, April 2005.

[17] Sanjay Govindjee, Gregory J. Kay, and Juan C. Simo. Anisotropic modelling and numerical simulation of brittle damage in concrete. *International Journal for Numerical Methods in Engineering*, 38:3611–3633, 1995.

[18] P.H Feenstra. *Computational Aspects of Biaxial Stress in Plain and Reinforced Concrete*. Phd thesis, Delft University of Technology, November 1993.

[19] F. J. Vecchio and M. P. Collins. Compression response of cracked reinforced concrete. *Journal of Structural Engineering*, 119(12):3590–3610, 1993.

[20] Kjell Magne Mathisen. Lecture 2: Solution of nonlinear equilibrium equations. Lecture notes in TKT4197 at Norwegian University of Science and Technology, 2016. Department of Structural Engineering, NTNU.

[21] E. Basler. Untersuchungen $\ddot{u}$ber den sicherheitsbegriff von bauwerken. *Schweizer Archiv $f\ddot{u}$r angewandte Wissenschaft und Technik*, 4, 1961.

[22] A.C. Cornell. A probability based structural code. *ACI Journal No. 12*, 1969.

[23] A.M. Hasofer and N.C. Lind. Exact and invariant second-moment code format. *Journal of the Engineering Mechanics Division*, 100, 1974.

[24] Finn-Idar G. Giske, Bernt Johan Leira, and Ole Øiseth. Long-term extreme response analysis of marine structures using inverse sorm. *Proceedings of the ASME 2017 36th International Conference on Ocean, Offshore and Arctic Engineering*, 2017.

[25] COMREL 9.0.0. Strurel software, May 2017.

[26] C.G. Bucher and U. Bourgund. A fast and efficient response surface approach for structural reliability problems. *Structural Safety*, 7:57–66, 1990.

[27] Malur R. Rajashekhar and Bruce R. Ellingwood. A new look at the response surface approach for reliability analysis. *Structural safety*, 12(3):205–220, 1993.

[28] Jorge Rebaza. *A First Course in Applied Mathematics*. John Wiley & Sons, 2012.

[29] Lucia Faravelli. Response-surface approach for reliability analysis. *Journal of Engineering Mechanics*, 115(12), 1989.

[30] Jochen Köhler. L07 - system reliability. Lecture notes - Safety Aspects in Civil Engineering, 2016. Department of Structural Engineering, NTNU.

[31] Thomas Zimmermann, David Lehký, and Alfred Strauss. Correlation among selected fracture-mechanical parameters of concrete obtained from experiments and inverse analyses. *Structural Concrete*, 17(6):1094–1103, 2006.

[32] Jochen Köhler. L06 - introduction to structural reliability - first order reliability method. Lecture notes - Safety Aspects in Civil Engineering, 2016. Department of Structural Engineering, NTNU.

[33] Morten Engen, Max A.N. Hendriks, Jochen Köhler, Jan Arve Øverli, and Erik Åldstedt. A quatification of the modelling uncertainty of non-linear finite element analyses of large concrete structures. *Structural Safety*, 64:1–8, 2017.

[34] Edward B. Haugen. *Probabilistic Approaches to Design*. John Wiley & Sons, 1968.

[35] Jochen Köhler. L10 - code calibration, design assisted by testing. Lecture notes - Advanced Structural Design, 2016. Department of Structural Engineering, NTNU.

[36] Mario Pimentel, Eugen Bruhwiler, and Joaquim Figuiras. Safety examination of existing concrete structures using the global resistance safety factor concept. *Engineering Structures*, 70:130–143, 2014.

[37] Bård Pedersen and Reidar Kompen. Compressive strength and e-modulus of sv-40 concrete. Technical Report 177, Norwegian Public Roads Administration, December 2013. A study on the impact of aggregates.

[38] J. G. M. van Mier and J. P. Ulfkjær. Round-robin analysis of over-reinforced concrete beams - comparison of results. *Materiaux et Constructions*, 33:381–390, 2000.

[39] Alfred Strauss, Thomas Eschbacher, Peter Kendický, and Vladimir Benko. Tragkapazität schlanker druckgleider. *Beton- und Stahlbetonbau*, 12:845–856, 2015.

[40] Jitao Yao and Kaikai Cheng. Discussion of sensitivity factors and dominating variable for design value method. *KSCE Journal of Civil Engineering*, 21:37–44, 2017.

A Blueprint

The drawings produced by IABSE can be found in the following pages. The two drawings only differ in type of concrete grade. The first document corresponds to the column with concrete grade C45, while the second drawing belongs to the column of concrete grade C100. The drawings are produced by engineer Marian Kisăc and therefore written in Slovak.

REZ A-A
M 1:5

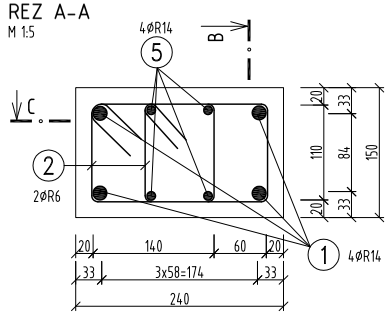

REZ D-D
M 1:5

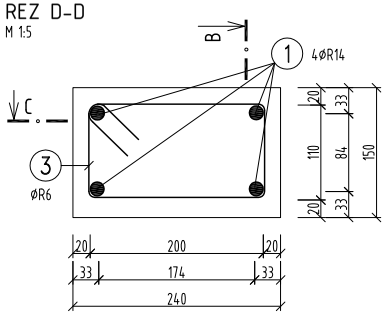

STĹP S 1.1

TVAR
M 1:25

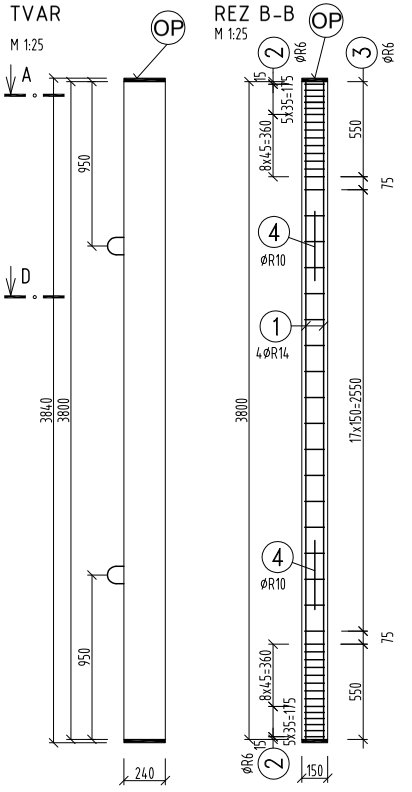

REZ B-B
M 1:25

REZ C-C
M 1:25

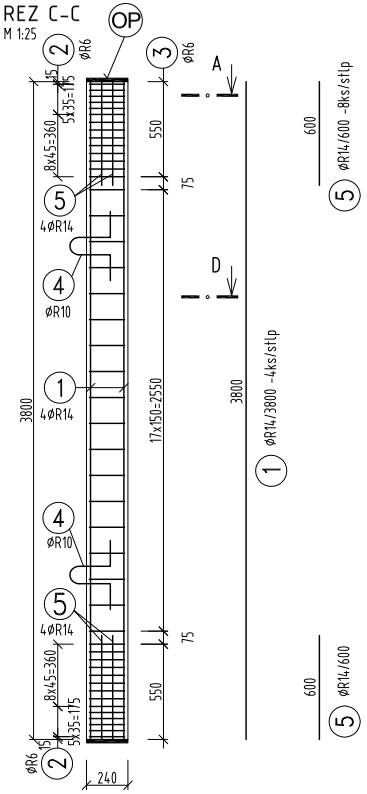

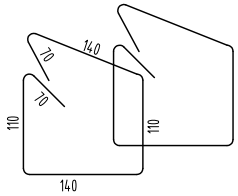

2 ØR6/640 -56ks/stlp

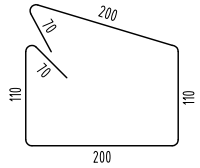

3 ØR6/760 -18ks/stlp

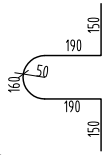

4 2ØR10/840 -2ks

OP OCEL. PLATNICKA 240/150/20, SPOLU 2x5,7=11,4kg

ŠPECIFIKÁCIA VÝSTUŽE-OCEĽ B 500B

CISLO PRUTA	ø PRUTA (mm)	DLZKA PRUTA (m)	POCET	CELKOVA DLZKA (m)		
				ø6	ø10	ø14
1	14	3.80	4			15.20
2	6	0.64	56	35.84		
3	6	0.76	18	13.68		
4	10	0.84	2		1.68	
5	14	0.60	8			4.80
SPOLU	DLZKA m			49.52	1.68	20.00
	HMOTNOS? kg/m			0.222	0.617	1.208
	HMOTNOS? kg			10.99	1.04	24.16
	HMOTNOS? kg			36.19		

BETÓN: 0,137m^3

Poznámky:

Stĺpy betónovať vo vodorovnej polohe položené na užšej hrane (150mm)

Výstuž č.(5) privariť k oceľovej platni

Jednotlivé položky výstuží sú kótované vonkajšími rozmermi

HMOTNOSŤ 342,5kg
BETÓN C45/55 KRYTIE 20mm
OCEĽ B 500B VYHOTOVIŤ 7x

SKÚŠOBNÁ VZORKA STĹP S 1.1	
VÝKRES TVARU A VÝSTUŽE	M 1:25 M 1:5 FORM.: 2 x A4
VYPRACOVAL : Ing. Marian Kišac 10.2013	C.V.: 1

REZ A-A
M 1:5

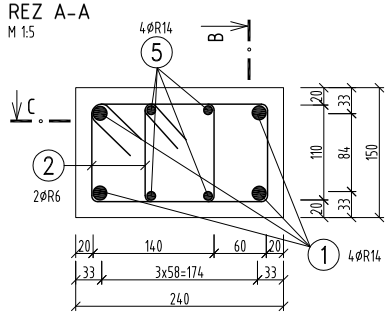

REZ D-D
M 1:5

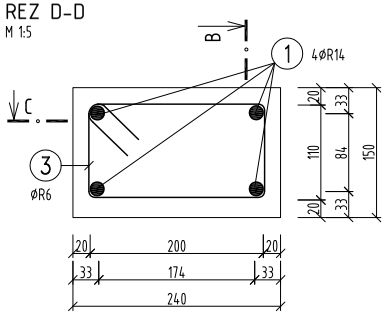

STĹP S 1.1

TVAR
M 1:25

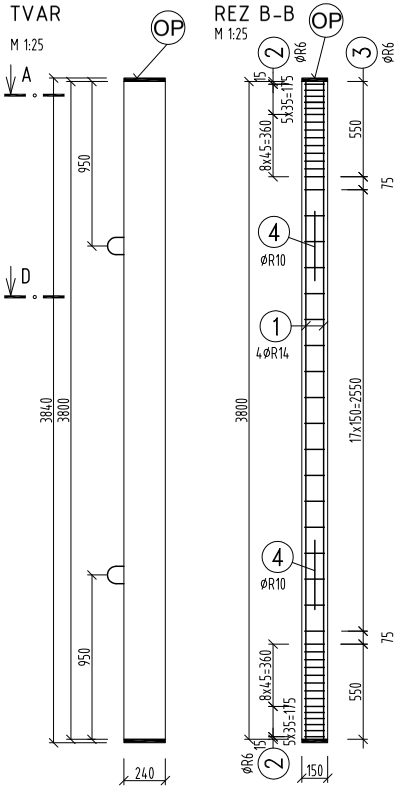

REZ B-B
M 1:25

REZ C-C
M 1:25

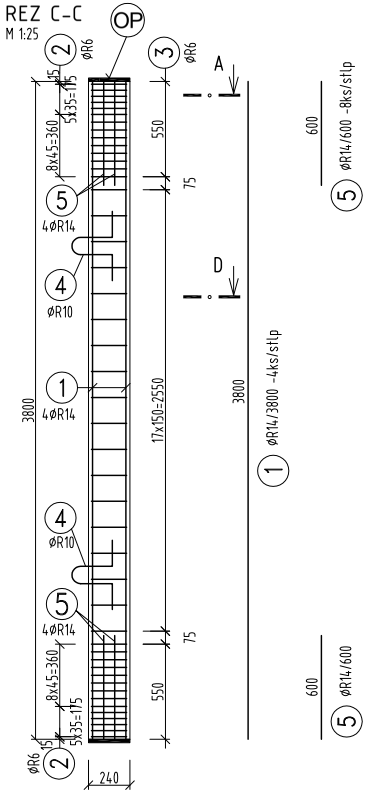

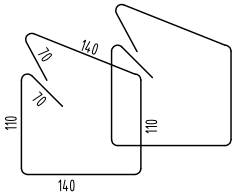

2 ØR6/640 -56ks/stlp

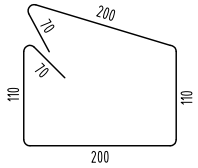

3 ØR6/760 -18ks/stlp

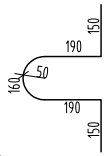

4 2ØR10/840 -2ks

OP OCEL. PLATNICKA 240/150/20, SPOLU 2x5,7=11,4kg

ŠPECIFIKÁCIA VÝSTUŽE-OCEĽ B 500B

CISLO PRUTA	ø PRUTA (mm)	DLZKA PRUTA (m)	POCET	CELKOVA DLZKA (m)		
				ø6	ø10	ø14
1	14	3.80	4			15.20
2	6	0.64	56	35.84		
3	6	0.76	18	13.68		
4	10	0.84	2		1.68	
5	14	0.60	8			4.80
SPOLU	DLZKA m			49.52	1.68	20.00
	HMOTNOS? kg/m			0.222	0.617	1.208
	HMOTNOS? kg			10.99	1.04	24.16
	HMOTNOS? kg			36.19		

BETÓN: 0,137m^3

Poznámky:

Stĺpy betónovať vo vodorovnej polohe položené na užšej hrane (150mm)

Výstuž č.(5) privariť k oceľovej platni

Jednotlivé položky výstuží sú kótované vonkajšími rozmermi

HMOTNOSŤ 342,5kg
BETÓN C100/115 KRYTIE 20mm
OCEĽ B 500B VYHOTOVIŤ 6x

SKÚŠOBNÁ VZORKA STĹP S 1.2	
VÝKRES TVARU A VÝSTUŽE	M 1:25 M 1:5 FORM.: 2 x A4
VYPRACOVAL : Ing. Marian Kišac 10.2013	C.V.: 2

B Parametric study

A thorough parametric study was performed in the process of developing a NLFE model of the problem. The parameters assumed to have a large impact on the resulting solution are the following.

- Boundary conditions and load application
- Finite element discretization
- Analysis procedure
- Material parameters

B.1 Method

A basis model was developed to test the sensitivity of change in different parameters. All parameters were kept constant except for the parameter in focus, and the response was compared to the basis model. The set parameters for the basis model are shown in Table B.1.

Parameter	Basis model
Element class	Solid
Element size	$\frac{b}{5}$
Interface	No interface
Load application	Prescribed displacement (Line load)
Symmetry	Horizontal symmetry plane
Material model	Model A, see Table 3.2
Iteration method	Full Newton-Raphson
Max no. iteration	30
Convergence criteria	Displacement (0.01) Energy (0.001)
Load steps	Size: 0.05 Number: 20
Analysis	Non-linear analysis
Solution method	Sparse Cholesky

Table B.1: Set parameters for the basis model

As a start, the parametric study considered the boundary conditions and load application parameters listed in Table B.2. The first parameter tested in the study was the use of a symmetry plane, as this would highly affect the CPU time of the analysis. From knowledge of the exper-

imental setup, see Figure 2.4, a line load was assumed to be the most accurate. Nevertheless, an analysis applying a point load was run to control and compare the stress distribution from the platens to the column. An analysis with the use of force control instead of displacement control was also run. The effect of an applied interface was tested in the parametric study. A divided interface able to demonstrate the welded connection between the four center bars of the longitudinal reinforcement and the platens was developed and controlled by a tension test before being applied to the compression analysis.

Symmetry	Load application	Interface
No symmetry	Line load (10mm displacement)	No interface
Horizontal symmetry plane	Point load (10mm displacement)	Divided interface
	Line load (100kN force)	Full interface

Table B.2: Parametric variables for the boundary conditions and load application

The choice of finite element discretization was a part of the parametric study as well. The change in parameters can be found in Table B.3. As mentioned in Section 4.4, three models of different element types were developed; 3D solid, 2D plane stress and 2D beam elements. It was assumed more accurate results for the 3D solid model, therefore the objective of this part of the parametric study was to verify satisfying results in comparison to the 3D model for the two latter models. The sensitivity of the mesh size was tested using the three maximum values from Guidlines of NLFEA [11] shown in Equation (4.8), and a lower value of $h/6$.

Element type	Element size
3D solid	$\frac{h}{5} = 30mm$
2D plane stress	$\frac{l}{50} = 76mm$
2D beam	$\frac{b}{5} = 48mm$
	$\frac{h}{6} = 25mm$

Table B.3: Parametric variables for the finite element discretization

The model was tested with several analysis procedure parameters, as listed in Table B.4, to determine the model sensitivity as well as the change in CPU time. Four different iteration methods were tested, and changes in load step sizes were applied. The convergence criteria used for the basis model is considered too loose, thus the criteria were tightened one-by-one

and both at the same time. Considering the use of an energy criterion, line search was not applied [20].

Iteration method	Convergence criteria	Load steps
Full Newton-Raphson	Displacement = 0.01 - Energy = 0.001	Size: 0.05 - Number: 20
Modified Newton-Raphson	Displacement = 0.001 - Energy = 0.001	Size: 0.10 - Number: 10
Secant Newton (BFGS)	Displacement = 0.01 - Energy = 0.0001	Size: 0.03 - Number: 34
Secant Newton (Crisfield)	Displacement = 0.001 - Energy = 0.0001	Automatic

Table B.4: Parametric variables for the analysis procedure

The material parameters applied to the model were assumed to have a large influence on the result. Therefore, a more refined study was done to the material parameters to further determine the sensitivity of each single parameter. The parameters listed in Table B.5 were in turn varied between the max and min values of the material sets developed throughout Section 4.2 and 4.3.

Parameter	Variation
f_{ck}	35 - 55 MPa
G_f	0.135 - 0.152 N/mm
f_y	450 - 550 MPa
f_t	2.0 - 4.0 MPa
E_c	28 - 45 GPa
E_s	180 - 300 GPa

Table B.5: Parametric study on the material parameters

B.2 Results and discussion

The results of the parametric study considering the boundary conditions and load application are shown in Figure B.1. By reducing the problem using a symmetry plane, the CPU time was reduced by 60%. The failure pattern seems to be symmetric and equivalent to the total model. There appeared to be close to no difference between applying a line load or a point load, and the check of stress distribution was satisfying for both situations. Using force control instead of displacement control led to large differences in maximum axial force, but the solution using force control led to a considerable increase in CPU, from 12 min to approximately 1 hour.

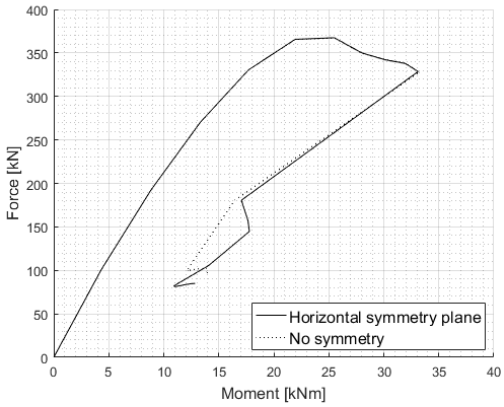

(a) Symmetry

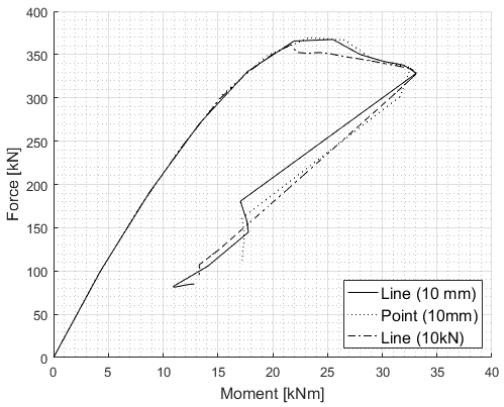

(b) Load application

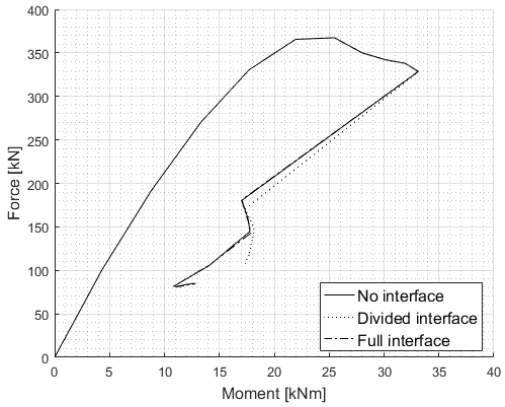

(c) Interface

Figure B.1: MN-diagram from parametric study on boundary conditions and load application

The application of different interfaces had negligible effect on the analysis result. The CPU time was unchanged and by studying the deformation plots from the tension test in Figure B.2, the wanted behaviour was obtained. Using a divided interface in the following analysis seemed to be a no regret option.

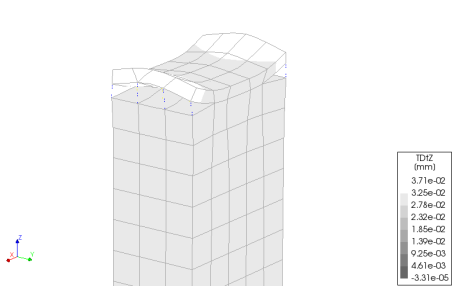

(a) Loaded part of column

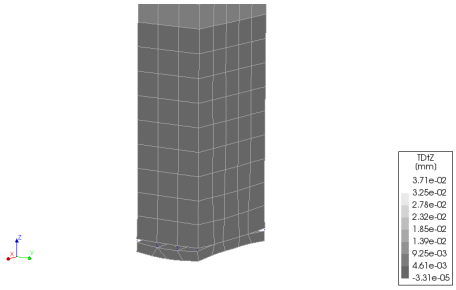

(b) Support

Figure B.2: Tension test: Contour plot of deformation in z-direction

Figure B.3 shows the results of the parametric study performed on the finite element discretization. As expected the difference between element types is noticeable, but a good relation between the 3D solid and 2D plane stress model was promising in regard to reducing CPU time. The 2D plane stress and 2D beam models reduced the CPU time by 93% and 95% respectively compared to the 3D model.

Using a smaller element size only seems to lift the point of maximum axial force while the remaining parts of the curve indicates a similar behaviour. The CPU time is notably increased by the reduction of element size and indicates a need to restrict further reduction to avoid excessive costs. Still, as recommended in Guidelines for NLFEA, the maximum element size should be set to $h/5 = 30mm$, and the larger elements as $b/5 = 48mm$ and $l/50 = 76mm$ should be avoided.

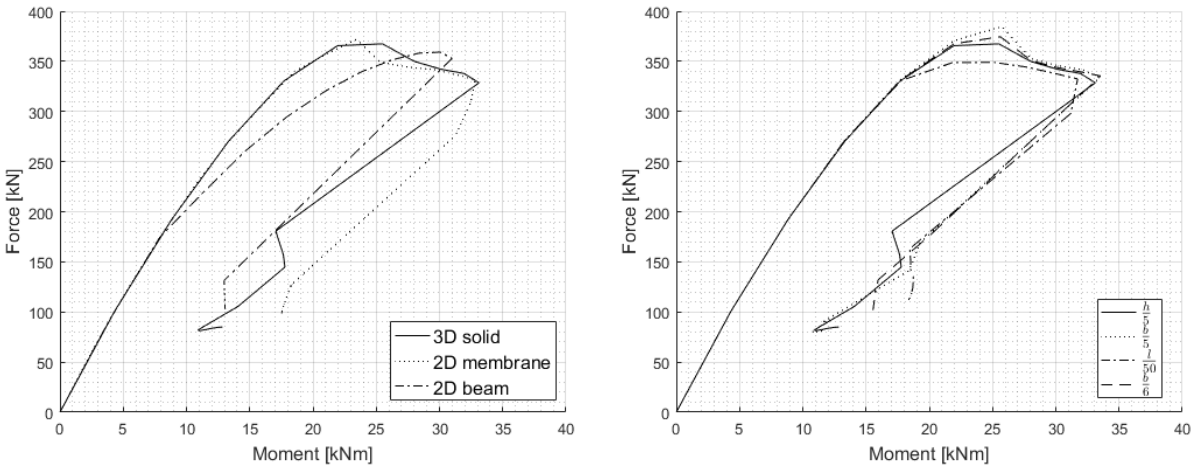

(a) Element type *(b) Element size*

Figure B.3: MN-diagram from parametric study on finite element discretization

The results of the parametric study on the analysis procedure are displayed in Figure B.4. The iteration method of Modified NR diverged around the failure point of the problem and was discarded in further analysis. The Full NR method converged in each step while the two methods of Secant Newton were unable to reach convergence at the point of maximum axial force and at failure. Considering the similar use of CPU time and the stability of the Full NR method, a choice was made to further use this method in continued analysis.

The basis model used convergence criteria considered as too loose, and naturally all steps in the analysis converged. Using tighter convergence criteria led to a slightly lower MN-curve. For

a tighter energy criteria all steps converged, leading to the conclusion that the loose displacement criterion is dominating. When tightening the displacement criterion convergence was still achieved in all points before failure, while points after never reached convergence. The CPU costs were increased, but to a smaller degree when tightening the criterion.

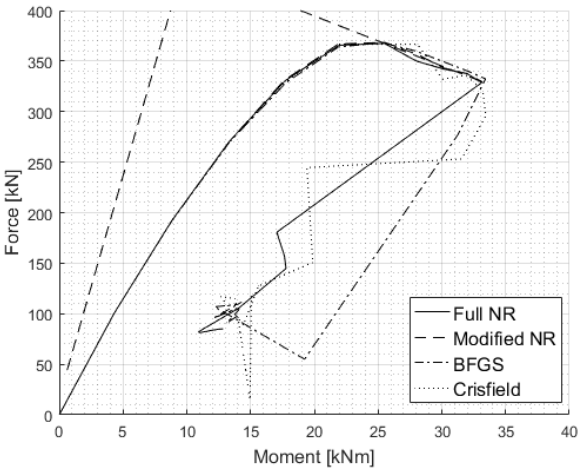

(a) Iteration method

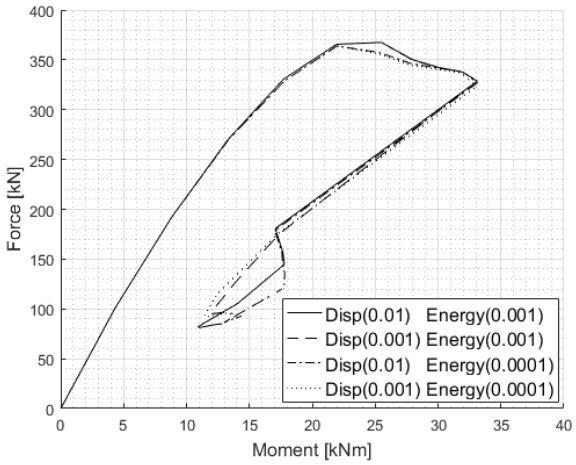

(b) Convergence criteria

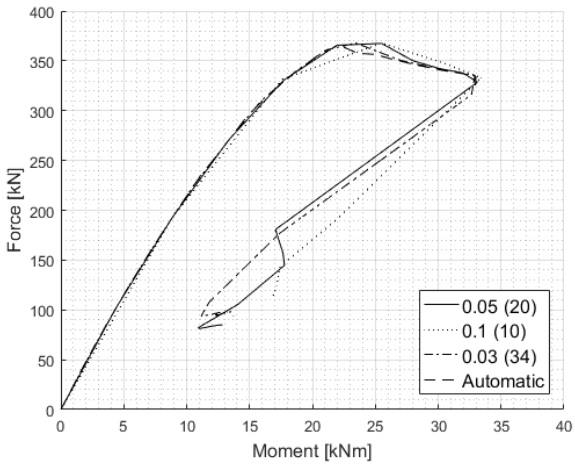

(c) Load steps

Figure B.4: MN-diagram from parametric study on analysis procedure

The results of the parametric study for the material parameters can be seen in Figure B.5. It's worth mentioning that the analysis was run with the 2D plane stress model using smaller load steps and finer mesh than for the basis model. The four parameters having a distinct impact on the response are f_c, f_y, E_s and E_c.

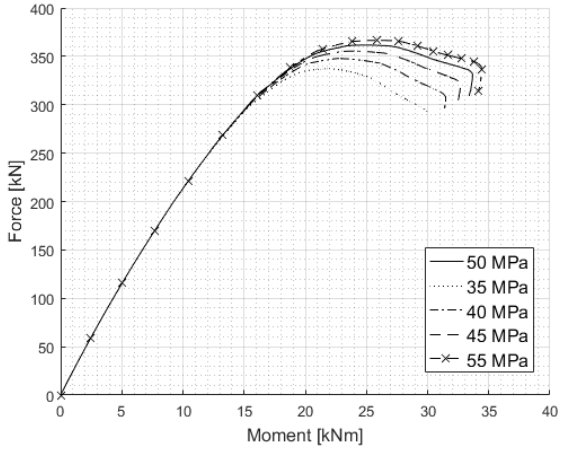

(a) Concrete compressive strength f_c

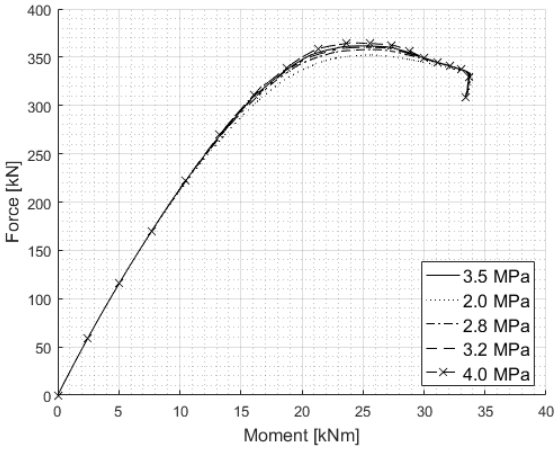

(b) Concrete tensile strength f_t

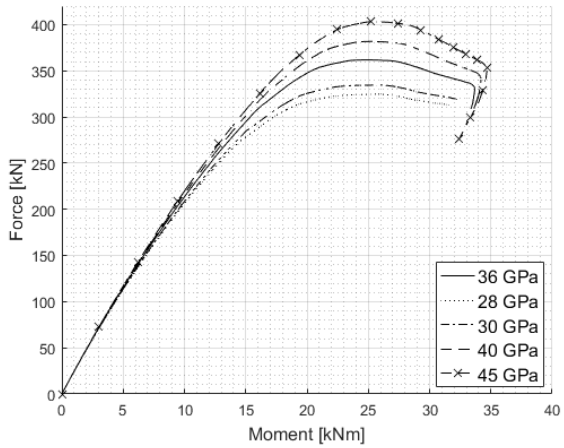

(c) Concrete stiffness E_c

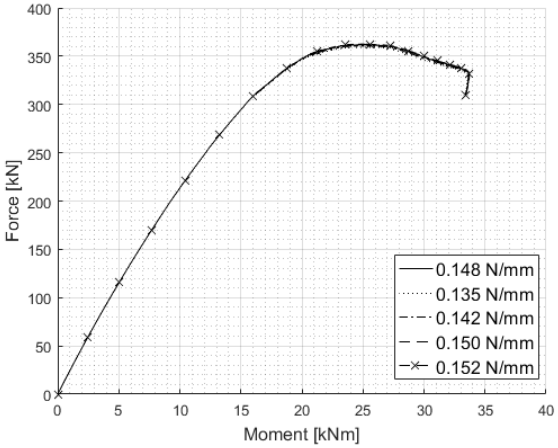

(d) Concrete fracture energy G_f

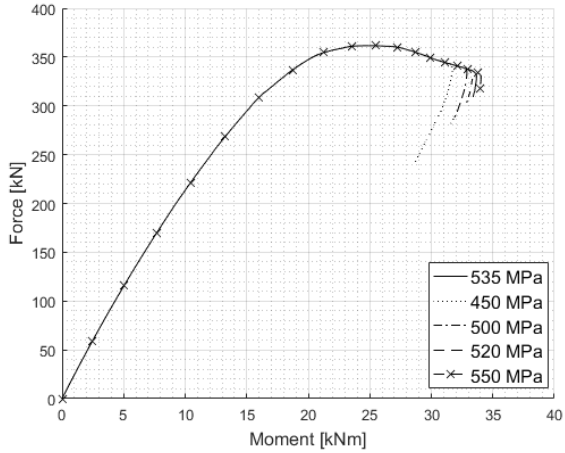

(e) Steel yield strength f_y

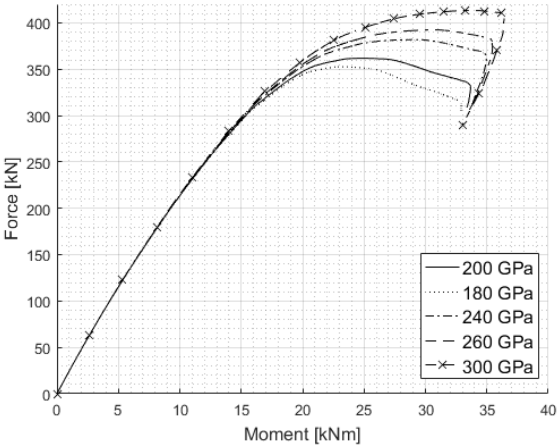

(f) Steel stiffness E_s

Figure B.5: Work diagrams from parametric study on material parameters

C Validation of the linear strain assumption

To test the assumption from EC2-1-1 of a linear strain distribution in the cross section, the global longitudinal strains at the mid span of the column was sampled from an FE-analysis of Column A with in-situ material parameters at different stages of loading. One sample was taken in the linear elastic regime at a load step where the elastic tensile strain limit of concrete was reached, one in the non-linear regime prior to flexural cracking, one at a load step just after cracking, and one final sample after reinforcement yielding. The force-displacement curve from the analysis is presented in Figure C.1, together with points of interest. The point of cracking is when the tensile strains in any integration point is larger than $2G_f/hf_{ct}$. The points of interest are:

- Pt. 1: Elastic tensile strain limit
- Pt. 2: Elastic compressive strain limit
- Pt. 3: Cracking
- Pt. 4: Maximum force
- Pt. 5: Maximum compressive stress
- Pt. 6: Yielding of reinforcement

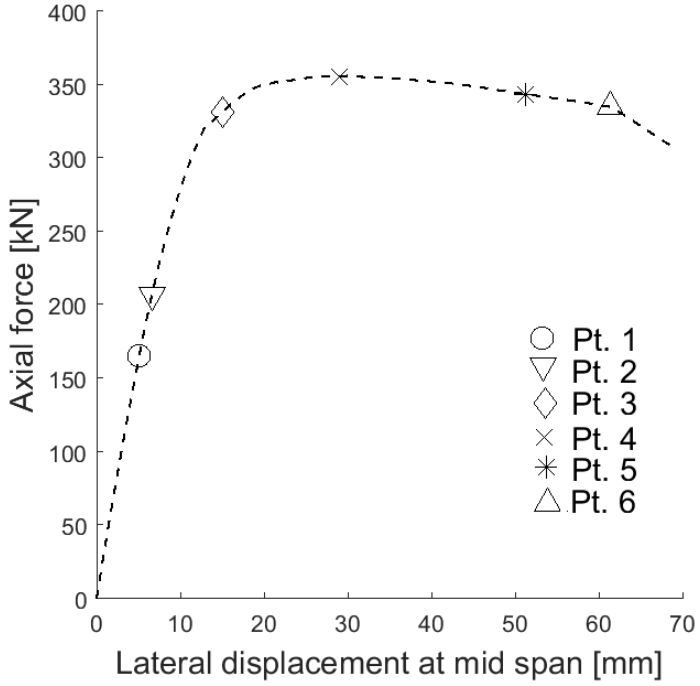

Figure C.1: Force-displacement curve with points of interest

Figure C.2 illustrates that the strain distribution prior to cracking is fairly linear, and the assumptions from EC2-1-1 are valid. Figure C.2c on the other hand reveals that the strain distribution in the tensile zone of the cross section after cracking is starting to become non-linear, with highly non-linear behaviour in Figure C.2d. The two large tensile strain peaks in Figure C.2d is a result of the embedded reinforcement model used in DIANA, as the strains in the reinforcement equals the strains in the surrounding concrete.

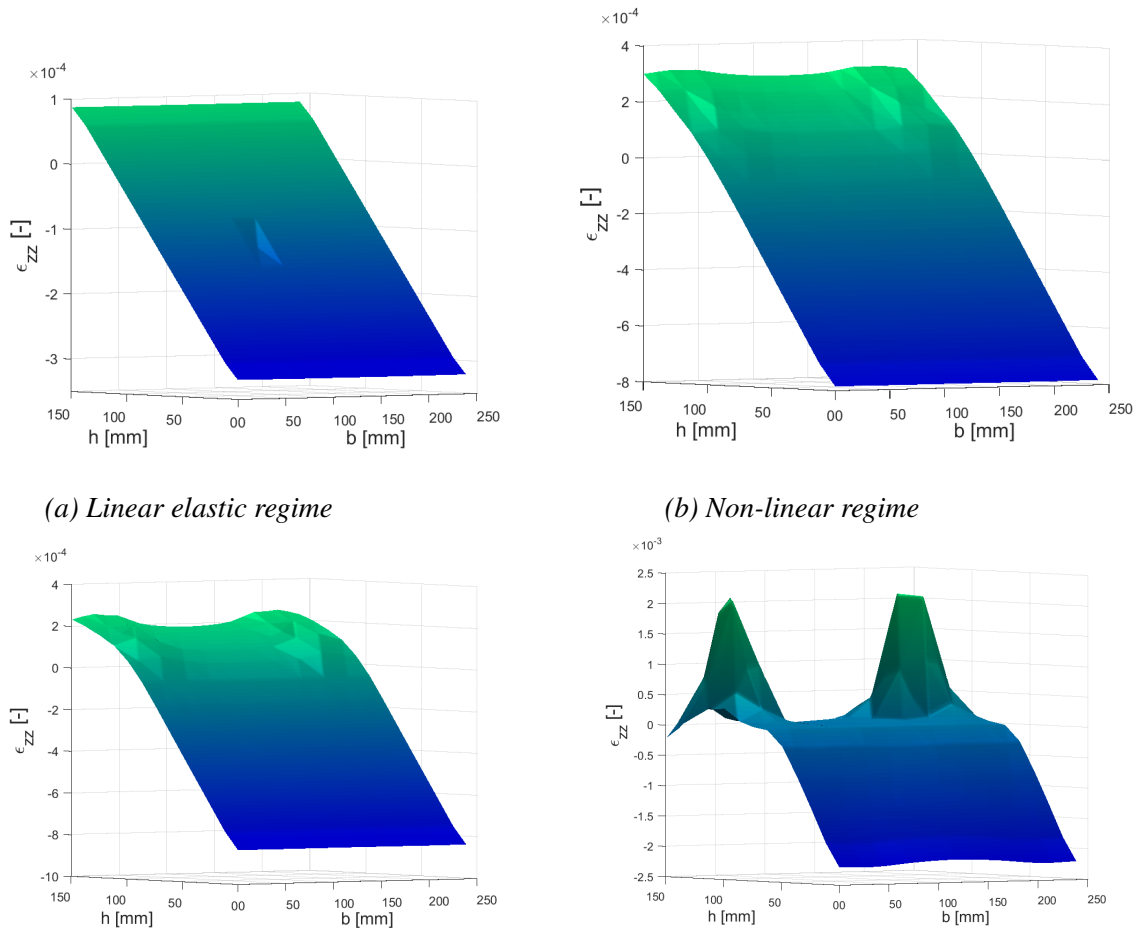

(a) Linear elastic regime

(b) Non-linear regime

(c) After flexural cracking

(d) After reinforcement yielding

Figure C.2: Global longitudinal strains ε_{zz} at the mid span of Column A

The non-linearity in the tensile strain distribution is likely caused by cracking in neighbouring integration points, as the strains were sampled between two flexural cracks. With the exponential tensile material definition of concrete the tensile strains become localized in the integration points that are cracked, while tensile strains in nearby integration points are reduced, thus causing a reduction in strains in the tensile zone of the cross section from which the sample was taken. The localization of tensile strains in the crack nearest to the mid span is illustrated in

Figure C.3a. Note that the strain figures are indicative only, and that the strain values are not equal to the strains in the integration points, but values projected to the nodes which include nodal averaging. The strain plots are only to be used for qualitative assessments.

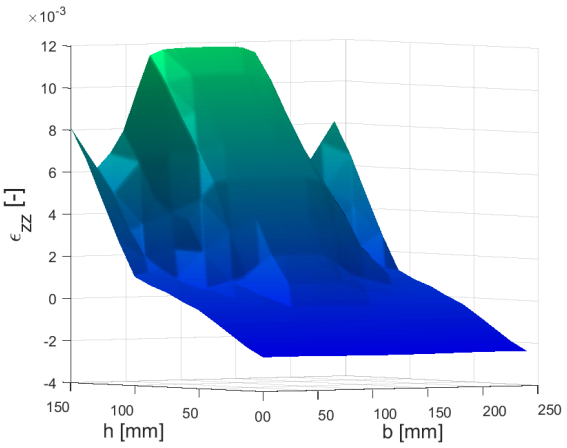

(a) Strains in crack

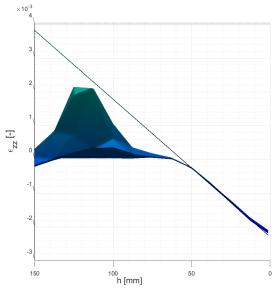

(b) Linear strain approximation at mid span

Figure C.3: Global longitudinal strains ε_{zz} in Column A after yielding of reinforcement

A linear strain plane, depicted in Figure C.3b was approximated by using the reinforcement strain values, to study whether the strains remain linear with respect to the reinforcements and the concrete compressive zone. The concrete strains were taken from Figure C.2d. Although the concrete cross section shows a non-linear deformation pattern, the materials that are still contributing to the cross-sectional capacity, namely concrete in compression and the longitudinal reinforcement, show a linear deformation pattern. These findings indicate that the linear strain assumption in EC2-1-1 is a valid approximation of the real structural behaviour. Figure 6.2c illustrates that the point of maximum moment from the FE-analyses are in agreement with the limit set in the analytic MN-diagram based on EC2-1-1 assumptions.

D Control of Matlab FORM and SORM algorithms

A total of five limit state equations were tested on the FORM algorithm:

1. $X_1 + X_2 - 60$
2. $X_1 + X_2 + X_3 - 80$
3. $X_1 + X_2 + X_3 + X_4 - 120$
4. $X_1 + X_2 + X_3 + X_4 + X_5 - 180$
5. $X_1X_2 + X_4^2 + X_1X_3 - 3500$

All of the random variables in the test were given the same lognormal distribution with $\mu_{log} = 3.9025$ and $\sigma_{log} = 0.1492$. The variables X_2, X_3, X_4, X_5 were correlated to X_1 by a correlation coefficient of 0.5. There was no correlation between the other variables. The convergence norm in both the Matlab script and COMREL was set to 0.0001. Note that these convergence norms represent two different norms. In COMREL it is given as the convergence criterion for β-point search, while it in the Matlab script is given as a vector length (see 5.2.2).

From the results in Table D.1 it is evident that the Matlab algorithm performs as intended. When introducing five random variables, COMREL did not manage to run the analysis.

Equation	COMREL β	Matlab β	Error [%]
1	3.877	3.8797	0.0696
2	5.593	5.5977	0.084
3	5.149	5.1532	0.470
4	N.A	3.6251	N.A
5	3.518	3.5218	0.108

Table D.1: Reliability indexes from COMREL and Matlab algorithm and relative error

To test the accuracy of the SORM algorithm, four non-linear limit state functions were tested in Matlab and compared to COMREL:

1. $X_1^2 + X_1X_2 + X_2^2 - 2100$
2. $X_1X_3 + X_3^2 + X_2 - 300$
3. $X_1X_2 + X_3X_5 + X_1X_4 - 880$
4. $X_1X_2 + X_3X_5 + X_1X_4 - 1500$

The distribution parameters are listed in Table D.2. There was no correlation between any of the variables.

Variable	μ	σ	PDF
X_1	50	5.0	Lognormal
X_2	20	1.0	Lognormal
X_3	10	3.0	Lognormal
X_4	40	10.0	Lognormal
X_5	5	0.5	Lognormal

Table D.2: Mean, standard deviation and distribution type of the random variables

The SORM probability of failure and relative error is listed in Table D.3. It is clear that the error is close to zero, and the Matlab SORM script performed as intended.

Limit state	COMREL P_f	Matlab P_f	Error [%]
1	1.55e-5	1.55e-5	0.000
2	1.93e-2	1.93e-2	0.000
3	1.09e-4	1.10e-4	0.917
4	2.54e-5	2.55e-5	0.394

Table D.3: SORM probability of failure in Matlab and COMREL

E Derivation of second order load effect

The governing equation for a beam-column loaded with an eccentrically placed compressive force is given by Equation (E.1), which has the solution given in Equation (E.2). Figure E.1 illustrates the problem.

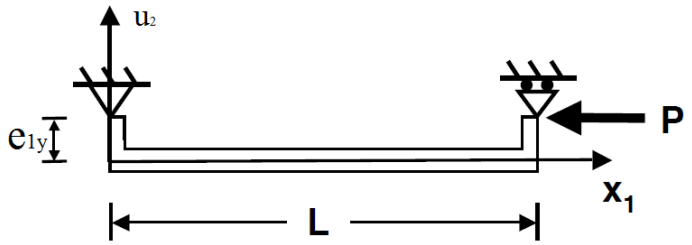

Figure E.1: Representation of load applied eccentrically [7]

$$\frac{d^2u_2}{dx_1^2} + \frac{Pu_2}{EI} = 0 \tag{E.1}$$

$$u_2 = Asin(\lambda x_1) + Bcos(\lambda x_1) + C + Dx_1; \quad \lambda^2 = \frac{P}{EI} \tag{E.2}$$

The boundary conditions to a pinned column with end moments equal to the force times the eccentricity, Pe_{1y}, are given as:

$$u_2(0) = 0, \qquad u_2(L) = 0, \qquad \frac{EId^2u_2}{dx_1^2}\Big|_{x=0} = -Pe_{1y}, \qquad \frac{EId^2u_2}{dx_1^2}\Big|_{x=L} = -Pe_{1y}.$$

These boundary conditions together with Equation (E.2), yields the final solution to the displacement along the column in Equation (E.3).

$$u_2 = \left(\frac{1 - cos\sqrt{\frac{P}{EI}}L}{sin\sqrt{\frac{P}{EI}}L} sin\sqrt{\frac{P}{EI}}x_1 + cos\sqrt{\frac{P}{EI}}x_1 - 1\right)e_{1y} \tag{E.3}$$

Note that when

$$P \to P_{cr} = \frac{\pi^2 EI}{L^2},$$

u_2 becomes unbounded ($u_2 \to \infty$).

A general concrete cross section with both tensile and compression reinforcement is illustrated in Figure E.2. A_s' is the compression reinforcement and A_s is the tensile reinforcement.

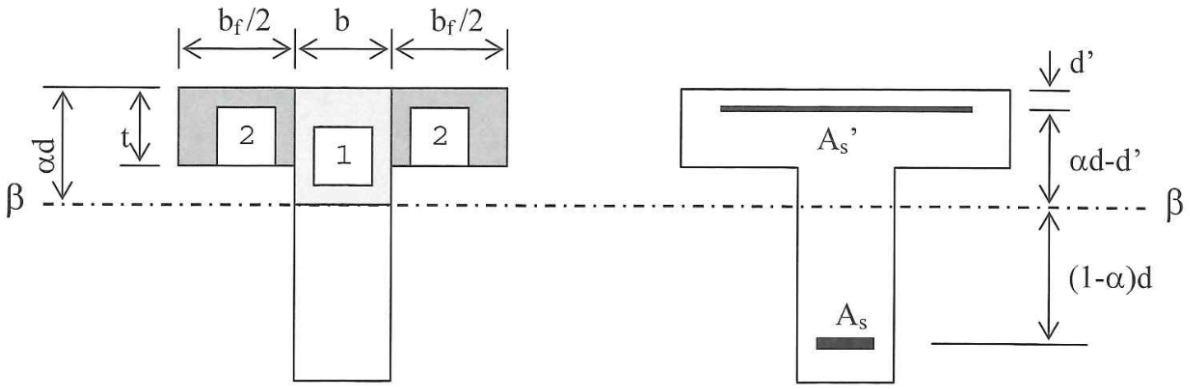

Figure E.2: Concrete and reinforcement contribution to the second moment of inertia [8]

Sørensen [8] states that the bending stiffness of such a cross section in stage II (cracked section) is given by Equation (E.4).

$$EI = E_{cm} I_{\beta\beta} + E_s (I_s + I'_s) \tag{E.4}$$

The concrete contribution, $I_{\beta\beta}$, is given by Equation (E.5), the tensile reinforcement contribution I_s by Equation (E.6) and the compression reinforcement contribution by Equation (E.7).

$$I_{\beta\beta} = \frac{b(\alpha d)^3}{12} + b\alpha d\Big(\frac{\alpha d}{2}\Big)^2 + \frac{b_f t^3}{12} + b_f t\big(\alpha d - \frac{t}{2}\big)^2 \tag{E.5}$$

$$I_s = A_s(1-\alpha)^2 d^2 \tag{E.6}$$

$$I'_s = A'_s(\alpha d - d')^2 - \frac{E_{cm}}{E_s} A'_s(\alpha d - d')^2 \tag{E.7}$$

F Validation of the MN-diagram

To test the accuracy of the MN-diagram, the Matlab script for constructing MN-diagrams was tested against finite element simulations in DIANA. The material model for the concrete was set to the non-linear relation given in Equation (3.1), while the parabolic model based on fracture energy was used in DIANA. The material model for the steel reinforcement was the same in both Matlab and DIANA. The load eccentricity was gradually increased in the finite element model to get cross-sectional failure at different combinations of axial force and moment to produce a piece-wise MN-diagram. Non-linear geometry was turned off, as only the cross-sectional capacity was of interest. The results are presented in Figure F.1, and shows the MN-diagram from Matlab as well as the DIANA-simulations.

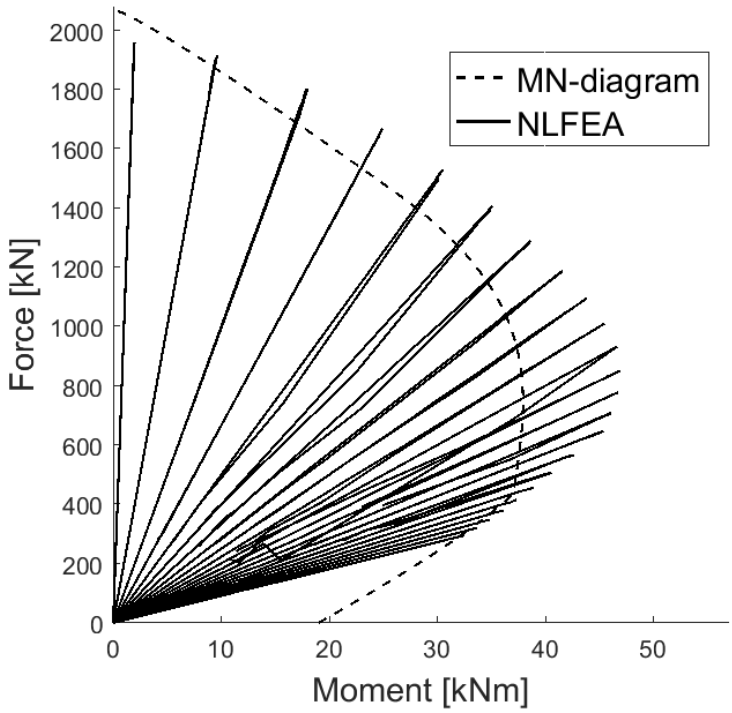

Figure F.1: MN-diagram and finite element simulations

Note that the two work diagrams that are closest to vertical give a lower capacity than the MN-diagram from Matlab. This is due to local compression failure at the point of load application in the FE-model, as a result of stress concentration effects. Also note that the FE-model gives a significantly higher capacity than the MN-diagram around the balance point. This may be a result of the different compression models used for concrete. In the failure region governed by reinforcement yielding the MN-diagram and FE-model seem to agree.